VYSOKÉ UČENÍ TECHNICKÉ V BRNĚ

BRNO UNIVERSITY OF TECHNOLOGY

FAKULTA ELEKTROTECHNIKY A KOMUNIKAČNÍCH TECHNOLOGIÍ
ÚSTAV BIOMEDICÍNSKÉHO INŽENÝRSTVÍ

FACULTY OF ELECTRICAL ENGINEERING AND COMMUNICATION
DEPARTMENT OF BIOMEDICAL ENGINEERING

IDENTIFICATION OF THE PARAMETERS OF AN ELECTROENCEPHALOGRAPHIC RECORDING SYSTEM

DIPLOMOVÁ PRÁCE
MASTER'S THESIS

AUTOR PRÁCE
AUTHOR

Bc. VERONIKA SVOZILOVÁ

BRNO 2015

VYSOKÉ UČENÍ TECHNICKÉ V BRNĚ

BRNO UNIVERSITY OF TECHNOLOGY

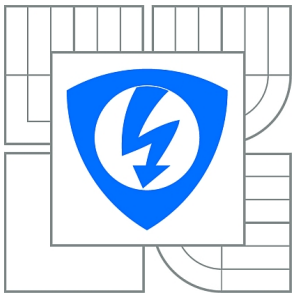

FAKULTA ELEKTROTECHNIKY A KOMUNIKAČNÍCH TECHNOLOGIÍ

ÚSTAV BIOMEDICÍNSKÉHO INŽENÝRSTVÍ

FACULTY OF ELECTRICAL ENGINEERING AND COMMUNICATION

DEPARTMENT OF BIOMEDICAL ENGINEERING

IDENTIFICATION OF THE PARAMETERS OF AN ELECTROENCEPHALOGRAPHIC RECORDING SYSTEM

IDENTIFIKACE PARAMETRŮ ELEKTROENCEFALOGRAFICKÉHO SNÍMACÍHO SYSTÉMU

DIPLOMOVÁ PRÁCE

MASTER'S THESIS

AUTOR PRÁCE — Bc. VERONIKA SVOZILOVÁ

AUTHOR

VEDOUCÍ PRÁCE — Ing. MARTIN MÉZL

SUPERVISOR

BRNO 2015

BRNO UNIVERSITY OF TECHNOLOGY

Faculty of Electrical Engineering and Communication

Department of Biomedical Engineering

Diploma thesis

Master's study field

Biomedical Engineering and Bioinformatics

Student: Bc. Veronika Svozilová ***ID:*** 136490

Year of study: 2 ***Academic year:*** 2014/15

TITLE OF THESIS:

Identification of the parameters of an electroencephalographic recording system

INSTRUCTION:

1) Learn the basic principles of recording and processing of EEG signals. 2) Make a review of the basic models used for EEG signal modeling. Implement the selected model in Matlab enviromenent. 3) Apply time-frequency spectral analysis for clinical EEG recording and also for the signals obtained from model implementation. Make comparison of both spectra. 4) Propose extensions of the basic model which include nonlinearities, model of impulse conduction, modelisation of electrode-electrolyte interface and others. 5) Perform experimentation with EEG phantom for model paramters identification and evaluation of the proposed model. 6) Make comparison of proposed models and discuss the results.

REFERENCE:

[1] SANEI, Saeid a Jonathon CHAMBERS. EEG signal processing. Hoboken, NJ: John Wiley, c2007, xxii, 289 p.
[2] DAVID, Olivier a Karl J. FRISTON. A neural mass model for MEG/EEG. NeuroImage. 2003, vol. 20, issue 3, s. 1743-1755.

Assigment deadline: 9. 2. 2015 ***Submission deadline:*** 30.7.2015

Head of thesis: Ing. Martin Mézl
Consultant: Alina Voda

prof. Ing. Ivo Provazník, Ph.D.
Subject Council chairman

ABSTRAKT

Elektroencefalografický záznamový systém slouží k vyšetření mozkové aktivity. Na základě tohoto vyšetření lze stanovit diagnózu některých nemocí, například epilepsie. Účelem této práce bylo zpracování signálu z toho systému a vytvoření modelového signálu, který bude s reálným signálem porovnán. Uměle vytvořený signál vychází z Jansenova matematického modelu, který byl dále implementován v prostředí MATLAB a rozšířen ze základního modelu na komplexnější zahrnující nelinearity a model rozhraní elektroda – elektrolyt. Dále bylo provedeno měření signálů na EEG fantomu a následná identifikace parametrů naměřených signálu. V první fázi byly testovány jednoduché signály. Identifikace parametrů těchto signálů sloužila k validaci daného EEG fantomu. V druhé fázi bylo přistoupeno k testování EEG signálů navržených podle matematického Jansenova modelu. Analýza veškerých signálů zahrnuje mimo jiné časově frekvenční analýzu či ověření platnosti principu superpozice.

KLÍČOVÁ SLOVA

Elektroencefalografický záznamový systém, mozková aktivita, Jansenův model, časově frekvenční analýza, Fourierova transformace, princip superpozice.

ABSTRACT

Electroencephalographic recording system is used to examine a brain activity. Based on this examination we can establish the diagnosis of certain diseases, such as epilepsy. The purpose of this study has been the signal processing and a signal generation which were compared with the real signal. Artificially generated signal is based on Jansen‘s mathematical model which has been also implemented in MATLAB and then that model has been extended to more complex model including nonlinearities and model electrode – electrolyte. Also a signal measurements on EEG phantom and identification of the parameters of these signals were performed. Firstly a simply signals were tested and the identification of their parameters has served to validate the EEG phantom. Secondly the created signal designed by Jansen model were tested also. Besides an analysis of all signals includes the time frequency analysis or a superposition principle testing.

KEY WORDS

Electroencephalographic recording system, brain activity, Jansen‘s model, time-frequency analysis, Fourier transform, superposition principle.

SVOZILOVÁ, V. *Identifikace parametrů elektroencefalografického snímacího systému.* Brno: Vysoké učení technické v Brně, Fakulta elektrotechniky a komunikačních technologií, 2015. 118 s. Vedoucí diplomové práce Ing. Martin Mézl.

PROHLÁŠENÍ

Prohlašuji, že svou diplomovou práci na téma „Identification of the parameters of an electroencephalographic recording system“ jsem vypracovala samostatně pod vedením vedoucího diplomové práce a s použitím odborné literatury a dalších informačních zdrojů, které jsou všechny citovány v práci a uvedeny v seznamu literatury na konci práce.

Jako autorka uvedeného diplomové práce dále prohlašuji, že v souvislosti s vytvořením této diplomové práce jsem neporušila autorská práva třetích osob, zejména jsem nezasáhla nedovoleným způsobem do cizích autorských práv osobnostních a jsem si plně vědoma následků porušení ustanovení § 11 a následujících autorského zákona č. 121/2000 Sb., včetně možných trestněprávních důsledků vyplývajících z ustanovení § 152 trestního zákona č. 140/1961 Sb.

Brno . . . .

(podpis autora)

Děkuji svému vedoucímu diplomové práce Ing. Martinovi Mézlovi za jeho ochotu, trpělivost a pomoc při tvorbě této diplomové práce. Dále děkuji svým francouzským konzultantům Dr. Alině Voda a Dr. Guillaumovi Becqovi za vedení a pomoc s praktickou částí mé diplomové práce a umožnění přístupu k jejich EEG fantomu.

CONTENT

LIST OF FIGURES

LIST OF TABLES

INTRODUCTION

Electroencephalographic recording system serves to the examination of a brain activity. For many decades this examination is used to diagnosis of diseases such as epilepsy or polio. In the EEG (electroencephalogram) signal there are a several types of waves whose changes are analysed. This type of examination is very important in medicine field and there have been several attempts to simulate a real EEG signal by artificial models, especially alpha and beta activity. The simulation of EEG-like signals helps to predict and diagnostic a brain diseases like epilepsy or polio.

Simulation of EEG-like signals is based on the effort to describe and generate EEG-like signals in the mathematical way. During the second half of the 20^{th} century to the present day, many mathematical models has been invented for that purpose. One of the appropriate mathematical model generating alpha activity is Jansen's model of a single cortical column. This model is based on the idea of a population of pyramidal neurons that interact with a population of an excitatory inter-neurons and with a population of an inhibitory inter-neurons. The extension of that mathematical model is Jansen's model of a double cortical columns that generates alpha and beta activity. The main idea of that extension is focused on an interconnection of two cortical columns by a connectivity constants. Based on that interaction between two cortical columns, alpha activity is generated by the first column and beta activity is generated by the second column.

In collaboration with the laboratory Gipsa-lab (Grenoble, France), their sponge phantom simulating a brain environment was used for signal experiments. These signal experiments included test signals serving to the identification of parameters of measuring system and alpha and beta activity signals generated by Jansen's models. Sponge phantom experiments simulated the real situation of acquisition of EEG-like signals. These experiments included nonlinearities, model of excitation conduction and model of electrode-electrolyte interface.

These sponge phantom experiments built on previous experiments whose task was to design and construct a valid EEG phantom. The main aim of these experiments was to implement alpha and beta activity generated by Jansen's models to the sponge phantom experiments and then output signals were analysed and compared to real ones.

1 NERVE CELLS

The CNS (Central Nervous System) consists of the nerve cells and the glia cells and their activity is the most important for EEG examination. In this part of my diploma I will describe construction of nerve cells and their function.

1.1 Construction of the nerve cells

Nerve cell (called neuron) consists of several main parts.

1.1.1 Cell body

Cell body is the one of the main part of the nerve cell. It is created by nucleus, cytoplasm and cell organelles. Nucleus has a globular or an oval shape and usually contains a small nucleolus. Cell organelles are located in the cytoplasm. These organelles are almost identical as organelles in the rest of somatic cells, [32].

1.1.2 Dendrites

Another part of the neuron is a dendrite. Dendrites are short projections which extend from the cell body. Dendrites are indispensable to action potential conduction. These projections are centripetal therefore they accept an input information called nervous excitement. On the dendrite's surface synapses are located which serve to connection of two neuron. Between two synapses there is the small aperture through which action potential conduction is realized, [32].

1.1.3 Axon hillock

Axon hillock is a place where the cell body is connected with the axon. It is a bridge for the signal propagation, [32].

1.1.4 Axon (nerve fibre)

Axon is the longest neuron's projection which ensures centrifugal action potential conduction from cell body. Axon is a conductive part of neuron and can be 1 meter long. Axon can have two sheaths. The first of them is an inner myelin sheath. This type of sheath is composed of a lipid substance myelin. Myelin sheath is interrupted Ranvier's cuts which accelerate action potential conduction. The second of them is an outer Schwann's sheath which is formed by glia cells. Myelin is an isolator so speed of action potential conduction is dependent on the thickness of myelin sheath. Both sheaths prevent the spread of the nerve impulses between neighboring nerve fibres, [32].

1.1.5 Nerve’s endings

Nerve endings are the output parts of an axon. They ensure secretion of the neurotransmitter which allows the transmission between neurons and between neurons and target cells, [32].

Whole construction of neuron is described below in Fig. 1.

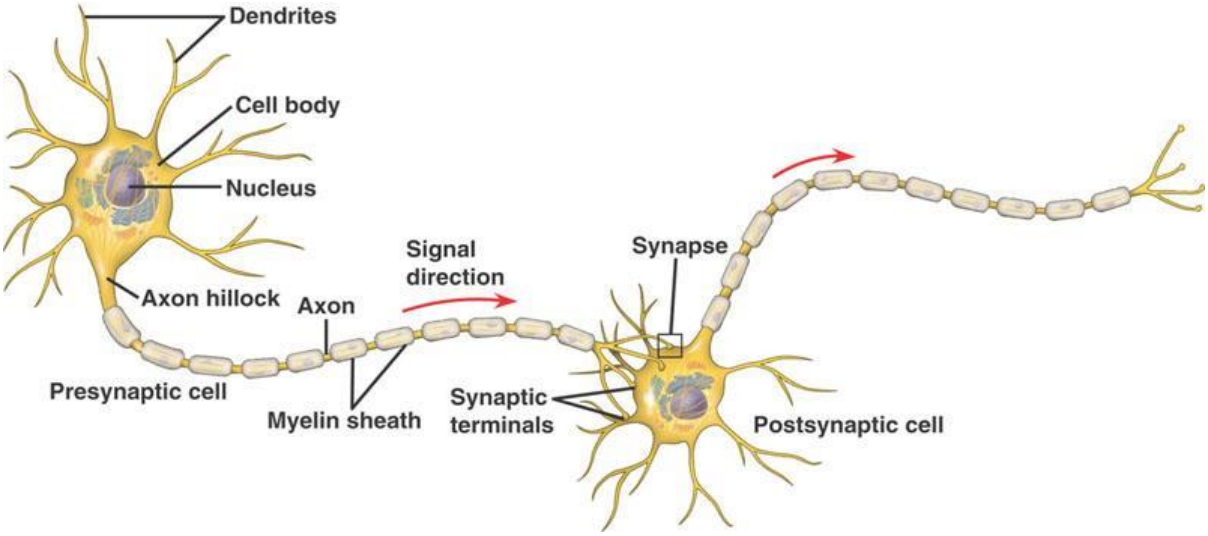

Fig. 1 Structure of the neuron, [30].

1.2 Generation of the action potential

The construction of neuron cells was explained in the previous chapter so now the generation of action potential is described.

Action potential (AP) is the transmitting information among neurons. Basically AP is result of the ion's exchange across the neuron membrane. It is a short time when membrane potential is quickly increased and then is quickly reduced so APs have temporary character. APs are created in the cell body and then continue in one direction along the axon.

AP represents a rapid change the resting membrane potential which caused by the supralimininal input. This rapid change is distributed to the next part of membrane. This rapid voltage change is connected with a change the permeability channels for sodium and potassium ions. AP can be evoked by the electrical or the chemical inputs which can lead to a local reduction of the resting membrane potential.

If the stimulus is sufficient the membrane depolarization will occur. If the membrane depolarization occurs the membrane potential will be changed during $0.5\ ms$ and its final value is about $+30mV$ (resting membrane potential is approximately $-70\ mV$). After this quick depolarization the membrane potential will be reduced and a quick repolarization will occur. In the phase of the repolarization the membrane potential returns to the value of resting membrane potential. When the membrane potential returns to its resting value the phase of the hyperpolarization appears. This phase is characterized by decrease membrane potential under its resting value. In final phase the membrane potential returns to its resting value and this phase takes $40\ ms$.

AP operates on the principle „all or nothing“, which means that there exits threshold value which must be exceeded to activate the membrane depolarization. As soon as the threshold value is exceeded the amplitude of action potential is not so important because properties of stimuli are encoded in the number of individual action potentials generated in a certain time series not in amplitude of action potential, [19].

All phases are introduced in this picture Fig. 2.

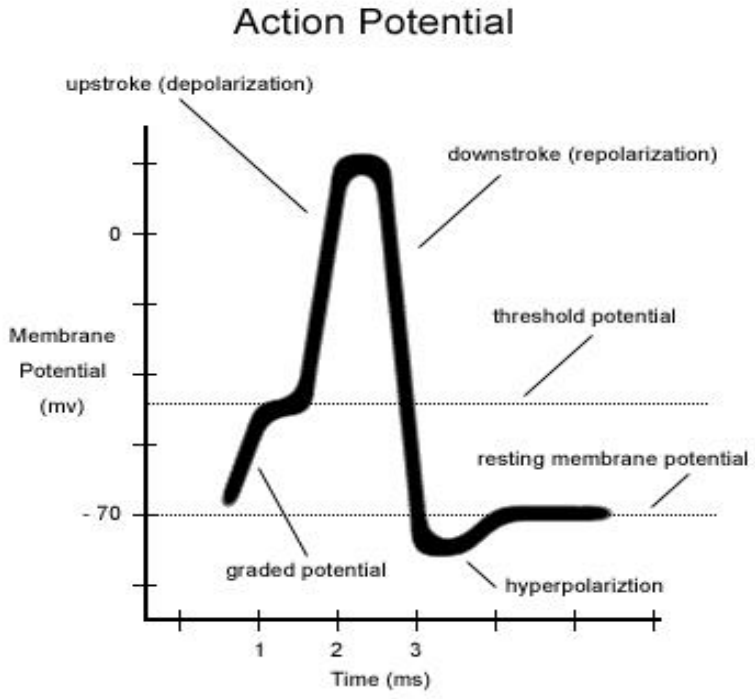

Fig. 2 The phases of the action potential, [7].

The processes (which are described above) are accompanied by changes in the composition outside and inside the cell. The resting membrane potential is characterized by a low concentration of sodium ions inside the cell and conversely a high concentration of sodium ions outsider the cell. This fact is due to size of sodium ions which are relatively large so the membrane is completely impermeable for them.

For potassium ions the situation is different. Potassium ions are cations (unlike the sodium ions which are anions) so their size is not so large. The membrane is not impermeable for them so potassium ions can go through membrane. Their concentration inside the cell is higher than outside the cell.

During the depolarization the sodium channels open a sodium ions move to the inside the cell and because of this fact the resting potential changes to the action potential. These sodium channels are created by specialized proteins which go through the membrane.

After reaching the voltage value about $30\ mV$ the sodium channels close and the membrane potential decreases to value of the resting potential. For certain time the creation of the action potential is blocked not to generate a new action potential. That is the reason why is the signal in the neuron characterized as „all or nothing“, [19].

1.3 Propagation of the action potential

Propagation of the action potential is implemented along the length of the neuron. The action potential spreads from the place of origin through the axon. The axon is encapsulated Swann's cells which help accelerate the propagation of the action potential. Due to the axon myelination here applies *saltatory* spreading the action potential. The signal doesn't spread continuously but the signal skips between the Ranvier's cuts.

This way of the propagation of the action potential increases its speed and significantly reduces the energy intensity of the process, [32].

2 EEG SIGNALS

EEG, i.e. the electroencephalogram, is the record of temporal changes of the electric potential acquired from the surface of the head. These temporal changes are caused by a brain activity and these changes are connected with changes of the human consciousness. EEG examination is based on this record, i.e. the electroencephalogram, [15].

2.1 EEG examination

EEG examination is the standard non-invasive method for functional examination of CNS's activity. Basic acquisition of the method consist of the set of electrodes which record signals from the head. These signals are sums of action potentials of single neurons. Problem is that these signals are highly attenuated because of a little conductive layer (the skull). Amplitude of these signals is attenuated to a level of microvolts. So typical EEG course looks irregular and chaotic but by the further analysis of the EEG signal we are able to recognize several basic types of waves of a certain frequency, [15].

2.1.1 Alpha waves

The first type of waves is Alpha waves which are located in the frequency range of $8 - 13\ Hz$. These waves are connected with condition of release. This status is represented by a state of alert relaxation of the mind. This condition is characterized by creativity, [11].

2.1.2 Beta waves

The second type of the waves is Beta waves which are situated in the range of $13 - 40\ Hz$. These waves are accompanied by condition in which people persist for predominant part of the day and they appear in the normal awake condition. At higher frequencies the stress can be found in humans and can be accompanied by the restlessness, a fear or an anger. In this condition here proceeds logical and analytical thinking, [11].

2.1.3 Delta waves

The third type is Delta waves which are located in the range of $0.5 - 4\ Hz$. They are measured in the condition of the deep sleep or in the condition of the unconsciousness. They are the slowest brain waves and these waves are accompanied by processes of the physical regeneration, [11].

2.1.4 Theta waves

These waves are situated in the range of $4 - 8\ Hz$. They respond to the condition of the deep relaxation, meditation or a low form REM (rapid eye movement) sleep. These waves indicate the condition in which the person is able to find an unusual solution to problems and in this condition an intuition is deepened, [11].

On the picture below we can see all these types of waves in the time process, Fig. 3.

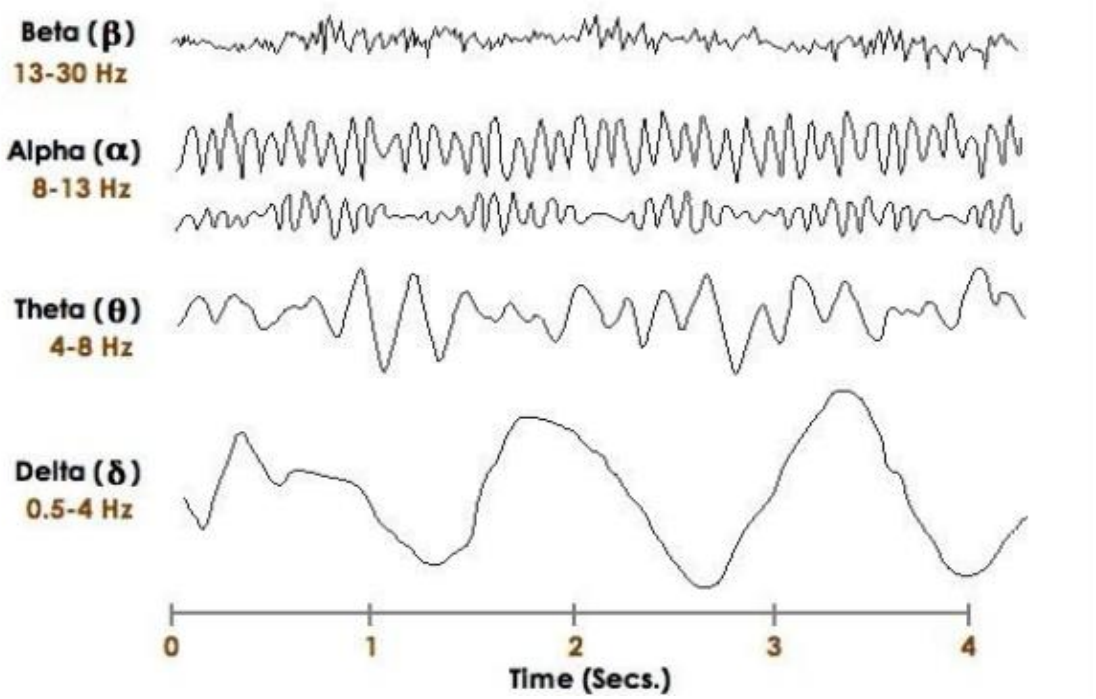

Fig. 3 The EEG waves, [31].

2.2 Construction of EEG device

EEG device called the electroencephalograph comprises a several parts which help measuring the electrical potential caused by the brain activity, [17].

2.2.1 Differential amplifier

As already stated, EEG measures and records the CNS's electrical potential through the set of electrodes which are located on the skull. Because of a little conductive layer (the skull) the electrical signals have the low amplitude so these signals must be amplified by the differential amplifier. The differential amplifier is used as the input amplifier (the preamplifier). This component is used for the minimization of the noise and for the amplification of the weak signals.

The differential amplifier is very sensitive and it has a high voltage gain. The differential amplifier has two inputs, the first of them is straight (active), the second of them is inverted (reference). This amplifier intensifies the voltage difference between two inputs, i.e. the amplifier deducts the value of the voltage on the inverted input from the value of the voltage on active input and then amplifies this difference. Moreover this process has one big advantage. If the same value of the noise voltage is brought equally to both inputs, the noise voltage will be subtracted from each other and at the amplifier output the value of the noise is not reflected, [17]. The differential amplifier is represented in the picture below, Fig. 4.

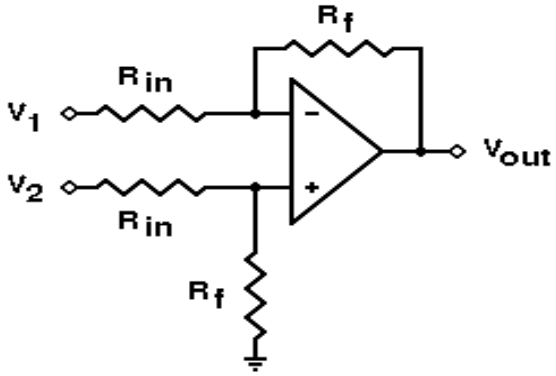

Fig. 4 The differential amplifier, [2].

2.2.2 Channels

The output of the differential amplifier is called channel. For each channel we need the one input amplifier. The number of signals which we can record is dependent on the number of channels. Signals can be modified during the procedure through channels for example using filters, [17].

2.2.3 EEG electrodes

Electrodes drain changes of the electric potential and together with a liquid medium create an electric potential in the resting state.

An electrical characteristic of electrodes is given by a kind of metal and a liquid medium. Electrodes made of silver are the most widely used. These electrodes together with medium of silver chloride are non-polarizable so they are suitable for EEG examination because they release satisfactory amount of current.

For the wiring of EEG electrodes we use the scheme which was united in 1957 on An International Congress of EEG and it is called „10-20“. In the sagittal and transverse plane electrodes are distributed over 20% or 10% but the sum in each plane must be 100%. Electrodes are marked with a letter (Fp…fronto-polar, F…frontal, P…parietal, T…temporal, O…occipital, C…central) and number for specification (odd numbers for left hemisphere, even numbers for right hemisphere), Fig. 5, [11][17].

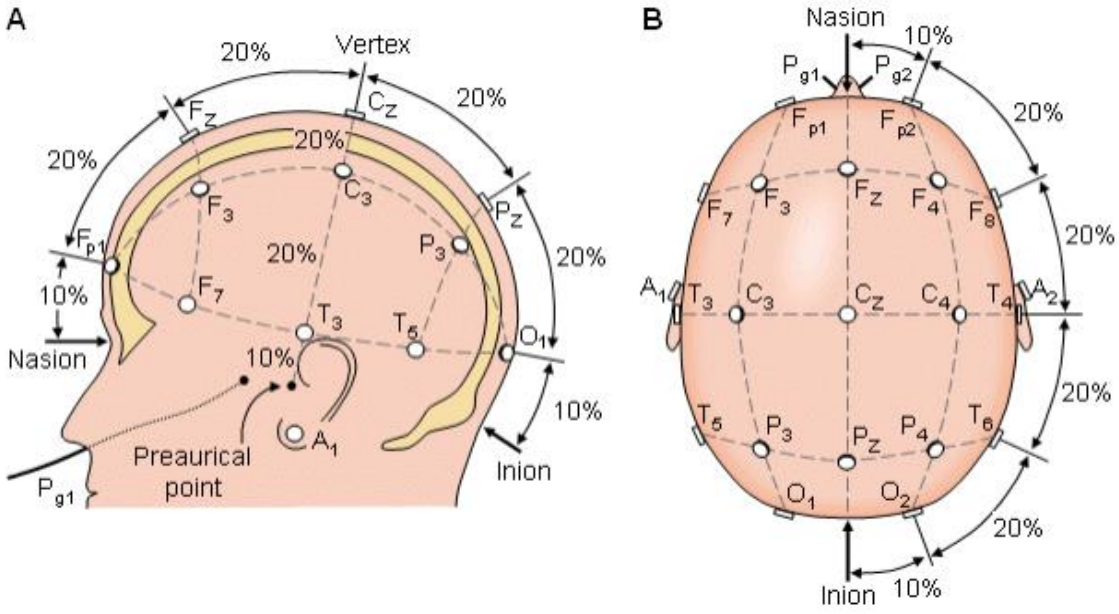

Fig. 5 The "10-20" system, [10].

For EEG examination there are two ways for the wiring electrodes. The first one is the unipolar wiring. Here we watch a difference between an active point on the scalp and a reference point on the scalp which has a zero potential. Reference electrode is usual situated on the earlobe, on the vertex or for example in the rear. This type of wiring is characterized by high levels of the detected signal so in the signal we can find information about an electric activity of the deeper layers of the brain. But this type of wiring EEG electrodes is also characterized by artifacts caused by an activity of the heart or muscles, [44]. The scheme of the unipolar wiring is introduced on the picture Fig. 6.

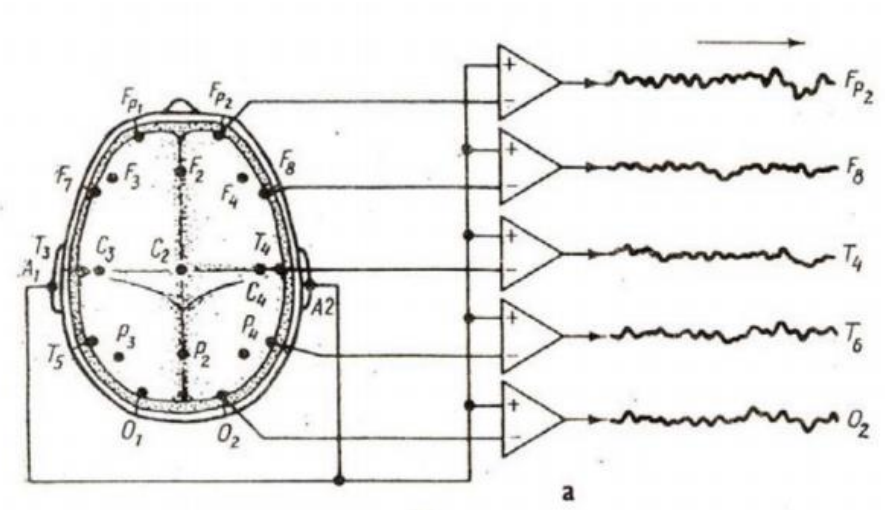

Fig. 6 The unipolar wiring, [44].

The second one is a bipolar wiring. We compare a potential between two points in a row on the scalp. One electrode of a pair is also used in a pair with the following electrode. So each electrode serves as a reference electrode for one pair and for the next pair this electrode serve as an active electrode, Fig. 7. Because of a short distance among electrodes this type of wiring is not optimal for measuring an electric activity of the deeper layers of the brain. An advantage is very good mapping the local differences in the signal amplitude, [44].

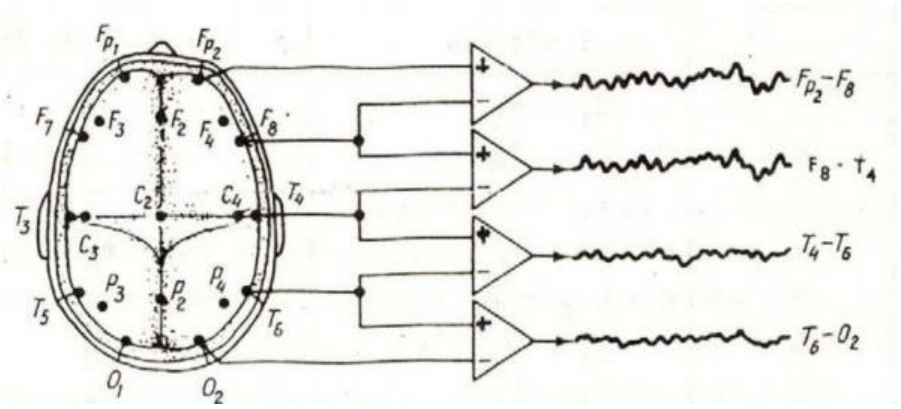

Fig. 7 The bipolar wiring, [44].

3 MODELING OF THE EEG SIGNALS

Modeling of the EEG signals is a very wide academic area that is divided into two main branches. The first branch of modeling EEG signals is about simulation of EEG-like waves corresponding to the normal EEG record without any health problems. Alpha and beta bands were described and designed by many mathematical models. Modeling of EEG-like signals, alpha and beta bands, is the basic to understand how a brain works.

The second branch builds on the first branch of EEG modeling introduced above. Scientists try to understand and predict a development of certain brain diseases based on the knowledge of the modeling of EEG-like signals, normal alpha and beta band. That branch is connected with an incident disease of the brain, epilepsy. Epilepsy is the very widespread brain disease that involves about $0.6 - 0.8\%$ of the population. Because of this fact there has been a need to describe and understand this illness which is accompanied by seizure. Therefore, modeling of the EEG signal is closely associated with the field called seizure prediction. This field is focused on the techniques of seeking the critical times of seizure procedure. The seizure prediction is considered useful to predict further attacks.

Because this diploma thesis is focus on the modeling of EEG-like signals, in this capture the overview of the suitable models that belong to the first branch of the modeling of EEG signals is presented. These models are based on the elementary neural mechanism and they describe the modeling of the neural populations, [1].

3.1 Macroscopic models

Even though the structure and behaviour of the brain is very complicated for the better understanding of the functional significance of the emergent dynamics several simplifications were introduced.

These simplifications are contained in *neural mass model*. This model is based on an idea that the neuronal network of the cortex is a spatially continuous network and the properties of neurons at one local area can be summarized in a state variables as the mean firing rates or the mean values of the cell membrane potential. The values of these variables correspond to an average neuron and they are a function of time and space.

There are two expectations. The first one, the function at the average dendrite is non-linear, the second one, the function at the average soma is linear.

As the input of the neural mass models a white noise is chosen because it accounts the influence of all neurons which are far away, [1].

3.1.1 Elementary macroscopic models

Firstly this type of models included only neurons with the excitatory interactions but later, the inhibitory interactions were involved. These excitatory and inhibitory properties of the neural mass were considered as two different neuronal populations. These population were connected to each other and their state was the mean firing rate at time *t*.

This model was described by set of differential equations because of the assumption of the similar behaviour of every location in both models, excitatory and inhibitory.

In spite of the fact that the neural mass models are very simple and it cannot describe the real situation very accurately, all the later neural mass models are extensions of these models.

The differential equations describing these models show nonlinear terms as a result of the thresholding effect at the dendrites so they should be qualitatively analysed. The EEG signal can be produced if the parameters of these models are suitably set, [1].

3.1.2 Freeman's model

This model was designed to explain the electrocortical dynamics of the olfactory bulb and prepyriform cortex. Unlike the previous elementary macroscopic models, Freeman's model is characterised by a set of a third order differential linear equation corresponding to the *pulse-to-wave* function of the average dendrite.

There are three levels of this model, *K0, KI, KII*. At the lowest level *K0*, there is no interaction between the neurons that are common in the input and the output. The higher level KI is based on the interactions of previous *K0* sets, either excitatory or inhibitory: *KIe* and *KIi*. The highest level of this model *KII* is based on a dense functional interaction between two *KI* sets and *KII* set is the same as the elementary macroscopic models mentioned in the previous part. The scheme of the connection topologies of these models are represented below, Fig. 8.

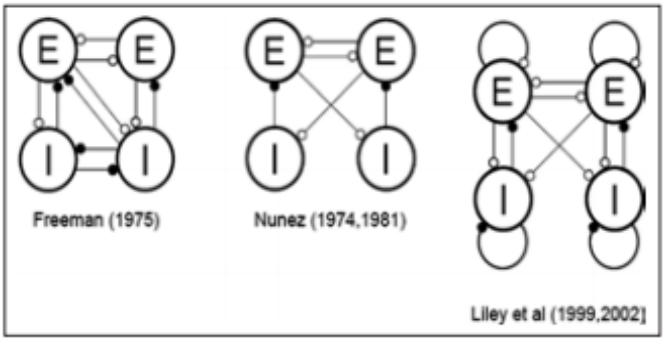

Fig. 8 Scheme of the connection topologies of introduced models, [1].

Freeman's model is determined by four nonlinearly coupled third order differential equations. The *wave-to-pulse* function of the average soma corresponds to nonlinearity. By Freeman's model the generation of the gamma band and the oscillatory activity can be simulated, [1].

3.1.3 Lopez da Silva's model

This model is very simple but also realistic model to simulate alpha waves of the EEG signals. It was observed that the response of the average soma to the pre-synaptic spikes corresponds to the second order. The average membrane potential rises to a peak and then decreases. So this innovation caused the strong resonance in the alpha band, [1].

3.1.4 Jansen's model

This model is an extension of Lopez da Silva's model and its main idea is based on that excitatory and inhibitory populations will interact such that oscillations appear. This model contains three populations of neurons, excitatory pyramidal cells, excitatory principal cells and inhibitory interneurons, represent a cortical area. Jansen's single-column model can simulate alpha waves and Jansen's double-column model can simulate alpha and beta waves, [1][16]. Its description and mathematical structure is presented in the next chapter because this model is the main issue of this diploma.

3.1.5 Nunez's global model

The scheme of this model is also represented in Fig. 8. As it can be observed in Fig. 8 in this model there is no interaction between inhibitory populations. The interactions are between excitatory populations and between inhibitory and excitatory populations. This model is global of electrorhythmogenesis by instantaneously considering short-term and long-term connections. Global models can be also created by an idea that the location is also considered as another variable in the differential equations. But Nunez's model offers a new perspective on the matter, [1][14].

3.1.6 Liley's model

The scheme of this model is shown in Fig. 8. There is no interaction between inhibitory populations but there is interaction between excitatory populations and also between inhibitory and excitatory populations. The new interaction in this model is *feedback.* Inhibitory and excitatory population interact with themselves and it correspond to two facts which were added to this model, effects of the synaptic reversal potentials and the transmission function of the axonal pulses in long range fibres. Due to the first fact, the effect of synaptic reversal potentials, the linear relation between the mean soma membrane potential and the synaptic input is transformed into an exponential relation. The autonomous limit cycle and chaotic oscillatory activity in the alpha band can be produced, [1][6].

4 JANSEN'S MODEL

This model is based on the idea that the cortical columns are the excitatory or the inhibitory population of the neurons that are very close connected and that are able to create EEG activity. Jansen model is inspired by the mathematical model designed by Lopes da Silva and Van Rotterdam. This mathematical model was designed to stimulate the spontaneous electrical activity of neurons recorded using the EEG. The main focus of this model is on the alpha waves.

The neuronal populations interact through the excitation and the inhibition which produces the alpha waves. Additionally Jansen model has the ability to simulate the evoked potentials which can be observed after the sense stimulation, for example the light or the sound stimulation.

The detailed description of Jansen's model is introduced below including the mathematical definition, [9] [16].

This model was chosen to simulate the normal alpha and beta activity and results of that simulation are introduced in the practical part of that diploma thesis.

4.1 Cortex

The cortex is the surface layer of the brain and creates the biggest part of the gray matter. The cortex has a special horizontal organization in layers of different types of cells. The cells which create this organization are not the same on the whole surface of the cortex. They have a different shapes, cell structure or dimension. The cortex is divided into the small regions and in the each region there are the cells which are the same or very similar.

The cortex comprises six layers of the neurons. The first layer (layer 1) is located on the surface, the last layer (layer 6) is located near the white matter. Two main types of the neuron can be described – projection neurons and local inter-neurons, [9]. Histological structure of the cerebral cortex is showed below, Fig. 9.

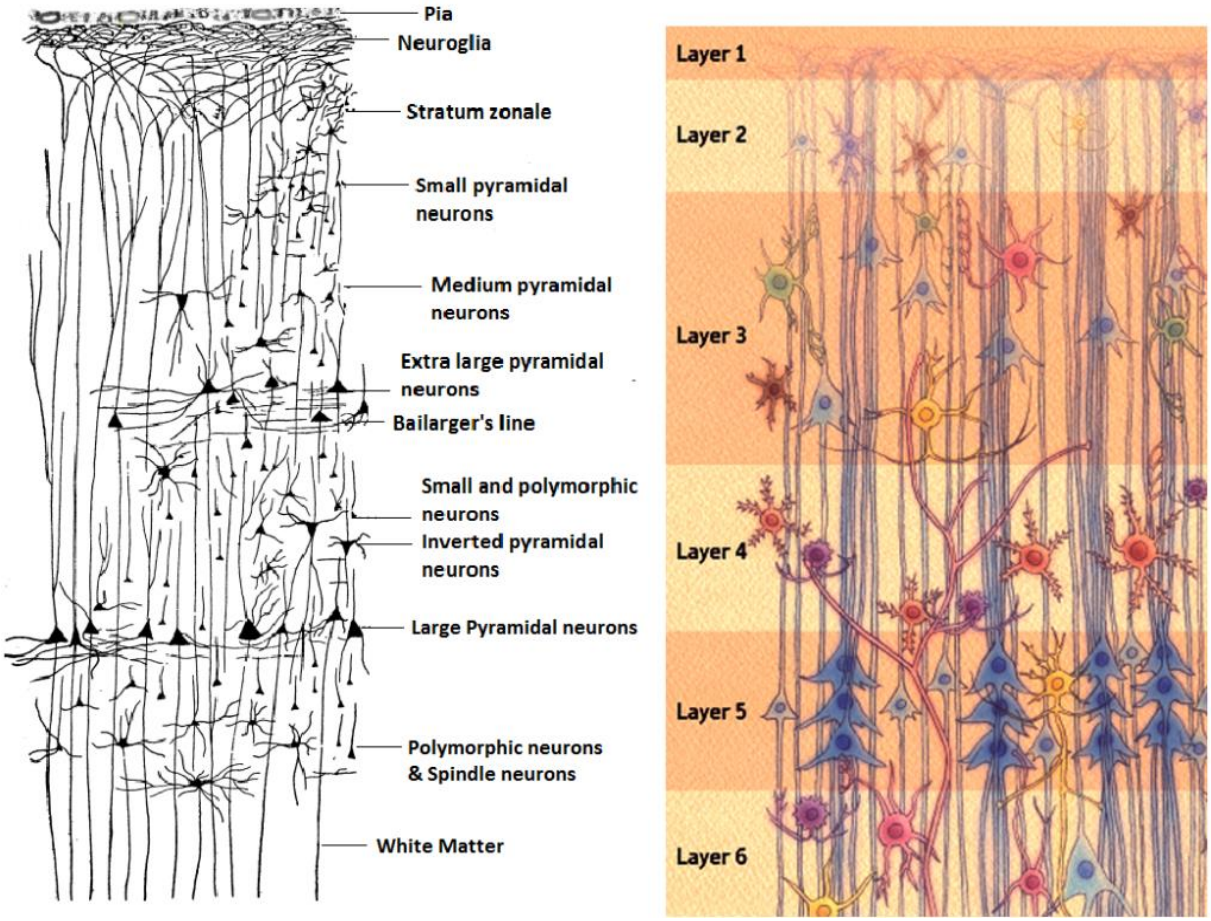

Fig. 9 The histological structure of the cerebral cortex with layers, [38].

Projection neurons are the main neurons which are the excitatory cells and many of them have the pyramidal cell body. These type of the neurons is located in layer 3, 5, 6 of the cortex. These neurons are very important for the transmission of the information from the one place to other place which is far from the original place, [9].

Local inter-neurons are the inhibitory cells which can be located in the each layer. These neurons create $20-25\%$ of the cortical neurons. Local inter-neurons can also transfer information but only among the neurons which are located in the same layer.

In the picture below, Fig. 10, there are showed the both type of the neurons through all the cortical layers. The red ones are the projection neurons and the black ones are local inter-neurons, [9].

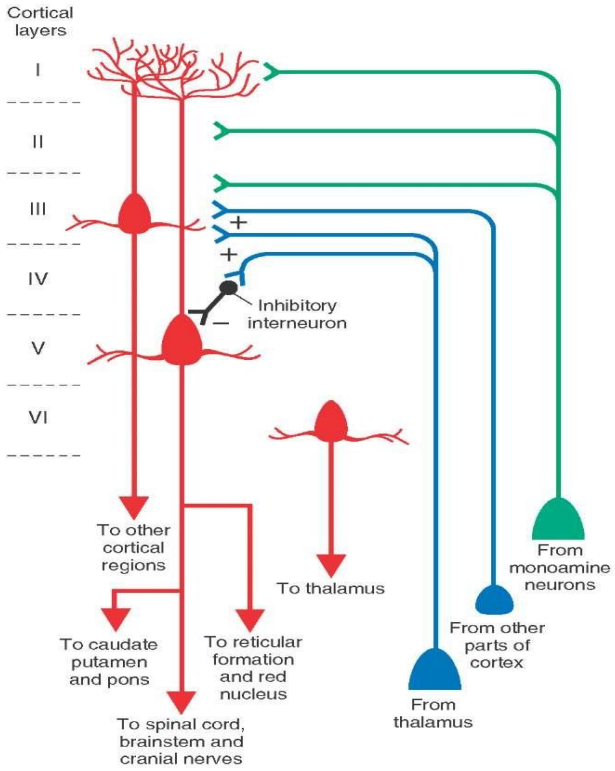

Fig. 10 The projection neurons and the local inter-neurons through all the cortical layers, [39].

4.2 Cortical columns

The neurons extend perpendicularly into the cortex and they are interconnected, so they create the cortical columns. This fact means if we start the stimulation then the same activity will be discovered in the whole layer.

Many of the cortical neurons bring their axons and dendrites from the surface of the cortex to the white matter and form anatomic structure of the cortical columns this way.

Nerve fibres mostly ends into the fourth layer where are connected with the stellate neurons. The stellate neurons, Fig. 11, lead their axons directly to the surface of the cortex and simultaneous parallel to the apical dendrites of the neighboring pyramidal neurons. Therefore the thalamocortical input is connected with the thin column of the pyramidal cells and because of this the same information is shared throughout the depth, [9].

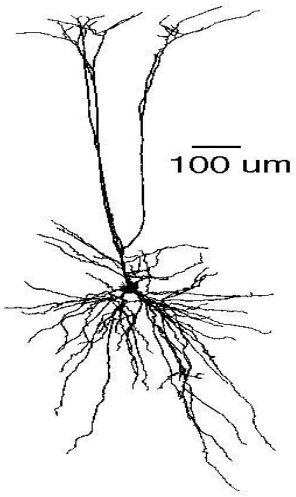

Fig. 11 The stellate neuron, [29].

This anatomic structure of the cortical columns was discovered by Vernon Benjamin Mountcastle in 1957. Professor Mountcastle performed experiments with electrodes and showed that neurons inside the cortical column exhibit the same activity and physiological unit *macrocolumns* was defined, Fig. 12, [9].

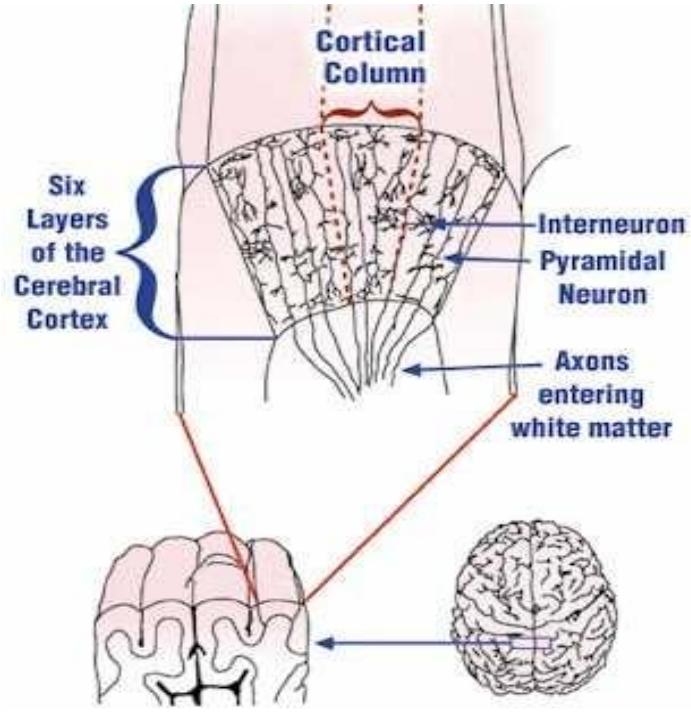

Fig. 12 The cortical column (macrocolumn), [27].

4.3 Structure of Jansen's single-column model

Jansen model represents the population of the pyramidal neurons which receives the feedback from the local inter-neurons located in the same column and the excitatory input from the other columns or the sub-cortical structures (for example as the thalamus). The scheme of Jansen model is represented below, Fig. 13.

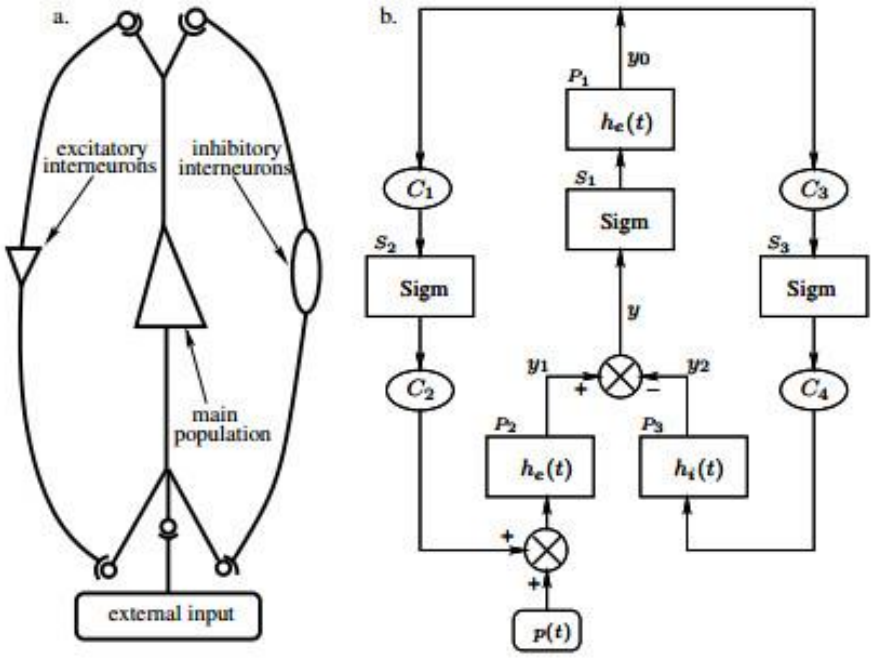

Fig. 13 Structure of Jansen a single-column model, [9].

The excitatory input can be represented by an average firing rate that can corresponds to a noise. In Fig. 13 the external input corresponds to the excitatory input and this input is marked as variable $p(t)$. According to the Fig. 13 Jansen model can be divided into the several parts, *boxes*, [9][16][5].

4.3.1 Post-synaptic block

This first box includes the blocks with the variables $h_e(t)$ and $h_i(t)$ for the excitatory and the inhibitory populations of the neurons. These blocks simulate synapses between the neurons populations. In this box the input is represented as the average value of the action potentials (the average firing rate of the pre-synaptic population). This input is converted into the average value of the post-synaptic potential through a second order differential linear transformation, (2), [9][16][5].

.

4.3.2 Sigmoid box

These boxes represent the cell bodies of the neurons and nonlinear transformation. This box transforms the average membrane potential of a neural population into an average firing rate. The function of the *Sigmoid* is introduced in the equation, (1).

$$Sigm(v) = \frac{2e_0}{1 + e^{r(v_0 - v)}} \tag{1}$$

The variable e_0 represents a half of the maximum firing rate of the neural populations, the variable v_0 represents the value of the potential for which a 50% firing rate is achieved and this variable can be understood as a firing threshold or as the excitability of the populations. The variable r represents the slope of the sigmoid at v_0. The curve of the sigmoid is symmetric about the point, v_0, e_0, Fig. 14.

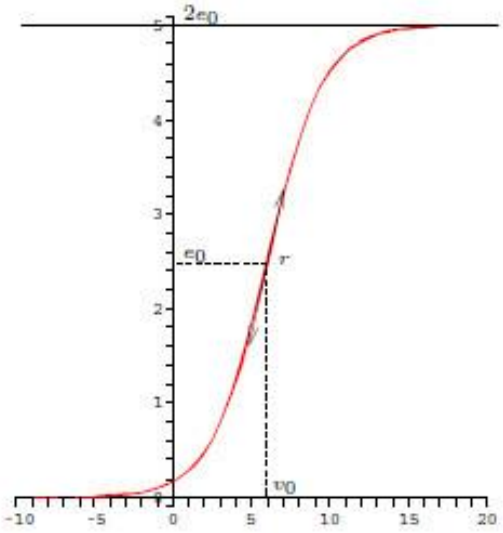

Fig. 14 Sigmoid graph, [9].

The shape of the sigmoid simulates characteristics of neurons. As long as the potential is under the excitable threshold neurons produce APs. The firing rate grows almost linear close the excitable threshold until saturation which is caused by the refractory period of neurons, [9][16][5].

4.3.3 Constants

Jansen model includes also constants C_i. These constants represent the power of the synaptic connection between populations so these constants indicate the number of synapses. The setting of these synapses is experimental and empirical but the strongest synapse is the first, C_1. For example the value of that constant for the simulation of alpha band is 135. Values of other constants are based on the strongest one, C_1, they are a proportional values of that constant, so second constant C_2 equals to 80% of $C_1$and constants C_3 and C_4 equal to 25% of C_1, [9][16][5].

4.4 Analytic description of Jansen's single-column model

The each post-synaptic block corresponds to solving differential equation, (2).

$$\ddot{y}(t) = Aax(t) - 2a\dot{y}(t) + a^2 y(t) \tag{2}$$

The variable A determines the maximal amplitude of the post-synaptic potential in the case of the excitatory population, in the case of the inhibitory population the parameter B is used instead of the parameter A. The variable a is a constant which represents a delay of the synaptic transmission in the case of the excitatory population, in the case of the inhibitory population the parameter b is used, [16][5]. The whole Jansen model can be described via three a second order differential equations, (3).

$$\ddot{y}_0(t) = AaSigm[y_1(t) - y_2(t)] - 2a\dot{y}_0(t) - a^2 y_0(t)$$

$$\ddot{y}_1(t) = Aa\{p(t) + C_2 Sigm[C_1 y_0(t)]\} - 2a\dot{y}_1(t) - a^2 y_1(t)$$

$$\ddot{y}_2(t) = Bb\{C_4 Sigm[C_3 y_0(t)]\} - 2b\dot{y}_2(t) - b^2 y_2(t) \tag{3}$$

The exact meaning of variables y_0, y_1, y_2 can be observed in Fig. 13.

4.5 Parameters setting for alpha activity in Jansen's single-column model

As it mentioned above, a single-column model was designed to simulate alpha activity. The setting of parameters should respect this fact. Parameters A, B, a, b have been set by Van Rotterdam. The overview of parameters setting is presented below, (4).

$$A = 3.25\ mV$$

$$B = 22\ mV$$

$$a = 100\ s^{-1}$$

$$b = 50\ s^{-1}$$

$$C_1 = 135$$

$$C_2 = 0.8C_1 = 108$$

$$C_3 = 0.25C_1 = 33.75$$

$$C_4 = O.25C_1 = 33.75 \quad \textbf{(4)}$$

As regards the remaining parameters, the variable v_0 can take different values because the excitability of cortical neurons can vary under the action of several substances. Because of the alpha activity simulation it is used $v_0 = 6\ mV$ suggested by Jansen.

It was suggested also $e_0 = 2.5\ s^{-1}$ and $r = 0.56\ mV^{-1}$ by Jansen and Rit. As the parameter $p(t)$ a white noise ranging from 120 to 320 pulses per second was used, it can be said that $120\ Hz$ is the lower limit and $320\ Hz$ is the upper limit of the range of a white noise.

The expected signals from a single-column model are introduced below. There are six two-seconds output signals where it is shown how the output from a single-column model is changing with a varying constants C_i, [9][16][5].

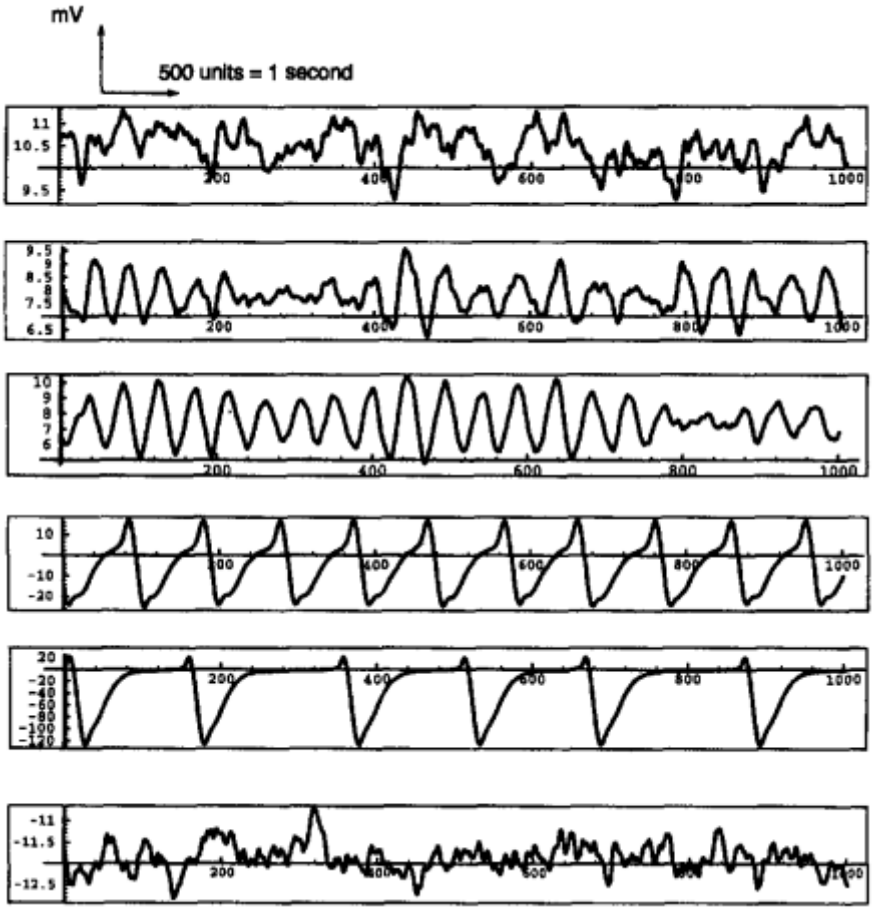

Fig. 15 Two-seconds output signals changing with a varying C_1 that equals 68, 128, 135, 270, 675, 1350 respectively, [16].

As it can be seen the first output from the top in Fig. 15 represents beta activity. With increasing C_1 the output is changing into alpha activity till the $C_1 = 135$. For cases $C_1 = 270$ and $C_1 = 675$ the output starts to move in the negative plane and for the last option $C_1 = 1350$ the output stays just in the negative plane and reminds beta activity, [9][16].

4.6 Structure of Jansen's double-column model

Jansen double-column model is an extension of Jansen single-column model. This type of Jansen model describes an interaction between two cortical columns. Each column is based on the same set of equations as the single-column model but the system of parameters is different for each column.

These two columns are connected into a loop where the each column is fed by two inputs. An external input can be different for each column, but in this case the external input is a white noise for both columns. Each column is also fed by output of the other column.

The double-column model extension includes two connectivity constants, K_1 and K_2. These constants are added into the loop before columns are fed by the other to attenuate the output of the column, [16].

The whole structure of Jansen double-column model is shown in the picture below, Fig. 16.

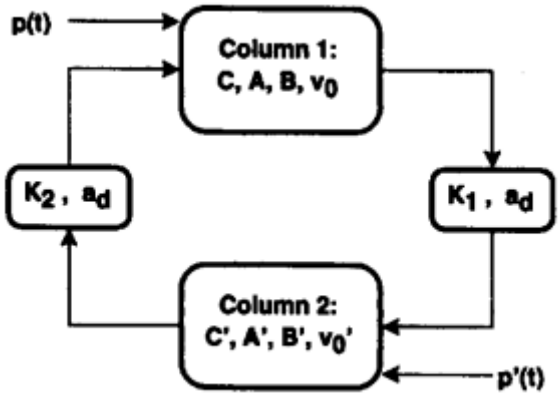

Fig. 16 Structure of Jansen double-column model, [16].

The aim of this extension was modeling situation where the one column may represent the visual cortex, while the second column models the prefrontal cortex. For the each cortical column we can assume the same cortical column model but situation with parameters system is different. In these cortical parts the structure of cells differs from one cortical area to the next. So each column will have the own parameters setting respecting the differences in cell structure.

The column representing the visual cortex was made to produce alpha activity. The prefrontal cortex was designed to generate beta activity.

As it can be observed in Fig. 16, there is the other important parameter, an intercolumn delay a_d. This parameter is related to delays connected with processing pathways of a visual stimulus by the prefrontal cortex and with the feedback to the occipital visual cortex. This delays are represented by linear transformation similar to the transformation used in the single-column model, $h_e(t)$ but with latency 3 times longer, $a_d \approx a/3$, [16].

4.7 Analytic description of Jansen's double-column model

The analytic description of this model will obtain twice as many variables as for a single-column model. In add there are variables describing the connection between column 1 and column 2. The set of equation is represented below:

$$\ddot{y}_0(t) = AaSigm[y_1(t) - y_2(t)] - 2a\dot{y}_0(t) - a^2 y_0(t)$$

$$\ddot{y}_1(t) = Aa\{p(t) + C_2 Sigm[C_1 y_0(t)] + K_2 y_{21}\} - 2a\dot{y}_1(t) - a^2 y_1(t)$$

$$\ddot{y}_2(t) = Bb\{C_4 Sigm[C_3 y_0(t)]\} - 2b\dot{y}_2(t) - b^2 y_2(t)$$

$$\ddot{y}_3(t) = A'aSigm[y_4(t) - y_5(t)] - 2a\dot{y}_3(t) - a^2 y_3(t)$$

$$\ddot{y}_4(t) = A'a\{p'(t) + C_2' Sigm[C_1' y_3(t)] + K_1 y_{12}\} - 2a\dot{y}_4(t) - a^2 y_4(t)$$

$$\ddot{y}_5(t) = B'b\{C_4' Sigm[C_3' y_3(t)]\} - 2b\dot{y}_5(t) - b^2 y_5(t)$$

$$\ddot{y}_{12}(t) = A'a_d Sigm[y_1(t) - y_2(t)] - 2a_d\dot{y}_{12}(t) - a^2 y_{12}$$

$$\ddot{y}_{21}(t) = A'a_d Sigm[y_4(t) - y_5(t)] - 2a_d\dot{y}_{21}(t) - a^2 y_{21}(t) \quad \textbf{(5)}$$

The first three variables, y_0, y_1, y_2, describe column 1, the next three variables, y_3, y_4, y_5, describe column 2. The last two variables, y_{12}, y_{21}, describe the connection between column 1 and column 2, [16].

4.8 Parameters setting for the spontaneous activity in Jansen's double-column model

In this section a simulation of the interaction between column 1 located in the visual cortex and column 2 located in the prefrontal cortex is described.

As it mentioned above, column 1 should simulate the visual cortex activity that means alpha activity. So the parameters setting will stay the same as in the single-column model case.

Column 2 is supposed to represent the prefrontal cortex activity that means beta activity. So the parameters setting are different.

The parameters setting was selected according to Jansen and Rit study variables that are different from the single-column model setting are introduced below, (6),[16][5].

$$A' = 3.25\ mV$$

$$B' = 17.6\ mV$$

$$C'_1 = 108$$

$$C'_2 = 86.4$$

$$C'_3 = 27$$

$$C'_4 = 27 \quad \textbf{(6)}$$

According to Jansen and Rit study, the connectivity constants, K_1 and K_2, were varied in the ranges. For the first one, K_1, it was between 0 and 8000 in steps increasing from 50 to 4000 units. For the second one, K_2, it was between 0 and 1500 in steps increasing from 100 to 500 units, [16]. The relationships between these two connectivity constants is shown below, Fig. 17.

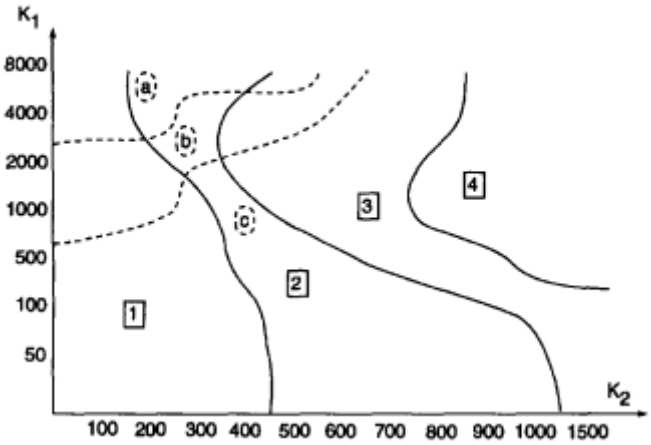

Fig. 17 Relationship between the connectivity constants, [16].

Picture Fig. 17 describes the relationship between the connectivity constants and its effect on the signals from the both columns. For example if the value of K_1 is between 0 and 500 units and value of K_2 is between 0 and 400 column 1 output will be alpha activity and column 2 output will be beta activity, [16]. Other combinations are shown below, Fig. 18.

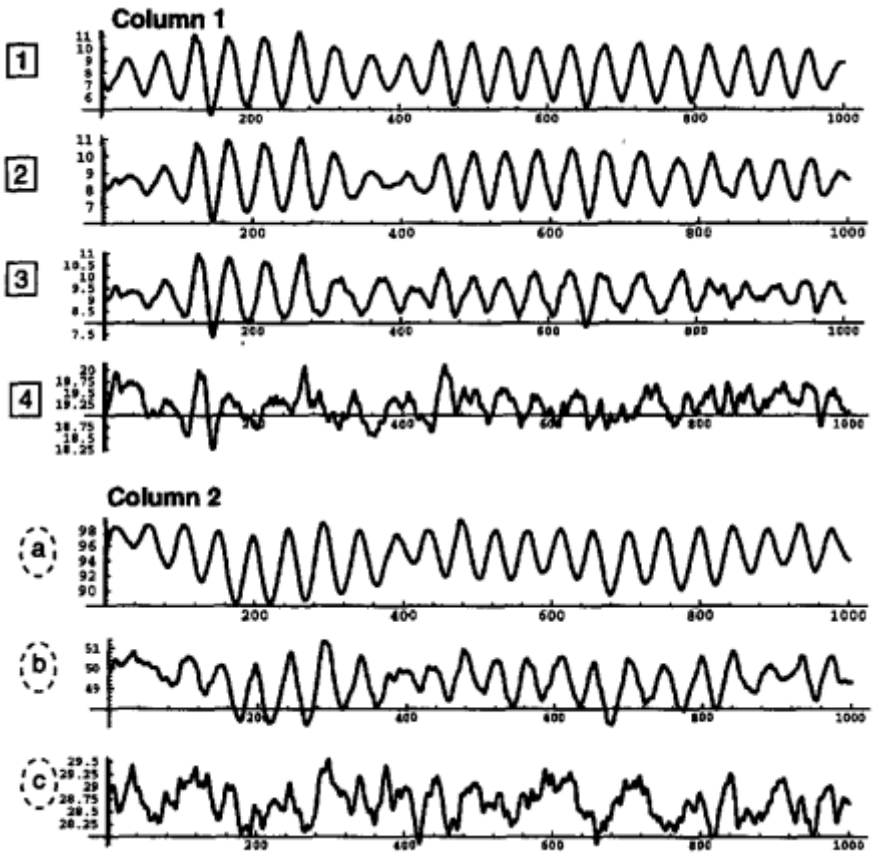

Fig. 18 Outputs from both column depending on the connectivity constants, [16].

The signals obtained from both Jansen's models were processed in practical part of this diploma. They were analysed and compared with real EEG-like signals, alpha and beta band. Also they were added to sponge experiments.

5 EEG ANALYSIS

The curve of the EEG recording is very complex and often vague. This curve changes in the time and very often in the EEG recording which is represented by this curve there are also recorded electric signals not from the brain but from the other physiological processes like winking, swallowing and change of the facial expression or from the technical device itself.

The EEG recording brings the information about the brain activity but the person who evaluates this recording should have lot of experiences in this field. In this complex group of curves we can distinguish a several basic elements called *graphoelements*. The most important graphoelement is the wave. The wave is the graphic recording and correspondents with the one electrical oscillation and has a several basic parameters, a frequency, the amplitude, a phase and a shape.

The frequency range is from $0.1\ Hz$ to $100\ Hz$, but ordinarily the upper limit is $70\ Hz$. This frequency spectrum is divided into the several bands, alpha, beta, delta and theta waves.

The amplitude characteristic is from $10\ \mu V$ to $1500\ \mu V$. The indicative range for alpha, theta and delta waves is divided into 3 bands. The first band is for the low amplitudes ($10-30\ \mu V$), the second one is for the medium amplitudes ($30-7\ \mu V$), the third band is for the high amplitudes (above $70\ \mu V$). For the beta waves the range of the amplitude characteristic is also divided into 3 bands, the first is for the low amplitudes (to $10\ \mu V$), the second is for the medium amplitudes ($10-25\ \mu V$) and the third is for the high amplitudes (above $25\ \mu V$), [8].

5.1 Artifacts

Artifacts are the biological phenomena which are not caused by the brain activity. Many types of the artifacts exist and can be divided to two categories based on their origin, [8]:

5.1.1 Biological

This group includes all of artifacts caused by the human activity, for example eyewink, muscle activity, perspiration, [8]. Typical example of the biological artifact is shown in the Fig. 14.

5.1.2 Technical

This group includes all other artifacts not caused by the human activity, for example a wrong electrode or a wrong shielding.

Artifacts are very unwanted because they complicate the assessment the EEG recording. So there exist a several methods for their filtering, [8].

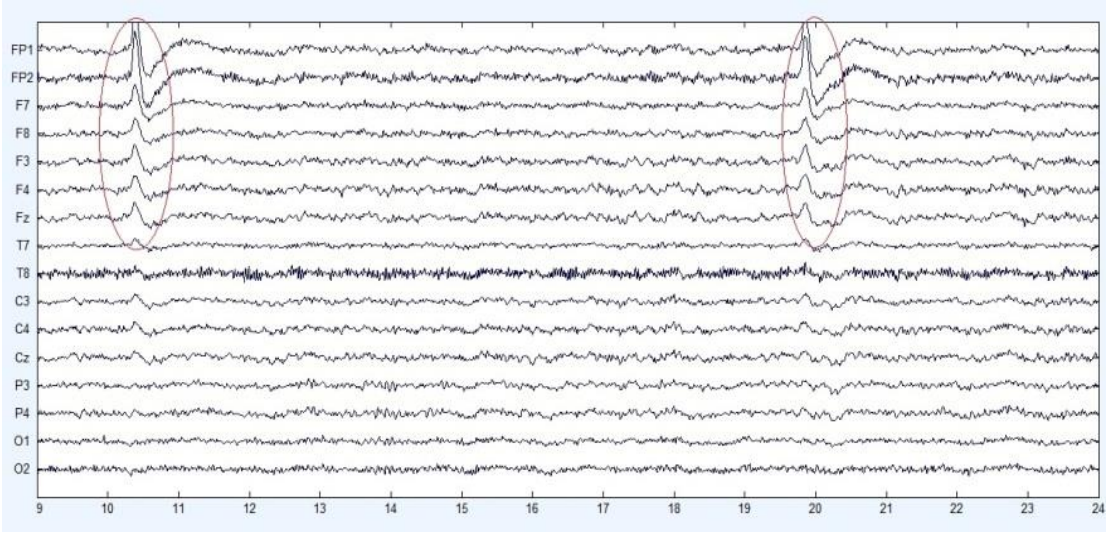

Fig. 19 The example of artifacts, eye blinking, [33].

5.2 EEG signal preprocessing

Main task of the preprocessing is the elimination of unwanted components which may occur in the EEG recording. During the measurement of brain activity artifacts can occur and there is a need to get rid of them directly during measurement or after the measurement, [8].

5.2.1 Elimination interference from the network (50 Hz)

In the EEG signal frequencies higher than $50\ Hz$ do not contain the important information so the most often method for elimination is a low-pass filtering which releases the low frequencies under $50\ Hz$.

This interference can be eliminated in the hardware by the wiring filter into the circuit or in the software by the subtracting $50\ Hz$ frequency from the EEG signal, [8].

5.2.2 Elimination fluctuation isoline

During the measurement the signal fluctuates and this is an unwanted phenomenon which can be eliminated by a highpass filtering with very low threshold frequency. The result will be subtracted from the original signal and the waveform remains steady, [8].

5.3 EEG signal processing

In the EEG signal processing there exist a several methods but the basic division is very simple. It can be divided into four main parts, time analysis, spectral analysis, brain mapping, time-frequency analysis.

5.3.1 Time analysis

This kind of the analysis we can use for monitoring the EEG signal in a time without any signal transformation. We can display and intensify some frequency spectrum and we can change a rendering speed.

Holter monitoring

This type of the monitoring takes 24 hours, Fig. 20. Holter recording contains the information about the brain activity and also about the heart activity (EEG and ECG measurements). Data from measurements are stored on the removable medium (smart card).

The evaluation and the analysis are performed after the completion of the measurement. This monitoring is very useful for the determination of phenomena that preceded an epileptic fit, [13].

Fig. 20 Holter EEG with ECG, [22].

5.3.2 Spectral analysis

This type of the analysis serves to the signal description via its frequency components. For the spectral analysis Fourier transform is used the most commonly.

Discrete Fourier Transform (DFT)

If the continuous periodic signal $f(t)$ is replaced by the chronological order (N samples) $f(nT)$ and if the sampling theorem is fulfilled, we can determine a matching set of N samples of the spectrum (7).

$$DFT\left(\frac{k}{NT_0}\right) = T_0 \sum_{n=0}^{N-1} f(nT_0) e^{-j\frac{2\pi kn}{N}} \ , k = 1,2, \dots, N-1 \tag{7}$$

The variable T_0 indicates a period of the sampling signal, k indicates the degree of the harmonic frequency spectrum, n indicates the serial number of the sample and N represents a set of signal samples, [8].

Fast Fourier Transform (FFT)

This type of Fourier Transform has a simpler calculation than the previous type so it is a less computationally demanding and the results of FFT and DFT are comparable. Let's X_0 to X_{N-1} be the complex numbers (8):

$$X_k = \sum_{n=0}^{N-1} x_n e^{\frac{2\pi i}{N} nk}, k = 0,1,2,\dots,N-1 \quad \textbf{(8)}$$

The transformation of the chosen part of the signal from the time domain to the frequency allows you to specify the exact number of waves in the frequency bands or specifies the frequency which is the most significant in the EEG recording, [8].

5.3.3 Brain mapping

This method is based on the mapping via Fourier Transform. Brain mapping uses a linear interpolation of the measured values. This topographic map shows the distribution of the brain activity. The generated graphic data are dependent on a several factors like the contact resistance of electrodes, Fig. 21, [42].

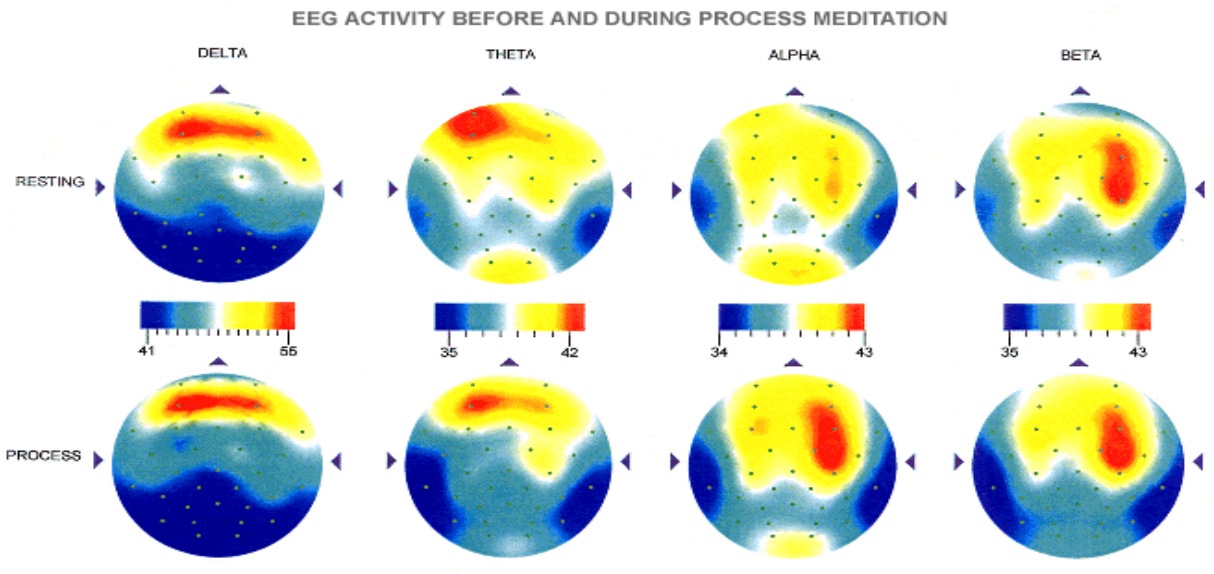

Fig. 21 The result of the brain mapping, [12].

5.3.4 Time-frequency analysis

EEG signals belong to the group of signals which have a transient nature. The analysis of these signals should consider the frequency content of each short periods of signal. In this case the spectrum is defined as a two-dimensional function (the first dimension is a time and the second one is a frequency).

Fourier Transform works with infinitely long signals. But in the practice the analysis is based on finitely long signal sections which are defined by the used window (window with the appropriate length and shape). This window should be moving along the timeline, [43].

Spectrogram

Spectrogram is a form of graphs and it is a time-dependent representation of the frequency spectral components. Spectrogram can represent an intensity of Short-Time Fourier Transform (STFT). STFT is a simple display sequence of Fast Fourier Transform (FFT) in time. Spectrogram could be shown as 2D image with the colour modulation (for example Fig. 22), but also as 3D image, [43].

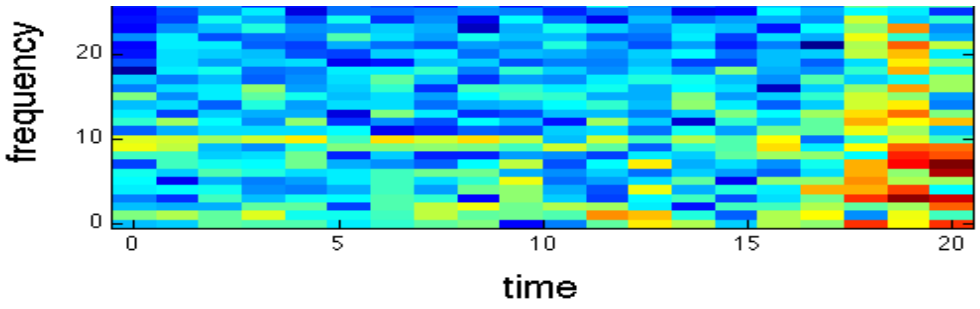

Fig. 22 The show of 2D spectrogram, [25].

This type of time-frequency analysis is often used and this analysis was used to the sponge experiments. Results of that analysis are represented in the practical part of that work.

6 SPONGE PHANTOM

Sponge phantom was developed in French laboratory Gipsa-lab in Grenoble to simulate a signal propagation in a brain environment during the acquisition signals. Sponge phantom is implemented into the system that consists of several parts that are introduced in this section, [23][24]. The scheme of this measuring system is shown below in Fig. 23. The sponge experiments and their results are shown in the practical part of that work.

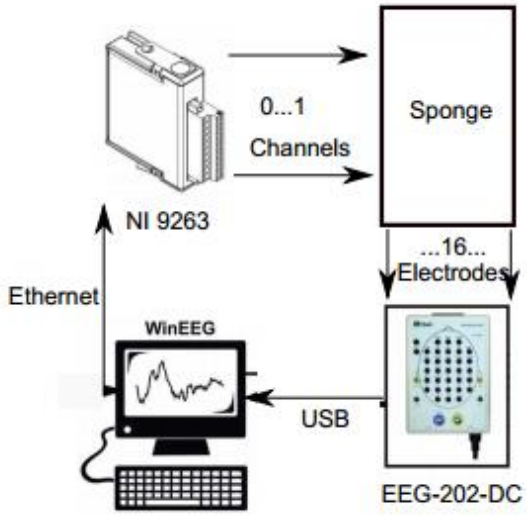

Fig. 23 The scheme of connection of the sponge experiments, [23][24].

6.1 WinEEG

WinEEG software has a two main functions. At first, this software was invented to record data. As it can be seen in Fig. 23, the output signals from the sponge are connected by a USB lead to PC where they can be recorded by this software. Secondly, this software is able to generate signals programmed in Python language. That fact was very useful for this diploma because signals of Jansen's model could be used as the inputs in the sponge experiment as well as simpler signals for verification of the system design., [23][24].

6.2 Data acquisition NI 9263

Data acquisition NI 9263 is a part of measuring system that connects a PC station with the sponge. It sends the inputs from a PC station, from WinEEG software, directly to the sponge, [23][24].

6.3 Sponge

Sponge with dimension 10.5 x 15.5 cm represents a medium that simulates the signal propagation in the brain. This sponge is filled by a phosphate buffer saline solution, PBS, in order to simulate the signal propagation in a brain as accurately as possible. The inputs are connected into the sponge by channels of NI 9263 and also the outputs are connected from sponge to the next part of this system EEG-202 DC, [23][24].

6.4 Mitsar EEG-202 DC

The outputs of this systems are conducted from the sponge by electrodes to Mitsar EEG-202 DC where they are amplified. So Mitsar EEG-202 DC is a DC amplifier that leads the amplified outputs from sponge to a PC station where the outputs can be recorded by WinEEG software, [23][24].

The real pictures of this system with all components are shown below. In Fig. 24 we can see almost all components of the measuring system.

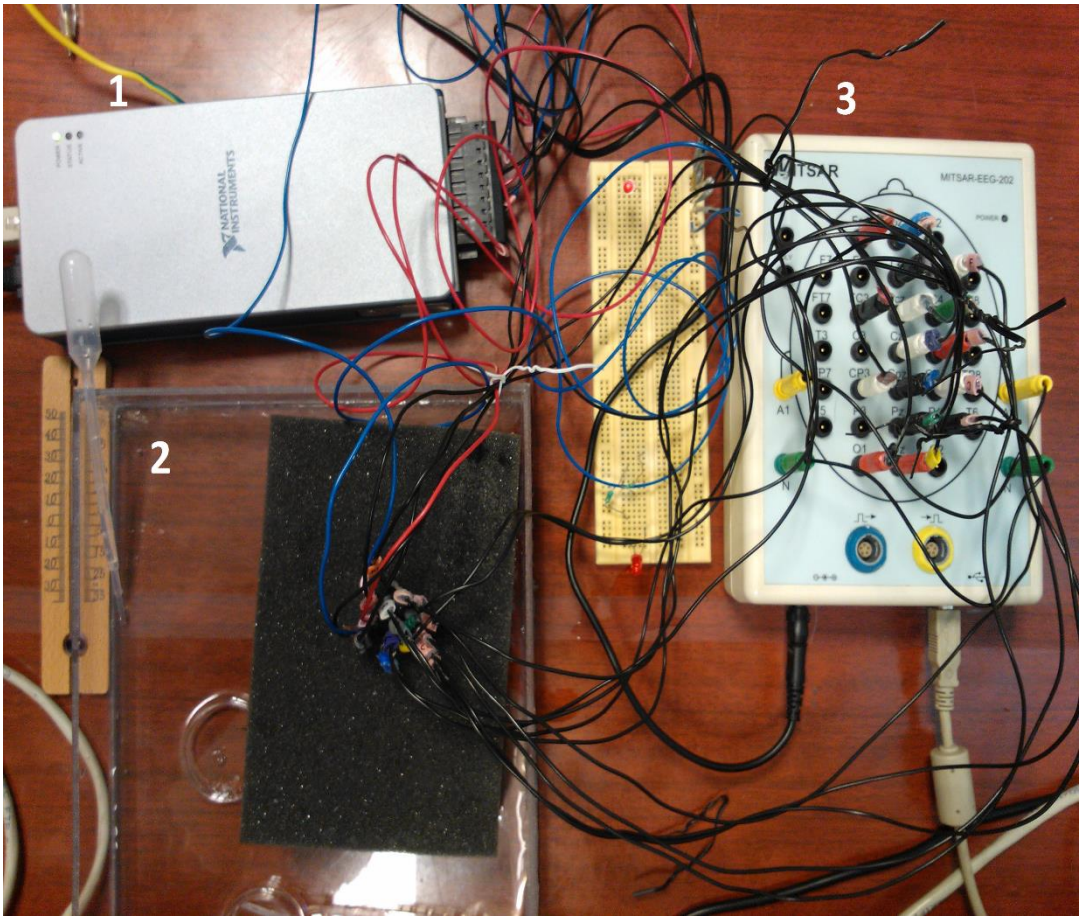

Fig. 24 The measuring system including the sponge phantom, 1 is NI 9263, 2 is sponge phantom and 3 is Mitsar amplifier.

In Fig. 25 there is another picture of the same system including a PC station.

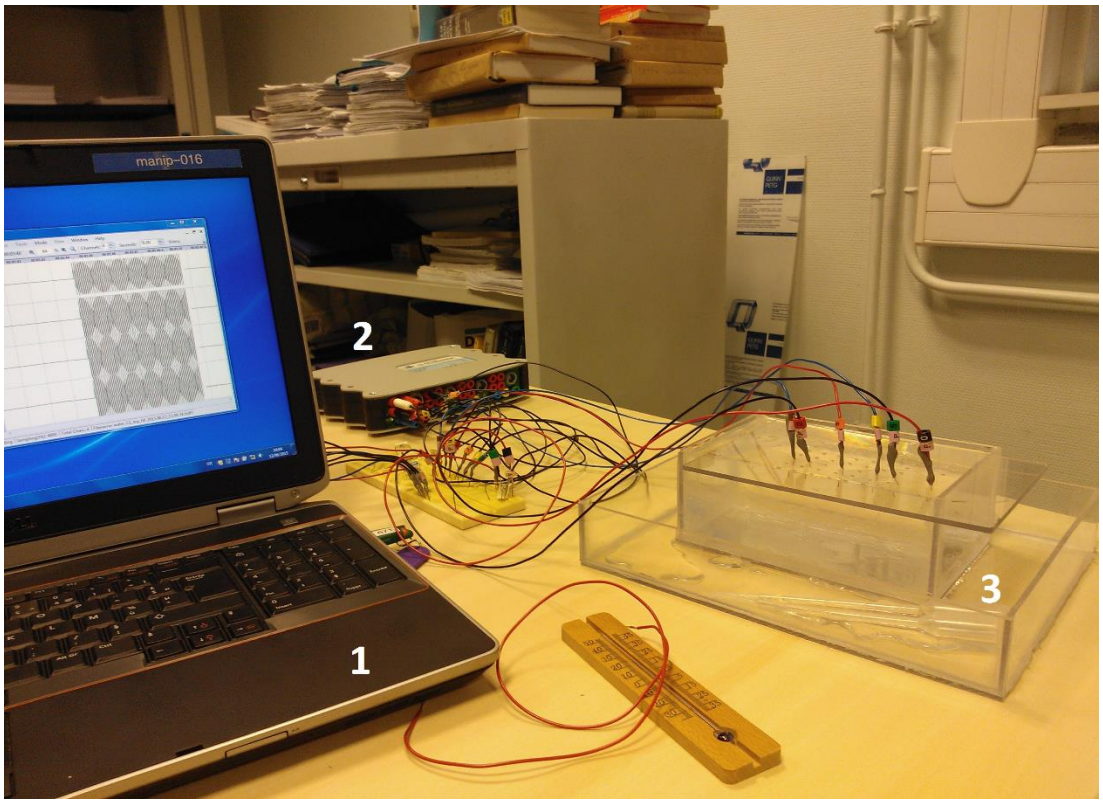

Fig. 25 The real picture of the measuring system with a PC station, 1 is a PC station with WinEEG software, 2 is NI 9263 and 3 is the sponge phantom.

7 IDENTIFICATION OF PARAMETERS OF SPONGE EXPERIMENTS

Sponge model was used like a measuring system for many experiments. The identification of model parameters was based on these experiments and results of these experiments are the main tasks of that work and they are introduced and evaluated in practical part.

Signals used in the sponge experiments contain containing three parts was used as inputs. Each part was useful for identification of different parameters.

The first part was called *spectroscopy*. This part was composed of 13 sinusoid trials, each of them with different frequency. This part served for an estimation of a complex gain and a phase.

The second part was a *step function* and response on this function served for an estimation of a time constant.

The last part included a *white noise*. This part was used in *Ident* toolbox, [37], and it served for a transfer function estimation.

The signal of lowpass filter is introduced below in Fig. 26. The red one is the input signal and the green one is the output signal. All three parts can be seen, *spectroscopy*, *step function* and *white noise* respectively.

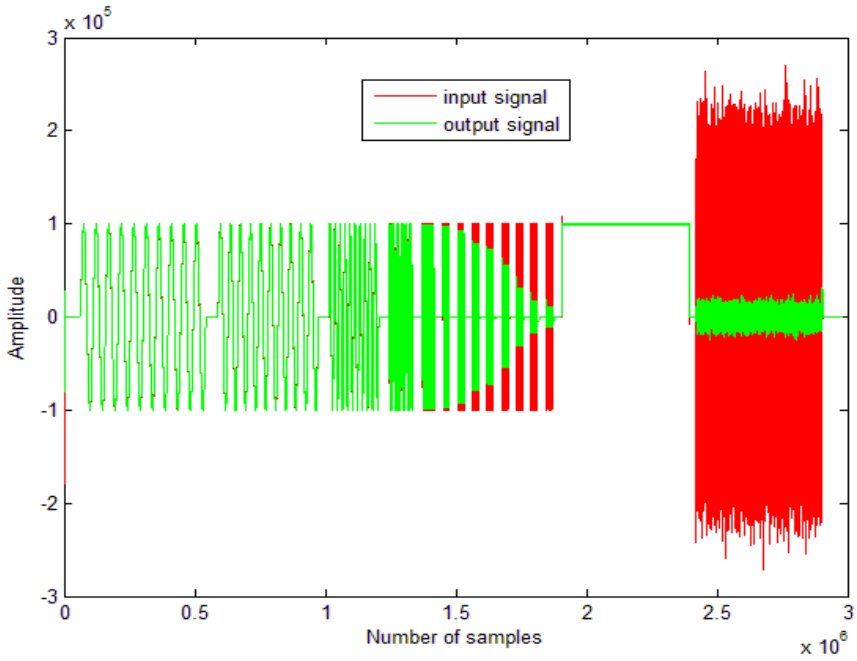

Fig. 26 The signal used in the sponge experiments simulating lowpass filter with three experimental parts, (loading.m).

7.1 Estimation of the complex gain and the phase

The first step was a development of own function called *spectro_tfe* that should compute the complex gain and the phase from the spectroscopy part.

Own function had several parameters, x_1, x_2, f_0, f_s. The parameter x_1 is the input sinusoid or signal, x_2 is the output sinusoid or signal, f_0 is the frequency of the sinusoid and f_s is the sampling frequency. The output parameters will be g and ϕ. The output g is the absolute value of the complex gain at f_0 and ϕ is the argument of the complex gain at f_0.

As a foundation of own function the equation for the complex gain was used. The equation for the complex gain G at one frequency of the sinusoid f_0 is represented below, (9).

$$G(f_0) = \frac{X_2(f_0)}{X_1(f_0)} \tag{9}$$

The parameter X_2 represents the Fourier transform of x_2, the output sinusoid or signal, the parameter X_1 is the Fourier transform of x_1, the input sinusoid or signal. Then parameters g and ϕ are estimated according to equation below, (10).

$$g(f_0) = |G(f_0)|$$

$$\phi(f_0) = \arg(G(f_0)) \tag{10}$$

The test of validation of *spectro_tfe* function was done in order to ensure the usefulness and accuracy of this function.

The test of *spectro_tfe* should include a comparison between two sinusoid signals, the first one should have a zero phase and the second one should have a varying phase.

After this validation the function *spectro_tfe* was applied to the experimental signals that corresponded to character of allpass, lowpass and highpass filters, simple ones as well as more complicated experimental signals, [4][28][40].

7.2 Estimation of the time constant

For this estimation the part of signal corresponding to the response of the step function was used.

For lowpass filter the time constant estimation is based on the equation for a transient response. The time constant estimation, τ, is shown below in Eq. (11).

$$h(t) = 1 - e^{\frac{t}{\tau}}$$

$$h(\tau) = 1 - e^{-1}$$

$$h(\tau) \approx 0.63 \tag{11}$$

So the time constant value corresponds to 63% of the step response.

For highpass filter the transient response is important too. The time constant estimation is similar as in the previous case, (12).

$$h(t) = e^{\frac{t}{\tau}}$$

$$h(\tau) = e^{-1}$$

$$h(\tau) \approx 0.37 \tag{12}$$

The time constant value for highpass filter corresponds to 37% of the step response.

For allpass filter the step response should be the same as for a step function so the time constant from this type of filter isn't defined, [3][18].

7.3 Estimation of the signal spectrum

In this section the *Ident* toolbox was used. The signal spectrums were estimated again but now not from the *spectroscopy* part but from the third signal part, a white noise part. Results from this section are comparable with results from the *spectro_tfe* application.

In addition, in the spectrum of simple experimental filters the cutting frequency can be observed. The expected value of the cutting frequency can be determined too to compare with the observed value of the cutting frequency, [4].

7.4 Estimation of the transfer function model

The main aim of this section was the find the parameters of a continuous transfer function model for allpass filter, lowpass filter, highpass filter using by Identification Toolbox and then these results should be compare with the theoretical equations defining the transfer functions for allpass, lowpass and highpass filters.

For modelling of filters the most suitable model structure for this process was ARX model structure, (13). The structure of the ARX model is sufficient for this simple model, [4] [35][36].

$$A(q)y(t) = B(q)u(t - n_k) + e(t)$$

$$A(q) = 1 + a_1 q^{-1} + \cdots + a_{n_a} q^{-n_a}$$

$$B(q) = b_1 + b_2 q^{-1} + \cdots + b_{n_b} q^{-n_b+1} \quad \textbf{(13)}$$

Where n_a corresponds to a number of poles, n_b corresponds to a number of zeros, n_k represents a delay and $e(t)$ is a white noise part, [4][35][36].

Because of comparing the results with theoretical assumption of the theoretical Fourier equations of the gain for allpass, lowpass and highpass filter in a function of the resistance R and the capacity C of components used in the filters are represented. This step is very important because it leads to define the ration of the output and input voltage. The ratio of the out and the input voltage corresponds to the transfer of the measured system. This estimated transfer (transfer function) was compared to the theoretical assumption of the Fourier equations and conclusions of that comparison are introduced in the practical part.

For the imagination a behaviour of integration and derivative circuits are described. The integration circuit, lowpass filter, is shown in Fig. 27.

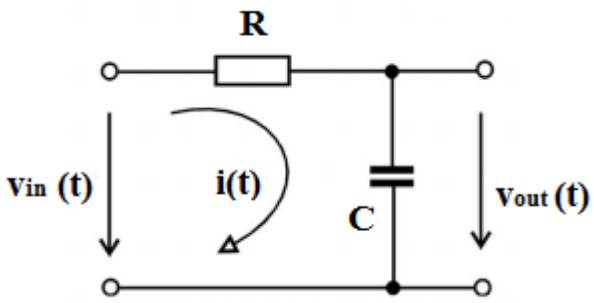

Fig. 27 Scheme for the integration circuit, lowpass filter, [20].

The input and the output voltage can be expressed by equation below, (14), [3][26][41].

$$v_{in}(t) = Ri(t) + \frac{q(t)}{C} = Ri(t) + \frac{1}{C}\int_0^t i(u)du$$

$$v_{out}(t) = \frac{q(t)}{C} = \frac{1}{C}\int_0^t i(u)du \tag{14}$$

Using Laplace Transform we get equations, (15):

$$V_{in}(s) = RI(s) + \frac{1}{Cs}I(s) = (R + \frac{1}{Cs})I(s)$$

$$V_{out}(s) = \frac{1}{Cs}I(s) \tag{15}$$

This type of filter divides a voltage in a ratio of the output voltage, v_{out}, and the input voltage, v_{in}. This ration is called a transfer, Eq. (16).

$$\frac{V_{out}}{V_{in}} = \frac{\frac{1}{Cs}}{R + \frac{1}{Cs}} = \frac{1}{RCs + 1} \tag{16}$$

The derivative circuit, highpass filter, contains the resistor and the capacity too, but its scheme is represented in Fig. 28.

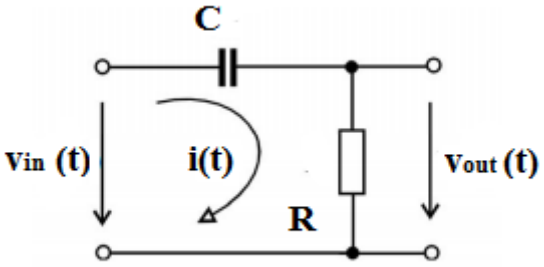

Fig. 28 Scheme for the derivative circuit, highpass filter, [20].

The output voltage can be defined according to equation below, (17), [3][26][41].

$$v_{in}(t) = \frac{q(t)}{C} + Ri(t) = \frac{1}{C}\int_0^t i(u)du + Ri(t)$$

$$v_{out}(t) = Ri(t) \tag{17}$$

Then after Laplace transform equations are represented below, (18).

$$V_{in}(s) = \frac{1}{Cs}I(s) + RI(s) = (R + \frac{1}{Cs})I(s)$$

$$V_{out}(s) = RI(s) \tag{18}$$

The transfer ratio for this circuit is described below, (19).

$$\frac{V_{out}}{V_{in}} = \frac{R}{R + \frac{1}{Cs}} = \frac{RCs}{RCs + 1} \tag{19}$$

After a numerical substitution the transfer function model for allpass, lowpass and highpass filter was received.

8 RESULTS OF JANSEN'S MODELS

In this section the practical part of that work begins. Own program of Jansen's single-column and double-column models is introduced here and the output signals are compared to the expected ones.

8.1 Jansen's single-column model

This basic Jansen's mathematical model (described in previous chapters) was implemented in Simulink in MATLAB. The structure of this model was created according to set of equations mentioned in the theoretical part where the detailed scheme of this model is mentioned too, Fig. 13.

The expected signals of this model are shown in Fig. 15 and for comparison the results of the own implemented model are introduced below in Fig. 29.

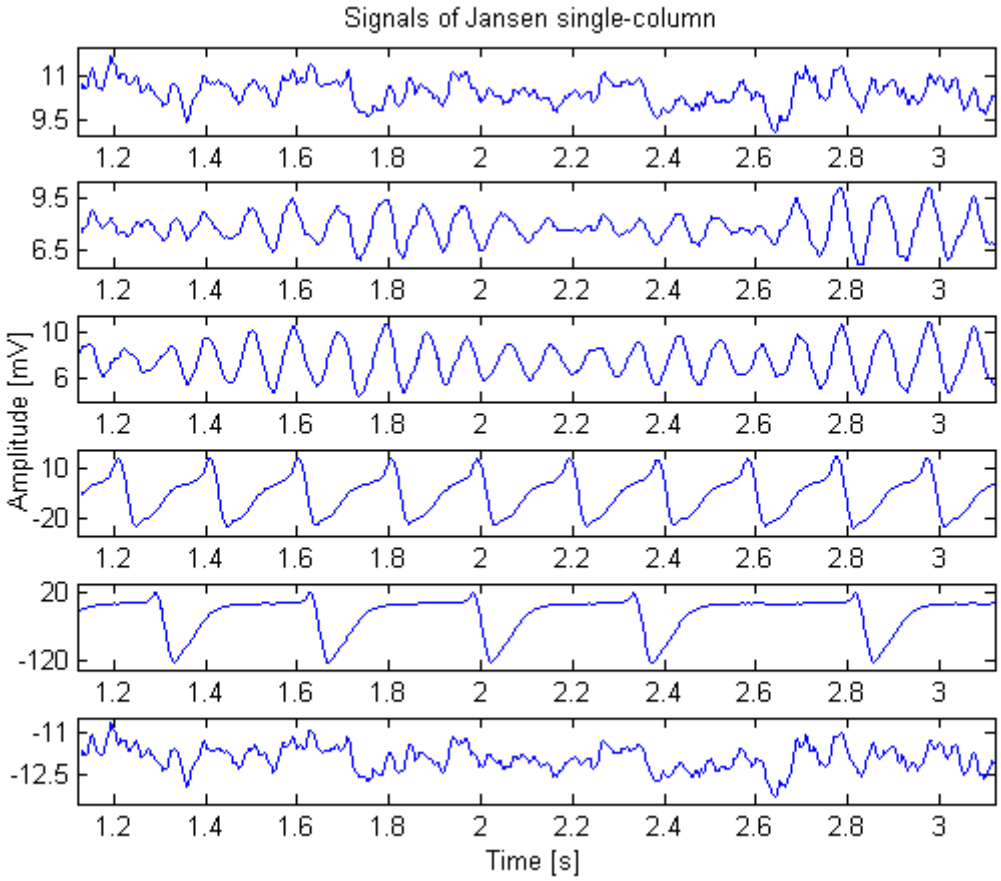

Fig. 29 Two-seconds output signals simulated in MATLAB with a varying C_1 that equals 68, 128, 135, 270, 675, 1350 respectively, (plot _single_column _model.m).

After comparison with the expected signals shown in Fig. 15 it can be observed that simulated signals are the same as the expected one. Beta activity was received for the low values of constant $C_1 = 68,128$ and for the highest value of constant $C_1 = 1350$. Alpha activity was received for the value of constant $C_1 = 135$. For the valid comparison the two seconds signals were simulated.

8.2 Jansen's double-column model

This model was the extension of the previous one. As it introduced in the theoretical part the extension was about addiction of two main variables, connectivity constants K_1, K_2 and delay a_d. The structure of this model was based on the set of the second order differential equation mentioned in the theoretical part, (5). The basic scheme of this model is shown below, Fig. 30. In this scheme all variables can be observed.

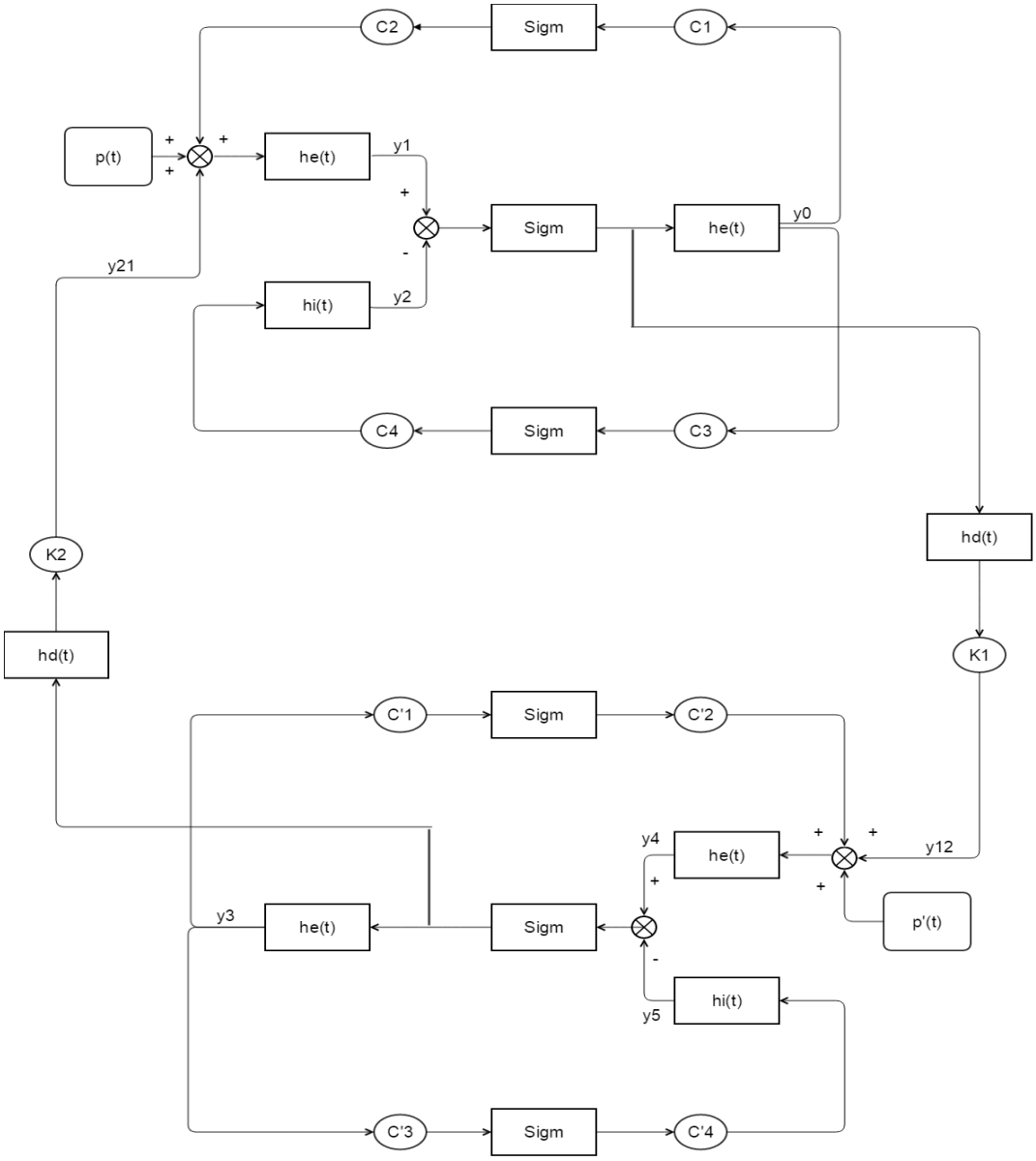

Fig. 30 Scheme of the double-column model.

Two signal were chosen for comparison with the expected signals and also for performing of sponge experiments. The first one is signal representing alpha activity in column 1 and beta activity in column 2. The connectivity constants were chosen in the range according to relationship of the connectivity constants shown in Fig. 17. The value of K_1 is 50 and the value of K_2 is 500 and the results are shown in Fig. 31.

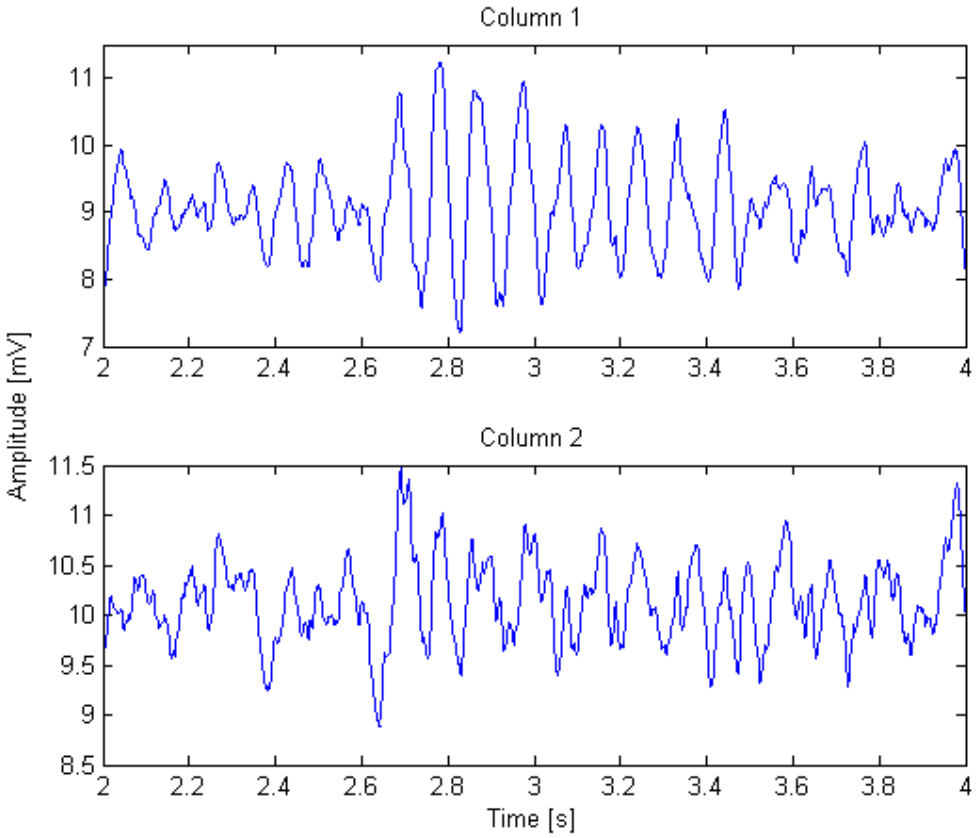

Fig. 31 Jansen signals representing alpha and beta activity, $K_1 = 50, K_2 = 500$, (plot_double_column_model.m).

The second signal was chosen to simulate alpha activity in both columns. So the value of K_1 is 7000 and K_2 is 10. The range of values of the connectivity constants was determined based on Fig. 17 where alpha activity is represented by the area 1 in column 1 and by the area a in column 2.

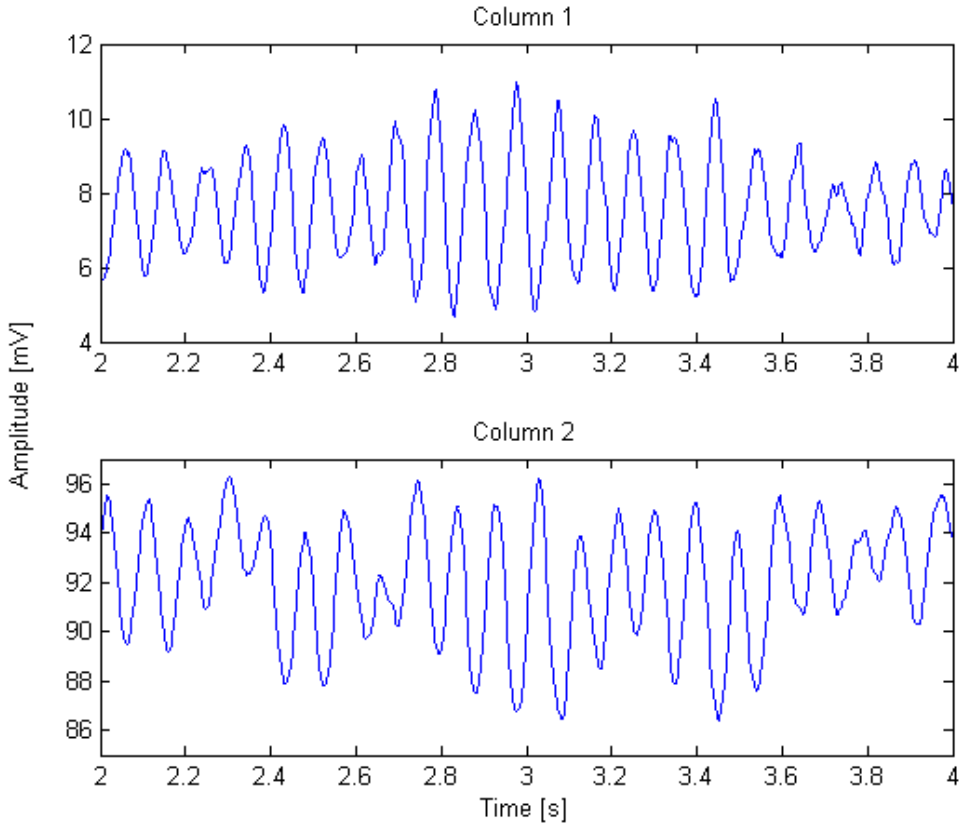

Fig. 32 Jansen signals representing alpha activity, $K_1 = 7000, K_2 = 10$, (plot_double_column_model.m).

Both signals from Jansen's double-column model were used to the time-frequency analysis. Their spectrograms were compared with the spectrograms of the real signals of alpha and beta activity.

8.3 Spectrograms of the real EEG-like signals and Jansen's signals

The time-frequency analysis was applied to both type of signals, the real ones and the simulated ones. The real signals were acquired from the online database *PhysioNet*, [34]. The signals corresponding to alpha and beta band were chosen and were resampled at the same sampling frequency as the simulated signals for the valid comparison.

Spectrograms are introduced below. For the spectrogram estimation the DTFT (Discrete Time Fourier Transform) algorithm was used with the Kaiser window with the length of 500 samples and overlap of 475 samples.

In Fig. 33 the spectrogram of the real signals are introduced and it can be observed both for alpha and beta activity. The spectrogram shows the highest power in the range of 8 Hz to 13 Hz for the alpha band and in the range of 13 Hz to 40 Hz for the beta band. The spectrogram of alpha activity shows significant frequency till 100 Hz. The range of alpha activity can be observed but the significant frequency can be found even for beta activity in this spectrogram. This fact is caused by a noise in these real signals. For the better spectrogram results some filtering method against a noise should be used and probably some sophisticated method for the better resolution of frequency bands should be used too.

The spectrogram of beta activity shows significant frequency almost till 100 Hz as the previous one, but the power of these frequencies is less than the power of frequencies from the previous spectrogram of alpha activity. It can be noticed that the frequency band of beta activity is present in this spectrogram but the frequency band of alpha activity can be observed here too. There are the same problems as in the previous case, additional noise and bad resolution of the frequency bands.

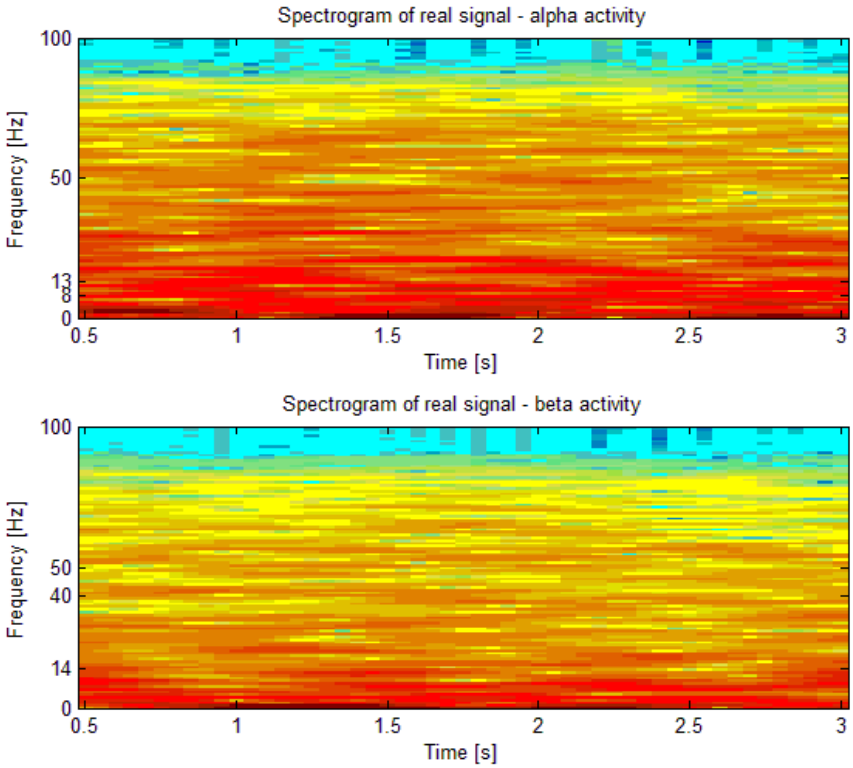

Fig. 33 Spectrogram of the real signals, alpha and beta activity, (plot_spectrogram_real.m).

Next spectrogram belongs to the simulated signal of Jansen's single-column model, alpha activity. In Fig. 34 the spectrogram corresponds to the theoretical idea and the frequency band typical for alpha activity is present. The simulated signals are not affected by a noise as the real ones and also other frequency components are not so significant as other frequency components in the real signals.

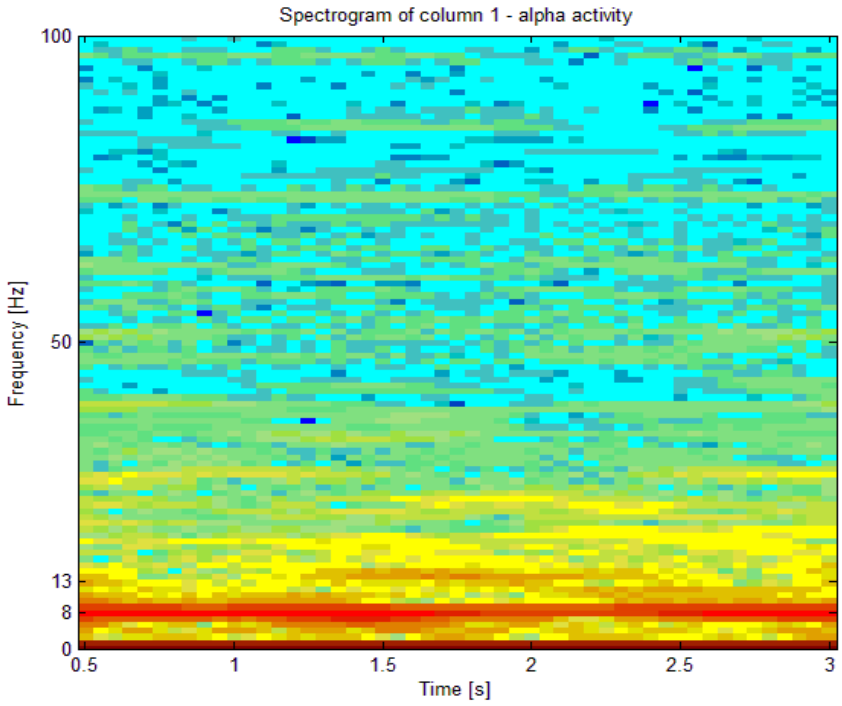

Fig. 34 Spectrogram of Jansen's single-column signal, alpha activity, (plot_spectrograms.m).

Finally the spectrograms were applied to the signals from Jansen's double-column model. Two signals were used, the first one should simulate alpha activity in the first column and beta activity in the second column, the second signal should simulate alpha activity in both columns.

In Fig. 35 the spectrogram shows significant frequency components correspond to alpha band, the expressive line can be seen in the range of 8 Hz to 13 Hz. The frequency components of beta band activity are present too but they do not have such as high intensities as the frequencies typical for alpha band.

The spectrogram of beta activity shows different situation. Overall the significant frequencies have less power than the frequencies in the previous case. So there are significant frequencies representing beta activity. The significant frequencies corresponding to alpha activity can be observed in the spectrogram of beta activity too but they do not have as high intensities as frequencies in the spectrogram of alpha activity.

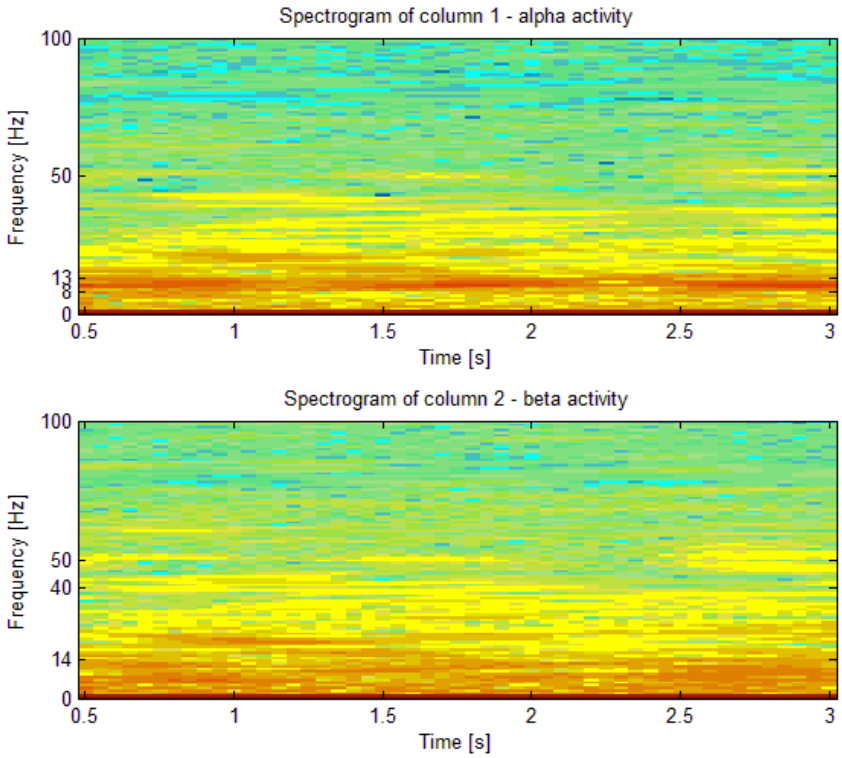

Fig. 35 Spectrogram of Jansen's double-column signals, alpha and beta activity, (plot_spectrograms.m).

The last spectrogram shows the spectrum of the signals representing alpha activity in both columns. The spectrograms introduced in Fig. 36 report the theoretical assumption that the frequencies corresponding to alpha activity should be present in this spectrum. In spectrograms of both columns that fact is obvious, the frequency range of alpha activity is present.

These signals describe the spectrum of alpha activity in the best way.

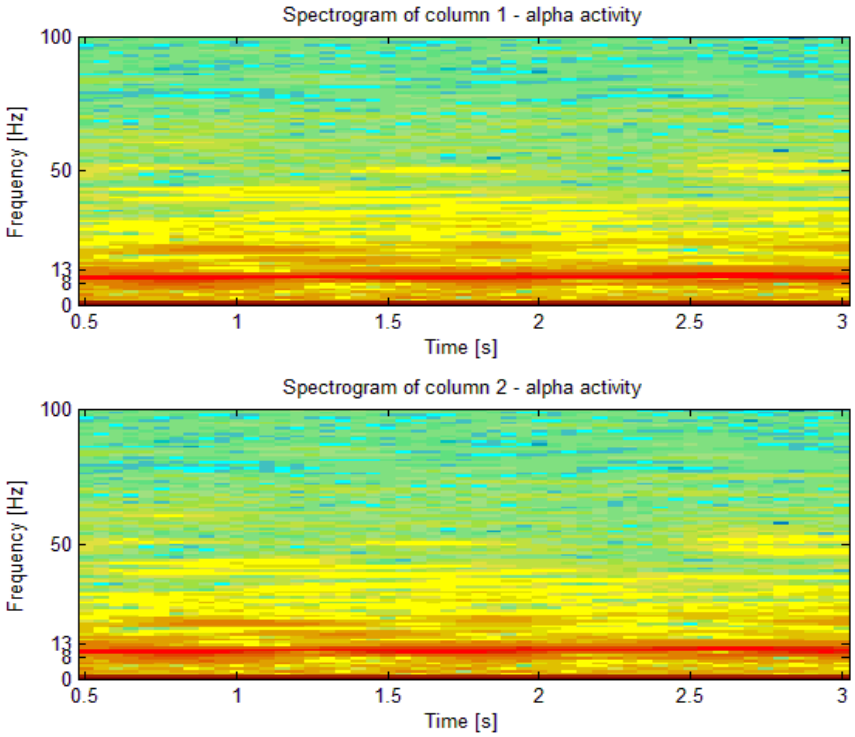

Fig. 36 Spectrogram of Jansen's double-column signals, alpha activity in both columns, (plot_spectrograms.m).

Signals from Jansen's model that have been represented in this section are used for next experiments with the sponge phantom.

9 RESULTS OF THE SPONGE EXPERIMENTS

In this section the results from sponge experiments are introduced. In these experiments the signals with three parts, *spectroscopy*, *step function* and *white noise*, were used as the input signals.

Results of the complex gain and the phase estimation, from the time constant estimation, from the signal spectrum estimation and from the transfer function estimation are presented.

Firstly, results of simple experiments corresponds to basic filters, allpass, lowpass and highpass filters are introduced.

Secondly, results of more complicated experimental signals are described. These signals are more addicted to the electrode setting.

9.1 Signals representing allpass, lowpass and highpass filters

Firstly, simple signals were used for these experiments. The input was still the same but because of varying conditions of measurements the allpass, lowpass and highpass filter were received as outputs. Settings of experimental signals are mentioned below, allpass Fig. 37, lowpass Fig. 38, highpass Fig. 39.

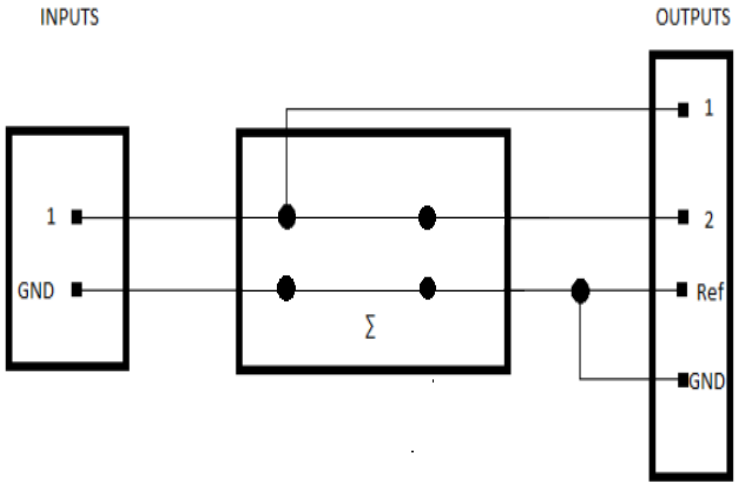

Fig. 37 The scheme of the system wiring for allpass filter.

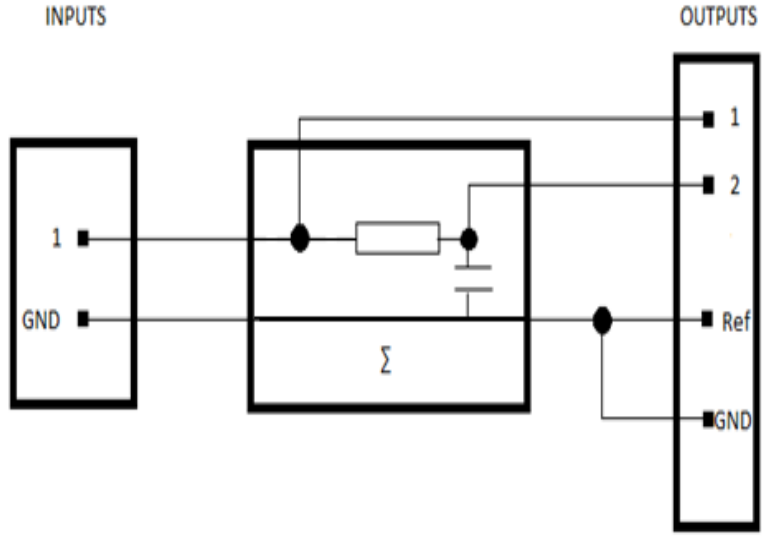

Fig. 38 The scheme of the system wiring for lowpass filter.

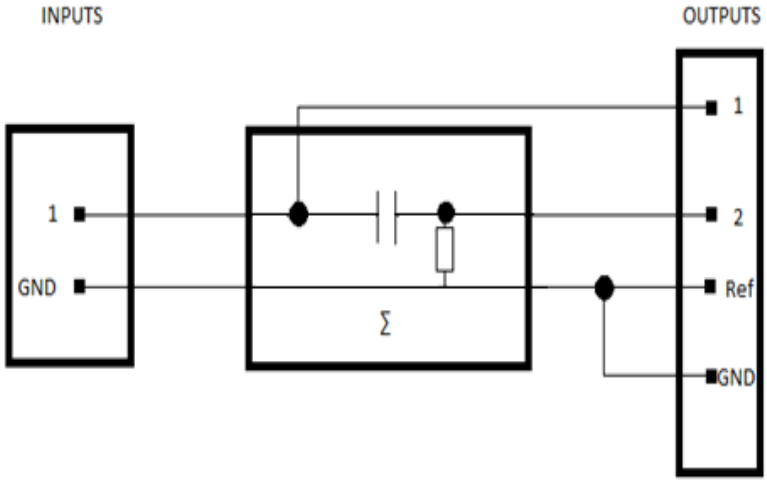

Fig. 39 The scheme of the system wiring for highpass filter.

Before applying the own function *spectro_tfe* to these signals the validation of this function should be performed.

9.2 Signals addicted to the electrode setting

In this section results of more complex experimental signals are represented. These signals are addicted to the electrode setting. In total three types of the electrode settings were used and they were described as S_1 in Fig. 40, as S_2 in Fig. 41 and as BIP (bipolar electrode setting) in Fig. 42, according to schemes below. Signals obtain two inputs and two outputs. Inputs are the sine waves with the same phase but mutually reversed with the different amplitudes. That is the reason why the frequency characteristic of each signal is estimated only for input 1.

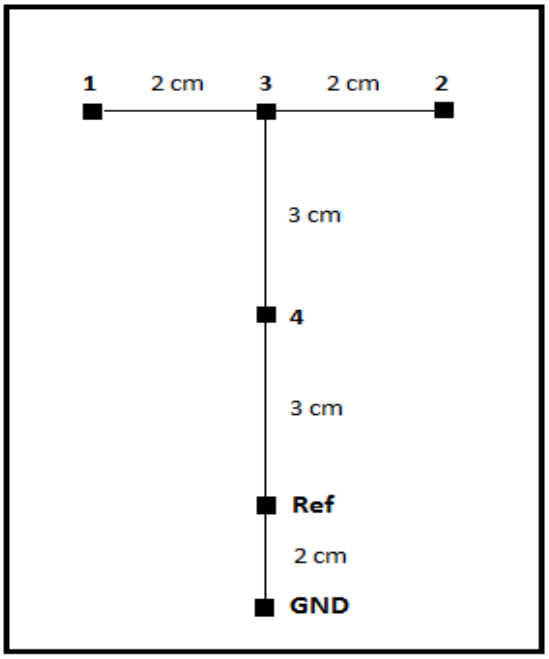

Fig. 40 Electrode setting with output middle line, S_1 setting.

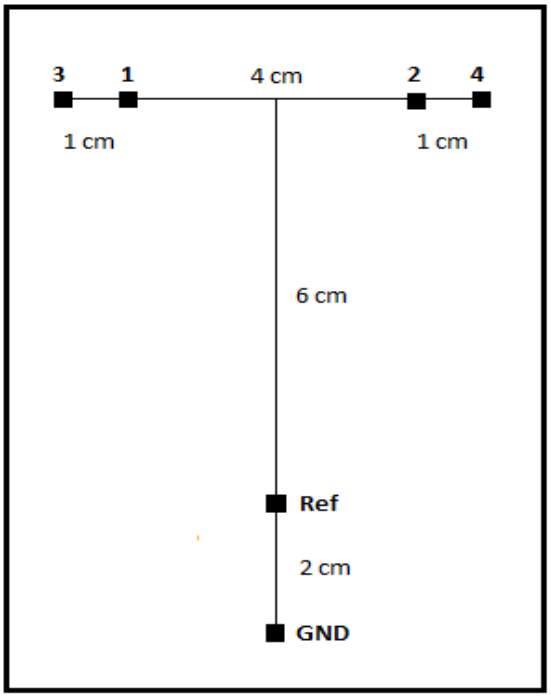

Fig. 41 Electrode setting with output horizontal line, S_2 setting.

For the first two settings the overview of electrode numbers stays the same, Tab. 1.

Tab. 1 Overview of electrode numbers.

Electrode number	Meaning
1	Input 1
2	Input 2
3	Output 1
4	Output 2

The different situation is for the last setting type, BIP. The setting, Fig. 42, with overview of electrode numbers, Tab. 2, are introduced below.

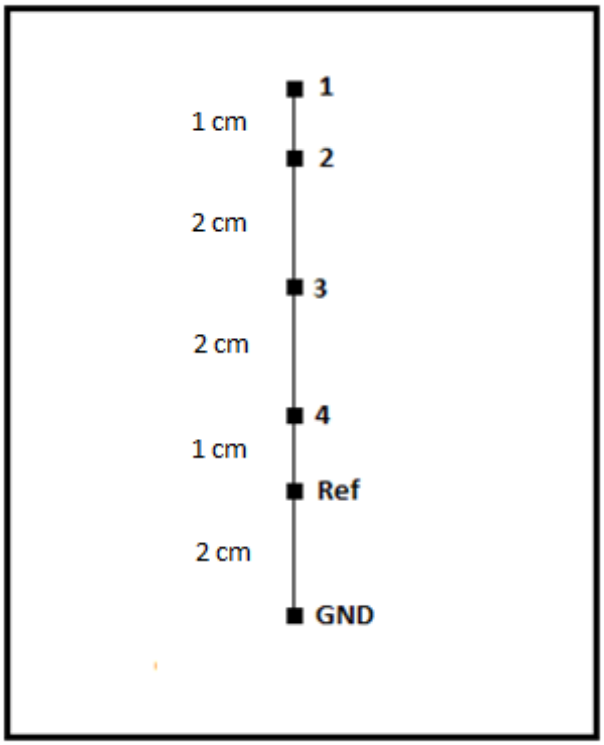

Fig. 42 Bipolar electrode setting, BIP setting.

Tab. 2 Overview of electrode numbers.

Electrode number	Meaning
1	Input
2	Output 1
3	Output 2
4	Output 3

For clarity shortcuts of these signals are introduced in a table below, Tab. 3.

Tab. 3 Shortcuts of signals.

Signal	Shortcut
sponge_C1_S1_ch0_2015.06.16_10.33.47.hdf5	C1_S1_ch0
sponge_C1_S1_ch1_2015.06.16_10.51.32.hdf5	C1_S1_ch1
sponge_C1_S2_ch0_2015.06.16_11.14.56.hdf5	C1_S2_ch0
sponge_C1_S2_ch1_2015.06.16_11.23.59.hdf5	C1_S2_ch1
sponge_C1_bip_01_2015.06.15_13.17.11.hdf5	C1_bip

9.3 Results of the estimation of the complex gain and the phase

The script for the validation called *unitary_test* generates a vector t containing time samples from 0 to 10 s with steps of 0.01 s, vector t contains even number of samples. The sampling frequency f_s is here 100 Hz. It also generates three signals x_1, x_2, and x_3 that are pure sinusoid with a frequency f_0 at 3 Hz. The phase of x_1 is zero. The phase of x_2 is $\frac{-2\pi}{4}$ and the phase of x_3 is $\frac{2\pi}{4}$. This test was done for $spectro\_tfe(x1, x2, f0, fs)$ to obtain the expected values. It was repeated for different vector t, t varying from 0 to 9.99 s with steps of 0.01 s, vector t contains odd number of samples.

In addition, the unitary test included a comparison between two sinusoid signals, the first one had a zero phase and the second one had a varying phase. The result of this comparison is represented below, it shows a match between the estimated ϕ_{est} and the expected ϕ, Fig. 43.

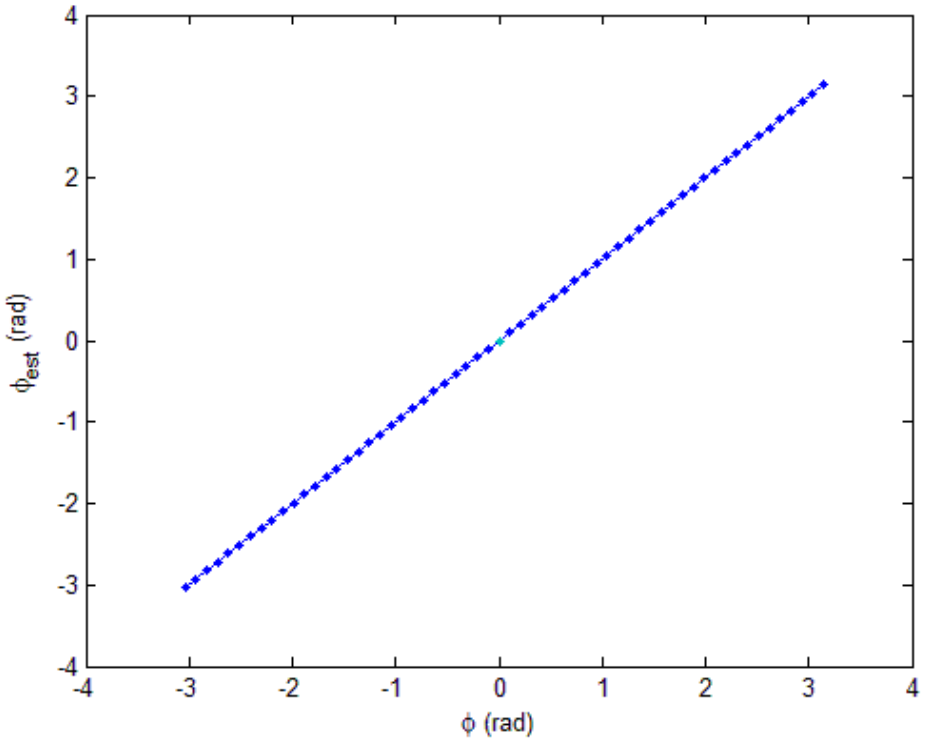

Fig. 43 Match between the estimated ϕ_{est} and the expected ϕ, (un_test.m).

After this successful validation the next step was the *spectro_tfe* application to filters, allpass, lowpass and highpass.

As it was mentioned in the previous chapter, the spectroscopy part of the signal contained one input and one output signal and both consist of 13 sinusoid trials with a different sinusoid frequencies so practically outputs of function spectro_tfe g and ϕ are vectors with 13 values that are plotted in frequency dependence.

Result of allpass filter is introduced below, Fig. 44.

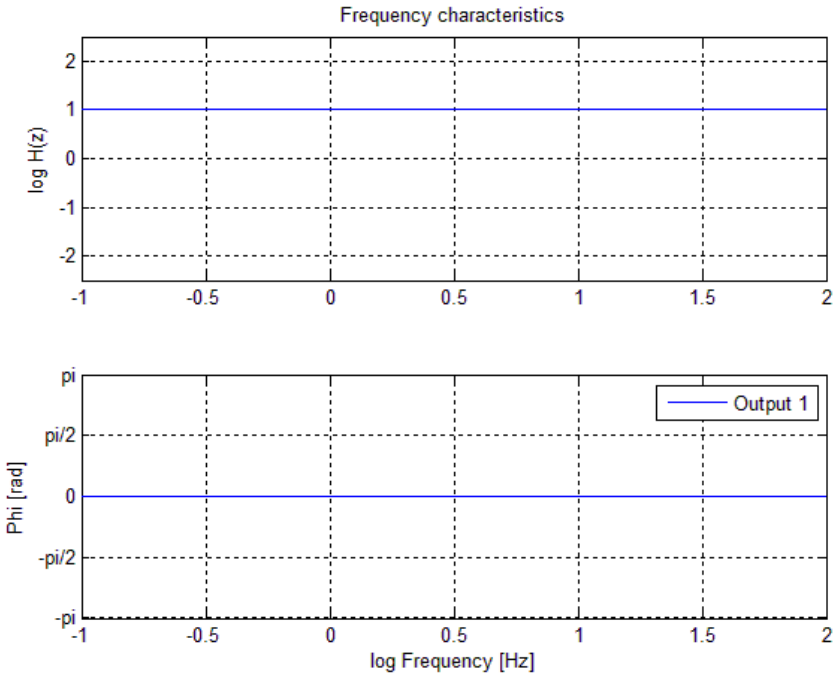

Fig. 44 The frequency characteristics for allpass filter (top – amplitude, bottom – phase), (figuring.m).

As it can be seen the variable *g* is represented by a zero line as well as *phi* variable. That means no frequency band is rejected.

Results of lowpass filter are shown in Fig. 45.

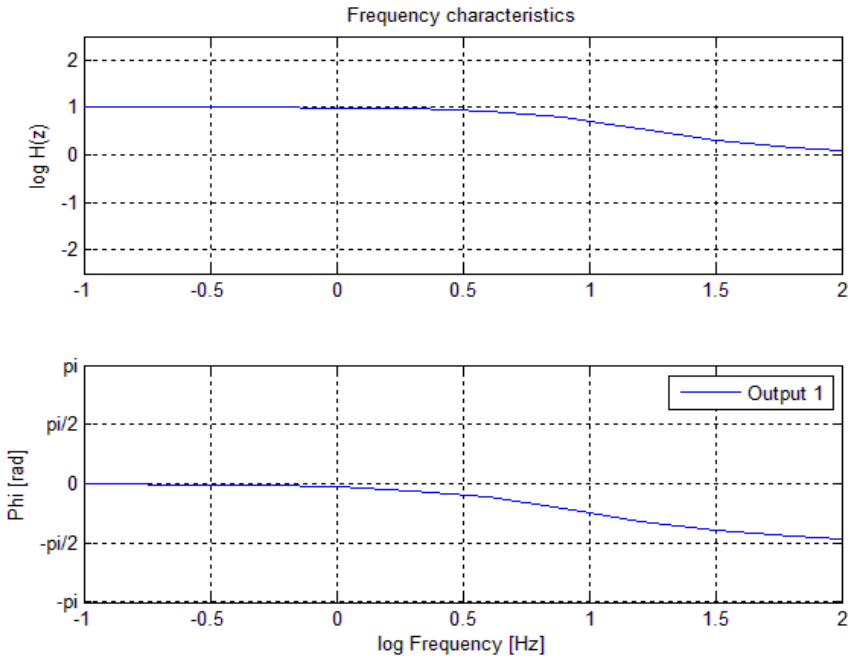

Fig. 45 The frequency characteristics for lowpass filter (top – amplitude, bottom – phase), (figuring.m).

The frequency characteristic for lowpass filter, Fig. 45, shows the band of the lower frequencies is released unlike the band of the higher frequencies that is not released.

Results of the last type of these experimental filters is highpass, results are represented in Fig. 46.

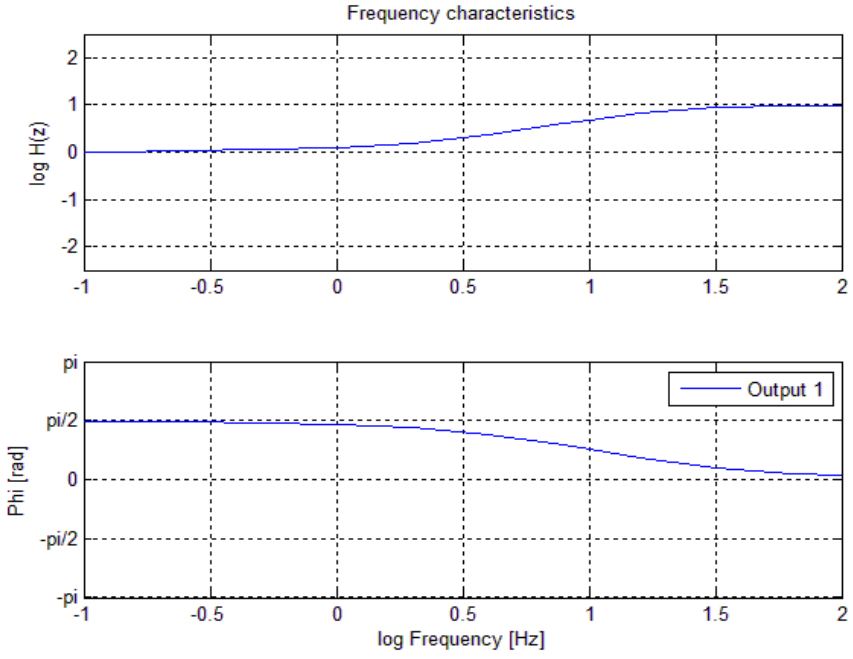

Fig. 46 The frequency characteristics for highpass filter (top – amplitude, bottom – phase), (figuring.m).

The frequency characteristic represented in Fig. 46 suggests that the band of the lower frequencies is rejected and the band of the higher frequencies is released.

The frequency characteristics for all experimental filters represented in this section confirm theoretical assumptions for these types of filters.

The function *spectro_tfe* was applied to signals addicted to the electrode setting from the sponge experiments. The solution concentration was c_1 that means $\frac{1}{2}$ of tablet per $1l$ for all of experiments. This concentration is not related to the physical unit but it was chosen based on the previous experiments.

The results of the frequency characteristics for each shortcut of signals described in Tab. 3 are shown below.

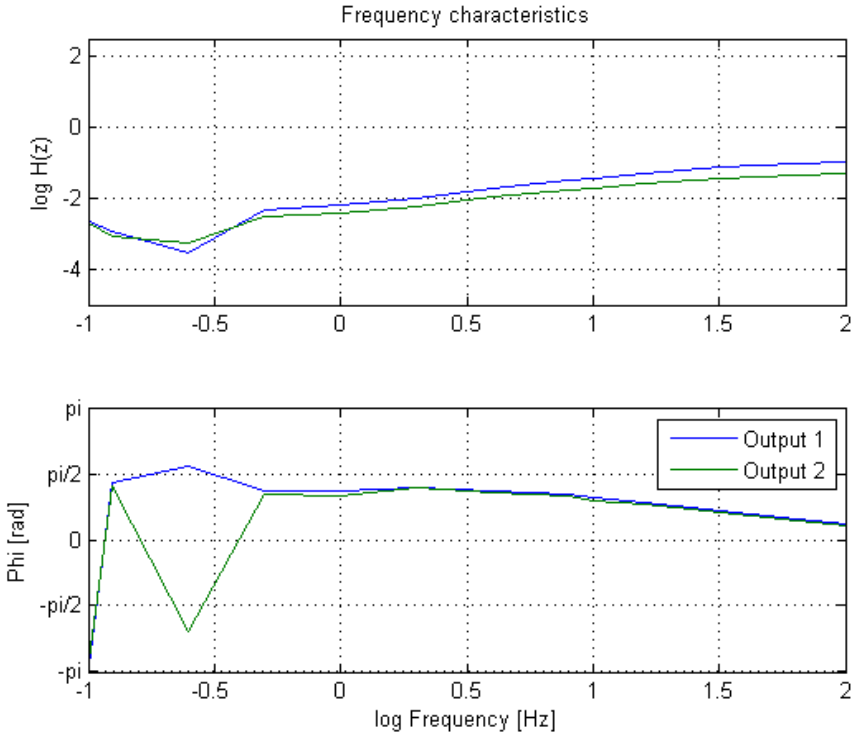

Fig. 47 The frequency characteristic of *C1_S1_ch0* signal, (figuring.m).

In Fig. 47 there is represented the frequency characteristic of the signal *C1_S1_ch0* that was designed according to S_1 electrode setting. This picture shows that results of both outputs are similar. Some attenuation of the amplitude of output 2 can be observed, this attenuation can be indicated by the longer distance between the input and output 2 than between the input and output 1.

All this system behaves like highpass filter. The amplitude is increasing and the phase is decreasing from $\frac{\pi}{2}$ to 0 as it is expected for highpass filters.

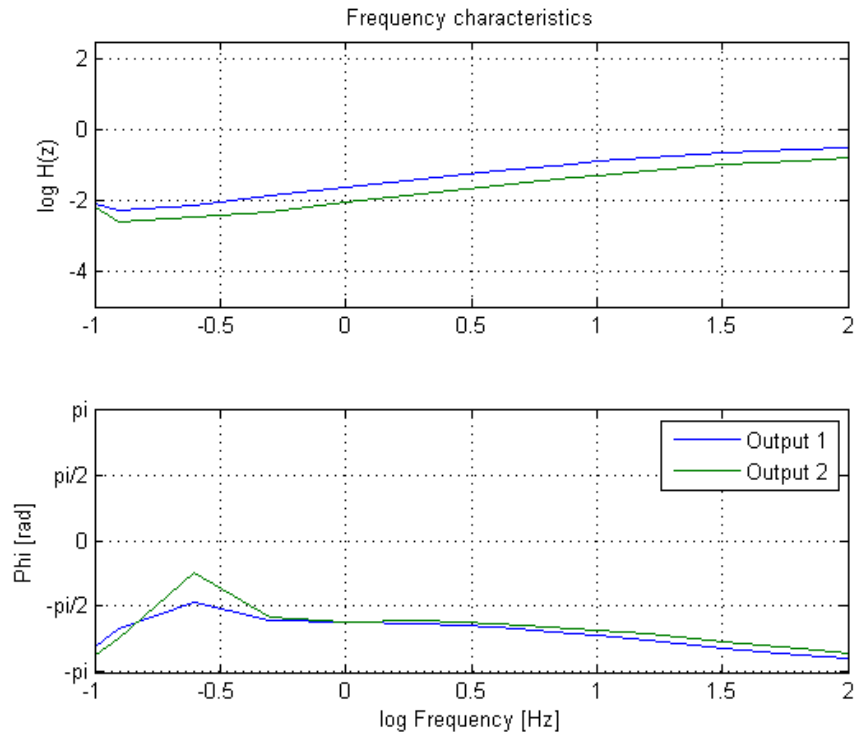

Fig. 48 The frequency characteristic of *C1_S1_ch1* signal, (figuring.m).

The frequency characteristic in Fig. 48 describes the signal with the same phase as the previous one but in this case the input is the inverted sine wave with the lower amplitude than the previous one.

The signal *C1_S1_ch1* was created by the electrode setting $S_1$and the match between output 1 and output 2 can be found. In the amplitude characteristic the attenuation of output 2 can be observed caused by the longer distance between this output and the input.

The whole system reminds highpass filter too. Typically phase decreasing from $\frac{-\pi}{2}$ to $-\pi$ and the amplitude increasing present in this frequency characteristic confirm this idea.

Results of signals with the electrode setting s_2 are presented below.

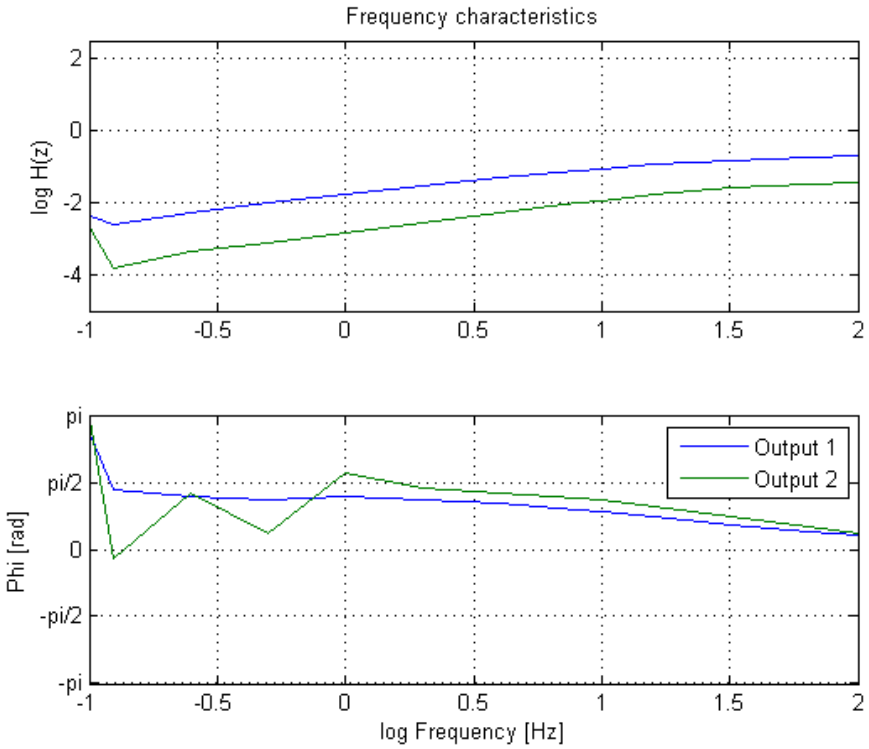

Fig. 49 The frequency characteristic of *C1_S2_ch0* signal, (figuring.m).

The attenuation between the results of output 1 and output 2 presented in the amplitude characteristic increased, Fig. 49. It is understandable because the distance between the input and output 2 was increased while the distance between the input and output 1 was decreased. So the differences in these distances caused the increase of the attenuation.

The system behaves as highpass filter too as it can be observed in the phase characteristic.

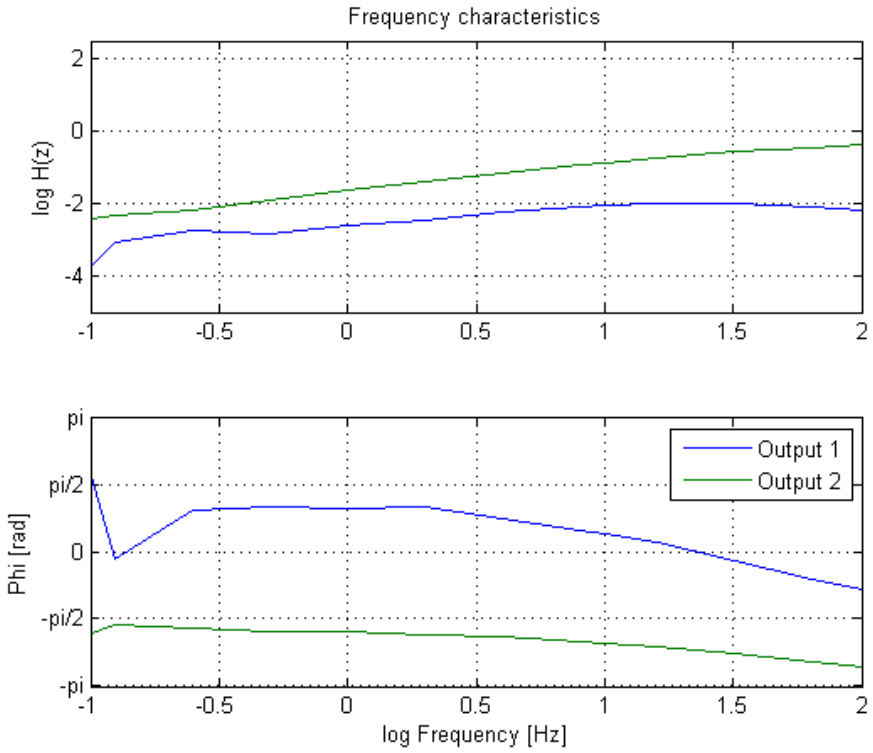

Fig. 50 The frequency characteristic of *C1_S2_ch1* signal, (figuring.m).

Results of the last signal designed by the electrode setting S_2 are mentioned above, Fig. 50. The sinusoid input had the same phase as the previous one but it was inverted and the amplitude was decreased. So practically inputs of the previous case were only switched between them.

Now results are a little bit different. The attenuation of the amplitude characteristic can be observed too but for output 1. Because the input switching now input 1 represents the inverted sine wave with the lower amplitude that represented input 2 firstly and that was closer to output 2. That is the reason why the amplitude of output 2 is higher than of output 1 and attenuation can be observed in the amplitude characteristic of output 1.

The system behaves as highpass filter too. The phase characteristics of outputs are shifted by π. The last analysed signal was created by the electrode setting BIP.

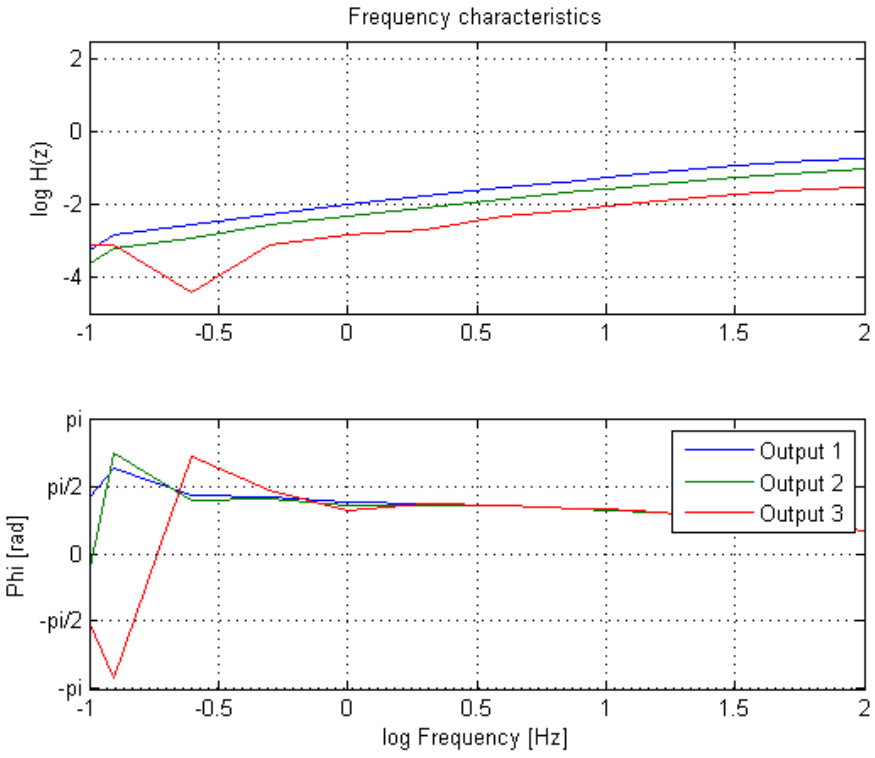

Fig. 51 The frequency characteristic of *C1_bip* signal, (figuring.m).

This system includes one input and three outputs and describes highpass filter as it can be seen. The attenuation of the amplitude characteristics can be observed and it depends on the distance between the input and outputs. So the lowest amplitude can be seen in the amplitude characteristic of the output 3, the furthermost output, the highest amplitude can be observed in the amplitude characteristic of output 1, the nearest output.

9.4 Results of the estimation of the time constant

In this section the step response part of these signals was used. For lowpass filter the theoretical assumption of the time constant is that the time constant value corresponds to 63% of the step response, as it mentioned in the previous chapter.

It can be observed in Fig. 52 that τ, tau, corresponds to 63% of the step response. The time constant τ equals 72^{nd} sample and it equals $0.015s$ according to the relationship below, (20).

$$\tau = \frac{N_i}{f_s} \tag{20}$$

Where N_i means the number of the sample corresponding to 63% of the step response. For this case $N_i = 72$. The variable f_s represents the sampling frequency that means $f_s = 4800\ Hz$.

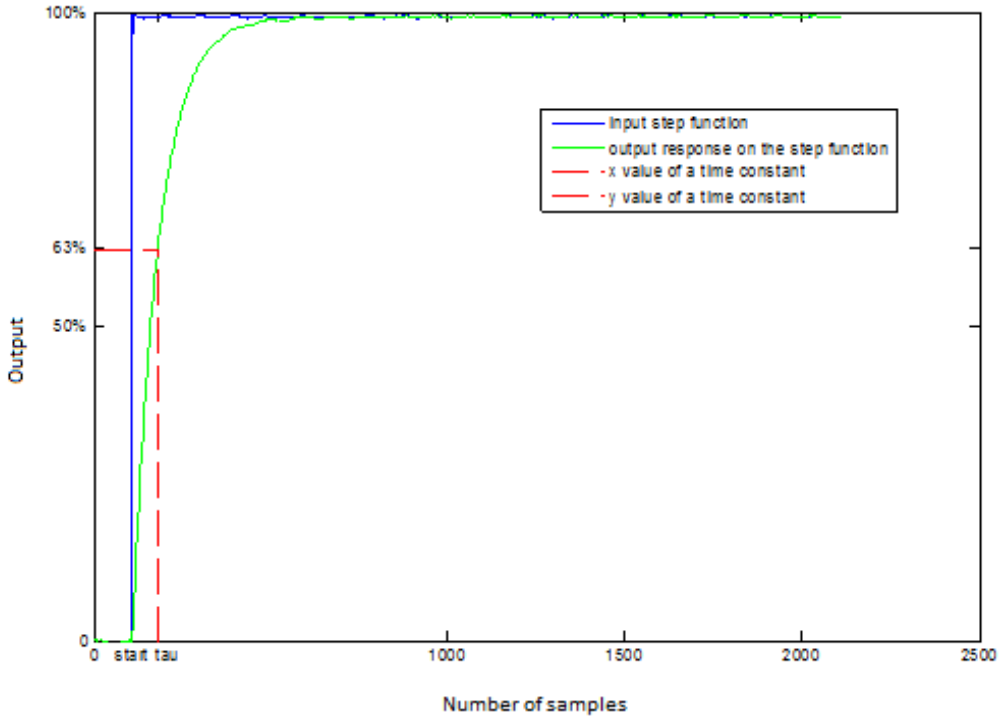

Fig. 52 Step response for lowpass filter with the time constant τ, (step_response.m).

For the highpass filter the theoretical assumption of the time constant value is that this value should correspond to 37% of the step response. The reason of this fact was shown in the previous chapter too.

The time constant τ equals 74^{th} sample and that equals $0.0154\ s$, according to the equation (20). But in this case the variable $N_i = 74$. The sampling frequency stayed the same. This results can be observed in Fig. 53.

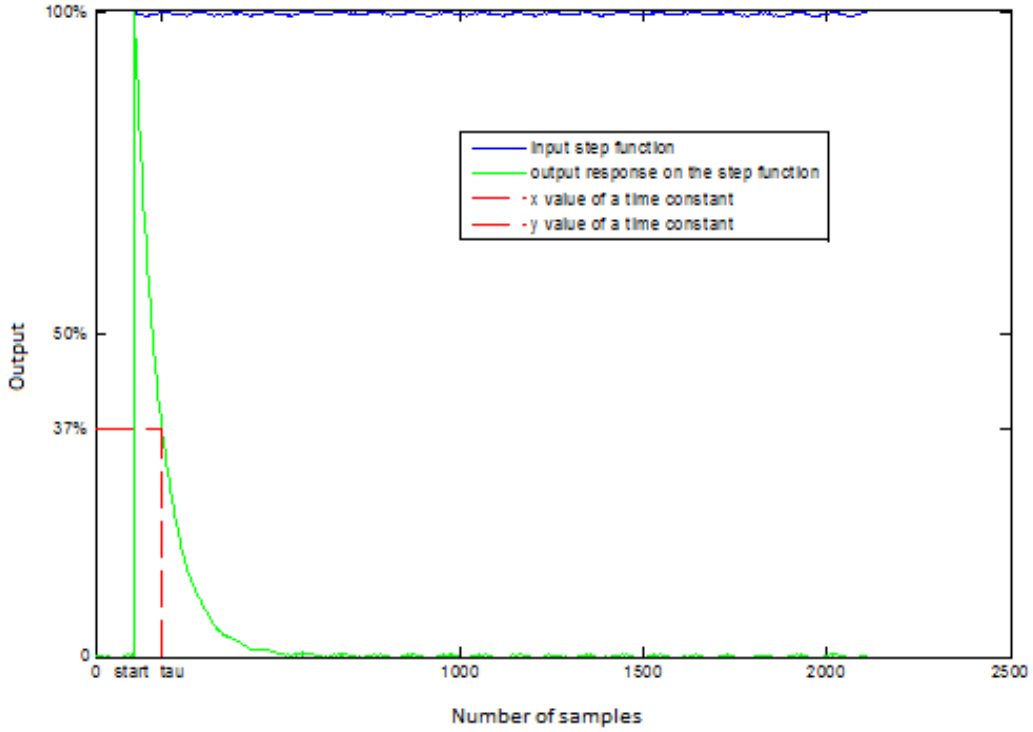

Fig. 53 Step response for highpass filter with the time constant τ, (step_response.m).

So the time constant for lowpass and highpass filters was found. For allpass filter the situation is different. The time constant of signal represents a delay between an input and an output. In the case of lowpass and highpass filters inputs and outputs are different so the time constant, the delay, should be non-zero value. But in the case of allpass filter the input and the output should be the same so the time constant, the delay, can be zero value.

The expected value of the time constant is acquired from the relationship below, (21).

$$\tau = RC \tag{21}$$

Parameters R represents a resistance and in this case $R = 15\ k\Omega$, C means a capacity and $C = 1\ \mu F$. So the expected value of the time constant is $0.015\ s$.

In the table below results are summarized, Tab. 4.

Tab. 4 Time constants for filters.

Allpass filter	-
Lowpass filter	0.015 s
Highpass filter	0.0154 s

All signals addicted to the electrode setting should behave as highpass filters that means a time constant of these signals is estimated from the response of the step function.

Due to the fact that these systems should correspond to highpass filters a time constant of each signal is a value equals to 37% of the step function response.

For the time constant calculation the equation above, (21), is used and the overview of time constants, Tab. 5, and results of all signals are represented below where time constants are marked as the variable τ.

Tab. 5 Overview of the time constants.

Signal		**Time constant**
C1_S1_ch0	Output 1	$\tau = 0.0046\ s$
	Output 2	$\tau = 0.005\ s$
C1_S1_ch1	Output 1	$\tau = 0.01\ s$
	Output 2	$\tau = 0.0063\ s$
C1_S2_ch0	Output 1	$\tau = 0.0056\ s$
	Output 2	$\tau = 0.0042\ s$
C1_S2_ch2	Output 1	–
	Output 2	$\tau = 0.0048\ s$
C1_bip	Output 1	$\tau = 0.0035\ s$
	Output 2	$\tau = 0.0035\ s$
	Output 3	$\tau = 0.0035\ s$

Time constants are identical with the value equals to 37% of the step response that is obvious from results represented in the last section, chapter 13.

The signal *C1_bip* was in the best quality, as it can be observed from the Tab. 5. Time constants of outputs were the same so it can be claimed that the whole system was delayed by $0.0035\ s$.

The result obtained from output 1 of *C1_S2_ch1* signal doesn´t represent highpass filter thus the time constant is not estimated. The step response of that signal is represented below in Fig. 54.

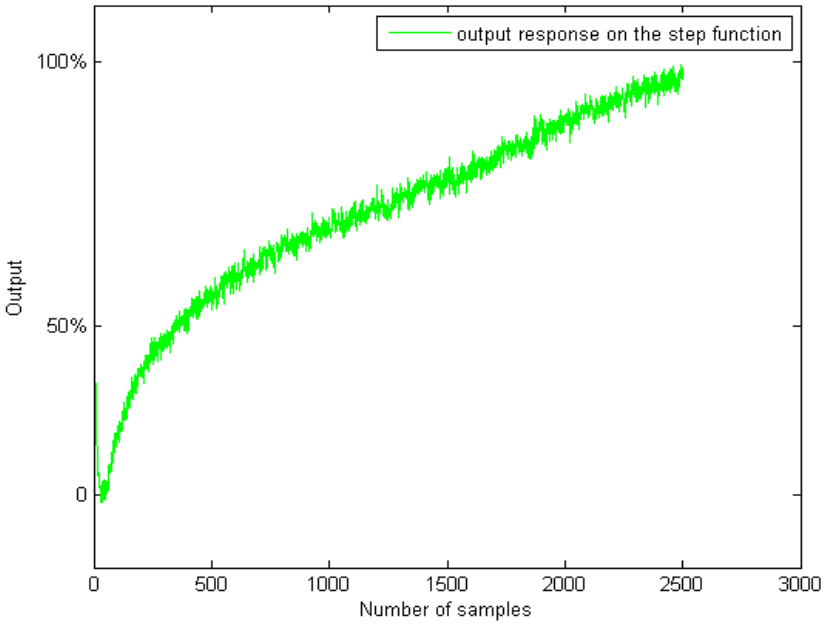

Fig. 54 The step response of *C1_S2_ch1* signal, output 1, (step_response.m)

9.5 Results of the estimation of the signal spectrum

The spectrum on the experimental allpass filter, lowpass filter, highpass filter using the Identification Toolbox was evaluated, Fig. 55.

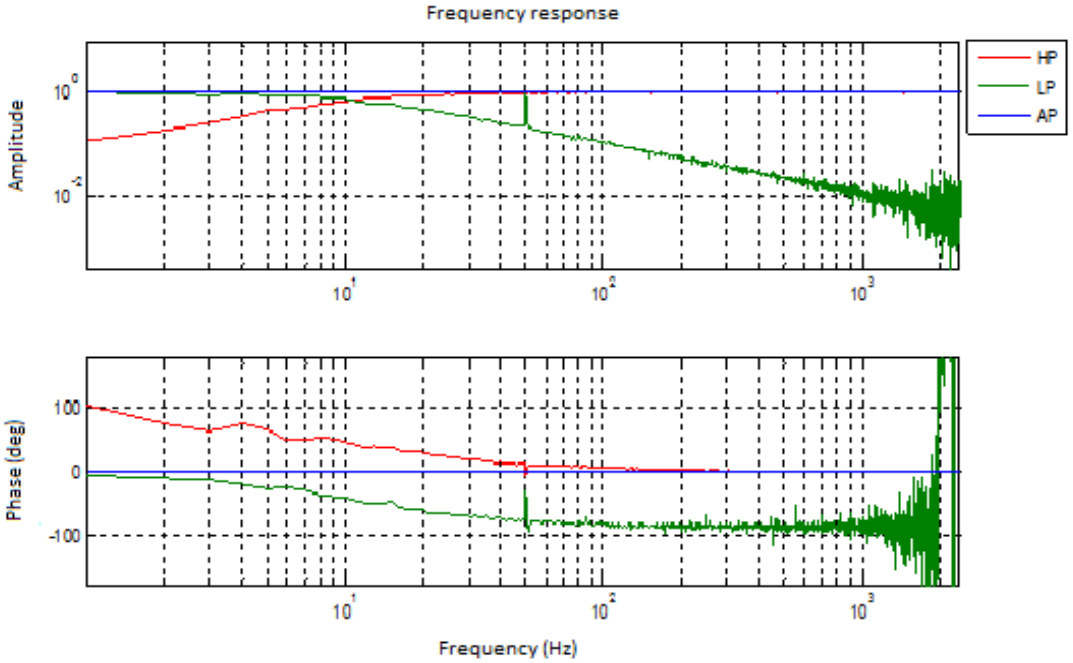

Fig. 55 Spectrum of the experimental filters, (AP.sid, LP.sid, Hp.sid).

In Fig. 55 the spectrum of all experimental filters and the cutting frequency with approximate value about 10.6 Hz can be observed. According to an equation for cutting frequency estimation (22), the value of the cutting frequency can be acquired.

$$f_c = \frac{1}{2\pi\tau} \tag{22}$$

Where the variable τ is the time constant defined in the previous step, so $\tau = 0.015\ s$. After the numerical substitution the expected value of the cutting frequency is $f_c \approx 10.6\ Hz$. The assumption of the cutting frequency value was confirmed by the signal spectrum of the experimental filters.

Spectrums of the white noise signal part were evaluated by *Ident* toolbox as it mentioned above. In pictures in the last section, chapter 13, frequency characteristics of signals representing highpass filters can be seen. They were compared with results of *spectro_tfe* function mentioned above. It is like a visual feedback that own function *spectro_tfe* was designed in the right way because spectrums estimated by function *spectro_tfe* and spectrums estimated by *Ident* toolbox match.

Cutting frequencies can be evaluated also according to the equation (22) and results are introduced in Tab. 6.

Tab. 6 Overview of cutting frequencies.

Signal		**Cutting frequency**
C1_S1_ch0	Output 1	$f_c = 34.6Hz$
	Output 2	$f_c = 31.83Hz$
C1_S1_ch1	Output 1	$f_c = 15.92Hz$
	Output 2	$f_c = 25.26Hz$
C1_S2_ch0	Output 1	$f_c = 25.42Hz$
	Output 2	$f_c = 37.89Hz$
C1_S2_ch2	Output 1	–
	Output 2	$f_c = 33.16Hz$
C1_bip	Output 1	$f_c = 45.47Hz$
	Output 2	$f_c = 45.47Hz$
	Output 3	$f_c = 45.47Hz$

9.6 Results of the estimation of the transfer function model

For the transfer function model prediction the *Ident* toolbox was used again. Specifically the section 'ARX Model Structure Selection' in Identification Toolbox was used. As it mentioned in the previous chapter, the structure of ARX model is simple and suitable for the prediction of the transfer function model enough.

From the theoretical description of the ARX model there are three main parameters, n_a, n_b, n_k. For the selection of the best-fit model the model performance for each combination of model parameters, n_a, n_b, n_k changing in a range from 1 to 10 was done.

For the modeling allpass, highpass and lowpass filters Transfer Function Models were chosen because of very good matches and simplicity either.

From previous step the best results were presented by Transfer Function Models containing only two parameters, n_a, n_b. The estimation of MSE (mean square error) and FIT (percentage of a compliance describing how the used mathematic definition matches with real data) was used to choose values of parameters n_a and n_b. Definition of MSE method is introduced below, (23).

$$SSE = \sum_{i=1}^{n} \omega_i (y_i - \hat{y}_i)$$

$$v = n - m$$

$$MSE = \frac{SSE}{v} \tag{23}$$

SSE means sum of squares due to error and this statistic method measures the total deviation of the response value from the fit to the response values. Next variable ω_i means weighting applied to each data point and usually it equals to 1, y_i means observed data value and $\hat{y}_i$ corresponds to predicted value from the fit. The residual degrees of freedom v corresponds to the number of response values *n* minus the number of fitted coefficients *m* estimated from the response values. MSE is a ration of the SSE to variable v, [21]. MSE value low and closer to 0 indicates a fit which is useful for prediction.

For comparison values of MSE and FIT for varying parameter n_a for lowpass filter are represented in Tab. 7. From this table it can be observed that the best choice is the first one because in this case here is the lowest value of MSE.

Tab. 7 Comparison of MSE and FIT values of lowpass filter.

(n_a, n_b)	**MSE**	**FIT [%]**
(1, 1)	132 850	94.98
(2, 1)	329 680	91.6348
(3, 1)	188 770 000	-100.701
(4, 1)	711 600	87.7102
(5, 1)	188 160 000	-99.8448

The same step was performed for highpass filter, Tab. 8, the first choice is the best too.

Tab. 8 Comparison of MSE and FIT values of highpass filter.

(n_a, n_b)	**MSE**	**FIT [%]**
(1, 1)	2 317	94.4783
(2, 1)	528 570	16.6017
(3, 1)	54 720	72.1666
(4, 1)	496 330	19.1857
(5, 1)	713 210	3.1245

Now, the best parameters for Transfer Function Models were obtained and the estimation of gains for these models can be done. Results are represented in table below, Tab. 9.

Tab. 9 Estimated gains of the transfer function models.

Type of filter	**Gain**
Allpass	$H(s) = \frac{1{,}001 \cdot s + 2{,}404 \cdot 10^5}{s + 2{,}404 \cdot 10^5} \approx 1$
Lowpass	$H(s) = \frac{0{,}007175 \cdot s + 66{,}67}{s + 66{,}64}$
Highpass	$H(s) = \frac{0{,}9932 \cdot s + 0{,}3725}{s + 66{,}63}$

The last step in this part was a substitution in the theoretical Fourier equation defined in the previous chapter.

For the next work one adjustment was done. The member RC was replaced by the time constant τ. Then the results are represented in table below, Tab. 10.

Tab. 10 Theoretical Fourier equation of the gain.

Type of filter	**Theoretical Fourier equation of the gain**
Allpass	$H(s) = 1$
Lowpass	$H(s) = \frac{1}{\tau s + 1}$
Highpass	$H(s) = \frac{\tau s}{\tau s + 1}$

According to Eq. (21) the variable τ was evaluated, the resistance $R = 15\ k\Omega$ and the capacity $C = 1\ \mu F$. The numerical value of the variable τ was put into equations from Tab. 10. Results are showed in Tab. 11.

Tab. 11 Theoretical gains of filters.

Type of filter	Theoretical gain
Allpass	$H(s) = 1$
Lowpass	$H(s) = \frac{66{,}67}{s + 66{,}67}$
Highpass	$H(s) = \frac{s}{s + 66{,}67}$

After comparison between the theoretical gains of the filters, Tab. 11 and gains of models, Tab. 9 we can observe deviations. The biggest deviation can be observed in the highpass filter. The highpass filter may include the lowpass component.

This process was repeated for signals representing highpass filters. Before the estimation of the transfer function models for each output the estimation of MSE and FIT was done to determine a number of poles and zeros based on the lowest value of MSE.

In tables in chapter 13 results are introduced. The lowest value of MSE represents the first combination of poles and zeroes for each output excepting output 1 of *C1_S2_ch1* signal. For this output the lowest value of MSE represents the second combination, Tab. 12, but the difference between this value and MSE value of the first combination is not so significant so the first combination of the number of poles and zeroes was taken to the estimation of the transfer function model because the model with the second combination of number of poles and zeroes is unnecessarily complicated.

Tab. 12 Comparison of MSE and FIT values of *C1_S2_ch1* signal.

	(n_a, n_b)	MSE	FIT [%]
Output 1	**(1, 1)**	90 590	46.3
	(2, 1)	90 467	47.48
	(3, 1)	90 480	47.47
	(4, 1)	110 040	42.08
	(5, 1)	8 650 900	-413.8
Output 2	**(1, 1)**	3 106 800	77.19
	(2, 1)	58 516 000	1
	(3, 1)	58 843 000	0.73
	(4, 1)	59 731 000	-0.01
	(5, 1)	59 726 000	-0.01

After the estimation of MSE and FIT values the transfer function models were evaluated and they are show in table below, Tab. 13.

Tab. 13 Estimated gains of the transfer function models.

Signal		Gain
C1_S1_ch0	Output 1	$H(s) = \frac{0.1256s + 46.64}{s + 728.2}$
	Output 2	$H(s) = \frac{0.0636s + 56.98}{s + 1252}$
C1_S1_ch1	Output 1	$H(s) = \frac{-0345s + 2.283}{s + 224.4}$
	Output 2	$H(s) = \frac{-0.1919s + 6.557}{s + 340}$
C1_S2_ch0	Output 1	$H(s) = \frac{0.2409s + 31.49}{s + 413.9}$
	Output 2	$H(s) = \frac{0.0413s + 4.703}{s + 415.4}$
C1_S2_ch2	Output 1	$H(s) = \frac{0.0036s + 0.5648}{s + 0.8046}$
	Output 2	$H(s) = \frac{-0.5229s - 18.84}{s + 480.2}$
C1_bip	Output 1	$H(s) = \frac{0.2497s + 46.27}{s + 757.6}$
	Output 2	$H(s) = \frac{0.1223s + 18.62}{s + 670.3}$
	Output 3	$H(s) = \frac{0.04087s + 6.055}{s + 639.5}$

As it was mentioned above these signals were supposed to be highpass filters so the transfer function models should correspond to this fact. But results in Tab. 13 shows to the several differences. Each transfer function model obtains even the lowpass part so for clarify and for the time constant estimation gains were rewritten according to the equations below.

$$H_{HP}(s) = A\frac{\tau s}{(\tau s + 1)}$$

$$H_{LP}(s) = A\frac{1}{(\tau s + 1)} \quad \textbf{(24)}$$

Results are represented here, Tab. 14.

Tab. 14 Highpass and lowpass part of the estimated gain of the transfer function model

Signal		Highpass part	Lowpass part
C1_S1_ch0	Output 1	$H_{HP}(s) = 0.124\frac{0.00137s}{(0.00137s+1)}$	$H_{LP}(s) = 0.06\frac{1}{(0.00137s+1)}$
	Output 2	$H_{HP}(s) = 0.0625\frac{0.0008s}{(0.0008s+1)}$	$H_{LP}(s) = 0.046\frac{1}{(0.0008s+1)}$
C1_S1_ch1	Output 1	$H_{HP}(s) = -0.34\frac{0.0044s}{(0.0044s+1)}$	$H_{LP}(s) = 0.01\frac{1}{(0.0044s+1)}$
	Output 2	$H_{HP}(s) = -0.187\frac{0.003s}{(0.003s+1)}$	$H_{LP}(s) = 0.02\frac{1}{(0.003s+1)}$
C1_S2_ch0	Output 1	$H_{HP}(s) = 0.25\frac{0.0024s}{(0.0024s+1)}$	$H_{LP}(s) = 0.076\frac{1}{(0.0024s+1)}$
	Output 2	$H_{HP}(s) = 0.0417\frac{0.0024s}{(0.0024s+1)}$	$H_{LP}(s) = 0.0113\frac{1}{(0.0024s+1)}$
C1_S2_ch2	Output 1	$H_{HP}(s) = 0.0036\frac{1.243s}{(1.243s+1)}$	$H_{LP}(s) = 0.702\frac{1}{(1.243s+1)}$
	Output 2	$H_{HP}(s) = -0.5\frac{0.002s}{(0.002s+1)}$	$H_{LP}(s) = -0.039\frac{1}{(0.002s+1)}$
C1_bip	Output 1	$H_{HP}(s) = 0.254\frac{0.0013s}{(0.0013s+1)}$	$H_{LP}(s) = 0.061\frac{1}{(0.0013s+1)}$
	Output 2	$H_{HP}(s) = 0.13\frac{0.0015s}{(0.0015s+1)}$	$H_{LP}(s) = 0.03\frac{1}{(0.0015s+1)}$
	Output 3	$H_{HP}(s) = 0.0426\frac{0.0015s}{(0.0015s+1)}$	$H_{LP}(s) = 0.0095\frac{1}{(0.0015s+1)}$

The time constants of the transfer function models could be determined and compared to the time constants estimated from the real systems.

Tab. 15 Overview of the time constants of models.

Model of signal		Time constant
C1_S1_ch0	Output 1	$\tau = 0.00137s$
	Output 2	$\tau = 0.0008s$
C1_S1_ch1	Output 1	$\tau = 0.0044s$
	Output 2	$\tau = 0.003s$
C1_S2_ch0	Output 1	$\tau = 0.0024s$
	Output 2	$\tau = 0.0024s$
C1_S2_ch2	Output 1	$\tau = 1.243s$
	Output 2	$\tau = 0.002s$
C1_bip	Output 1	$\tau = 0.0013s$
	Output 2	$\tau = 0.0015s$
	Output 3	$\tau = 0.0015s$

After a comparison of these values, Tab. 15, with the time constants of real signals, Tab. 5, it is obvious there are differences. For example the time constant of the real signal *C1_bip* is the same value for all output, $\tau = 0.0035\ s$, the time constants of the model of *C1_bip* signal almost respect the same rule. Only the time constant of output 1 is slightly different from others.

The highest value of the time constant of the transfer function models was received for output 1 of *C1_S2_ch0*. By *Ident* toolbox this model was evaluated but this model is not sufficient for the real system description. The match between the real signal and this model was very low, only 19%, in comparison with other models where this match was in a range of 60% to 90%. The real signal of output 1 of *C1_S2_ch0* was acquired in the same manner as the rest of signals but probably there was a measurement error. The different step response and the unexpected shape of the white noise part of this signal could support this claim.

10 RESULTS OF ANALYSIS OF JANSEN'S SIGNALS

This is the last section where the results from two analyses are introduced. The sponge experiments of Jansen's signals were processed and analysed. As the first Jansen's signal the signal simulating alpha activity in the first cortical column and beta activity in the second cortical column was used. As the second Jansen's signal the signal simulating alpha activity in both columns was used. The outputs from both signals were acquired from two setting combination like the previous ones, first setting S_1 and second setting S_2 were introduced in Fig. 40 and in Fig. 41.

For the clarity in Tab. 16 there are introduced shortcuts of Jansen's signals using in the sponge experiments.

Tab. 16 Overview of shortcuts of Jansen's signals using in the sponge experiments.

Full name of signals	**Meaning of signals**	**Shortcut**
sponge_C1_S1_Jansen1_2015.06.16_11.11.27.hdf5	Signals representing alpha and beta activity with the electrode setting S_1.	Jansen1_S1
sponge_C1_S2_Jansen1_2015.06.16_11.38.46.hdf5	Signals representing alpha and beta activity with the electrode setting S_2.	Jansen1_S2
sponge_C1_S1_Jansen2_2015.06.16_11.12.52.hdf5	Signals representing only alpha activity with the electrode setting S_1.	Jansen2_S1
sponge_C1_S2_Jansen2_2015.06.16_11.40.12.hdf5	Signals representing only alpha activity with the electrode setting S_2.	Jansen2_S2

10.1 Frequency analysis

The first analysis applied to the outputs from Jansen's sponge experiments was the frequency analysis, the power spectrums.

In each sponge experiments of Jansen's signals the input signals were repeated five times. For the frequency analysis these repetitions were averaged and then next analysis went on with only this averaged signals.

Signals were multiplied by Hamming window and then the Fourier transform was done. This analysis is useful to find out if the same significant frequency is present in the input signals and in output signals too. If the same significant frequency in inputs and in outputs is present the close relationship between inputs and outputs will occur. This relationship can prove that sponge medium simulating a brain is a proper conducting medium because this sponge medium keeps the continuity of the signal transmission and outputs are combinations of inputs. The results are introduced below.

Firstly in Fig. 56 the power spectrum of *Jansen1_S1* shows the significant frequency band in the range of 60 rad/s to 70 rad/s and that corresponds to range from 9.5 Hz to 11.1 Hz in inputs and also in outputs. The shape and the amplitude of the power spectrum are different for both inputs, the first one should represent alpha activity and the second one should represent beta activity. The amplitude of the significant frequency range of outputs is lower than the amplitude of the significant frequency range of inputs. So the relationship between inputs and outputs is present and outputs are uniformly affected by both inputs.

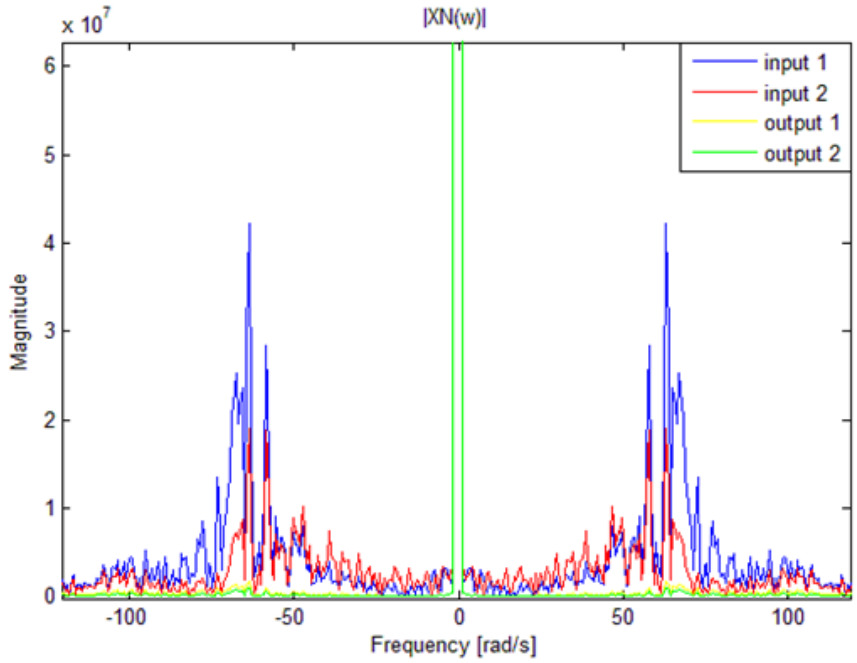

Fig. 56 The power spectra of *Jansen1_S1* signal, (plot_jansen_spectra.m).

Next power spectrum belongs to *Jansen1_S2*, Fig. 57. The significant frequency range is the same as in previous case, from 9.5 Hz to 11.1 Hz. The amplitude of this range present in the first output is lower than the amplitude of that range present in inputs but also it is higher than the amplitude of that range present in the second output. The first output is affected by the first input more than the second input as it can be seen from the scheme of the electrode setting S_2 present in Fig. 41. That means the amplitude of the significant frequency range in the first output should be higher than in the second output because the first output lays close to the first input that has a higher amplitude of the significant frequency range than the second input. This fact explains the low amplitude of that frequency range in the second output which is affected by the second input which has a lower amplitude of frequencies in general.

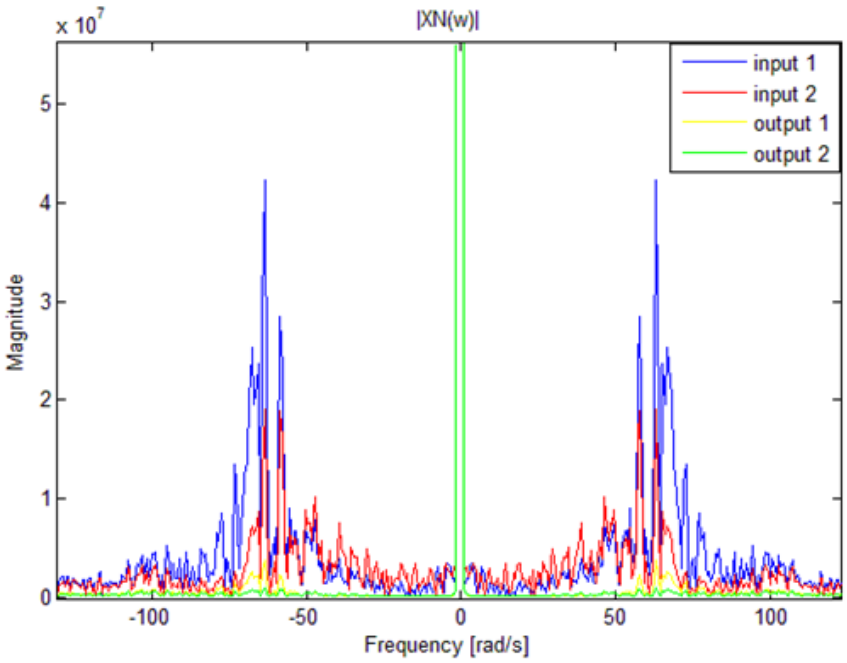

Fig. 57 The power spectra of *Jansen1_S2* signal, (plot_jansen_spectra.m).

The third power spectrum represents *Jansen2_S1* signal. The power spectrums of both inputs have similar shape and amplitude. It caused by fact that these inputs should simulate alpha activity only. The significant frequency range is still the same as in the previous case, from 9.5 Hz to 11.1 Hz. This range is present in outputs too but with the lower amplitude. The outputs are uniformly affected by both inputs and the farther output, the second output according to the scheme in Fig. 40, should have the lower amplitude of the significant frequency range than the closer output, the first output.

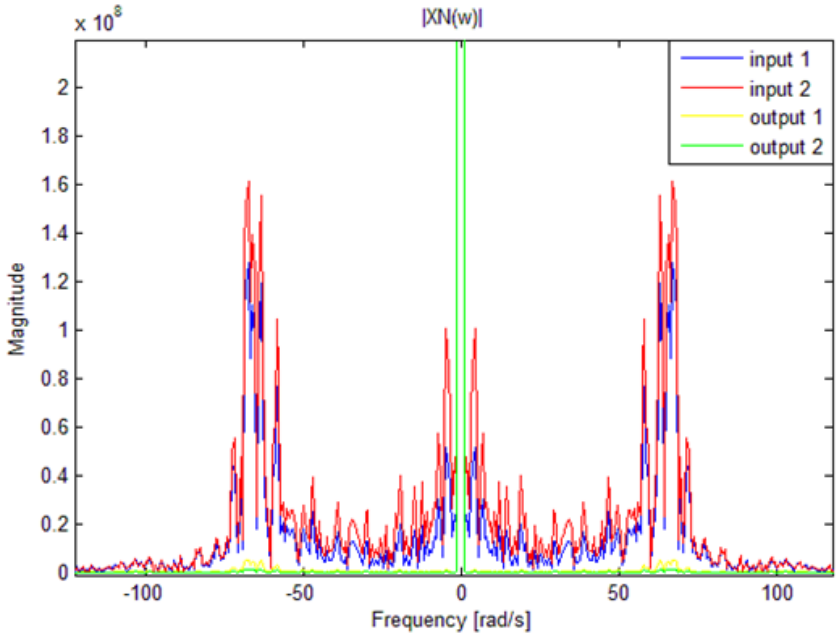

Fig. 58 The power spectra of *Jansen2_S1* signal, (plot_jansen_spectra.m).

The last spectrogram belongs to *Jansen2_S2* signal, Fig. 59. The significant frequency range is the same again, from 9.5 Hz to 11.1 Hz. The amplitude of that range in both outputs is the same because of the electrode setting S_2. The first output is affected by the first input and the second output is affected by the second input and because of the same type of signal in both inputs, alpha activity, in both outputs should be very similar signal with the similar amplitude of the all frequencies including the amplitude of the significant frequency range.

The outputs are combinations of the inputs. The effect of each input depends on the distance between that input and an appropriate output.

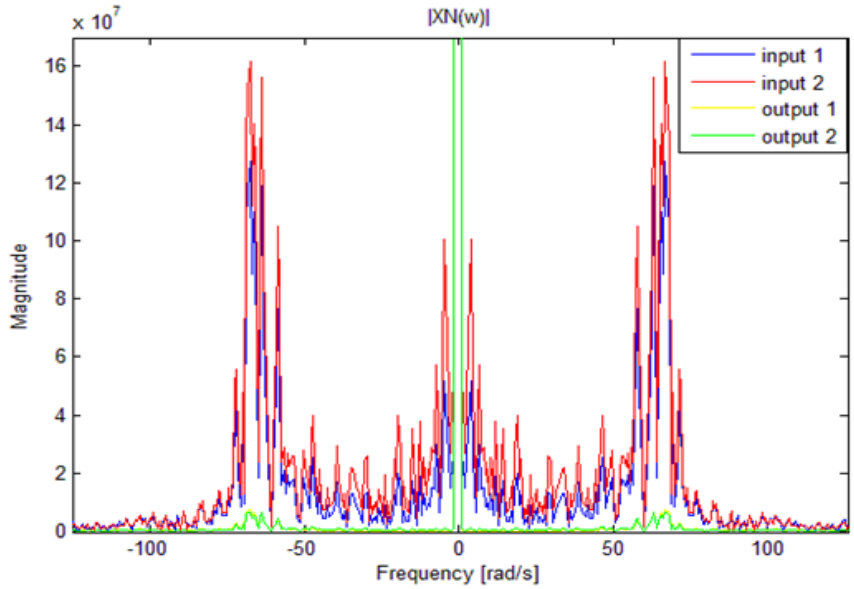

Fig. 59 The power spectra of *Jansen2_S2* signal, (plot_jansen_spectra.m).

10.2 Analysis of linear relationship between inputs and outputs

In this section the last analysis of Jansen's signals used in the sponge experiments is introduced. The last step was about finding a linear relationship between inputs and outputs to confirm that the sponge phantom is a convenient medium for a conduction of signals and that signals from this phantom are not subject to a big distortion. The linear dependence between inputs and outputs were found out according to a mathematical definition of a superposition principle introduced below, (25).

$$if \qquad \hat{y}(t) = \hat{h}_1(t) * x_1(t) + \hat{h}_2(t) * x_2(t)$$

$$and \qquad h_1(t) * x_1(t) \overset{FT}{\rightarrow} H_1(f)X_1(f)$$
$$h_2(t) * x_2(t) \overset{FT}{\rightarrow} H_2(f)X_2(f)$$

$$H_1(f)X_1(f) \overset{FT^{-1}}{\longrightarrow} h_1(t) * x_1(t)$$
$$H_2(f)X_2(f) \overset{FT^{-1}}{\longrightarrow} h_2(t) * x_2(t) \qquad (25)$$

Where $\hat{y}(t)$ means the output signal, $h_1(t)$ represents the impulse response in the time domain of the first input signal, $x_1(t)$ means the first input signal, signal from column 1, in the time domain, $H_1(f)$ is the impulse response of the first input in the frequency domain after Fourier transform application, $X_1(f)$ represents the first input, column 1, in the frequency domain after Fourier transform application. For the second input meanings of variables are analogical as for the first one. The convolution in the time domain passes to the multiplication in the frequency domain.

Firstly Jansen's signals were divided into systems including both inputs and only one output in order to determine the effect of both inputs on each output separately. Then each of these systems was recorded in *Ident* toolbox where the suitable model describing that system in the best way was estimated.

Based on testing of different models, the ARX model was evaluated as the best choice how to describe all of these systems. The impulse response of each ARX model was used to evaluate a convolution part of the mathematical equation shown above, (25).

As an example, one impulse response of that ARX model is shown below, Fig. 60.

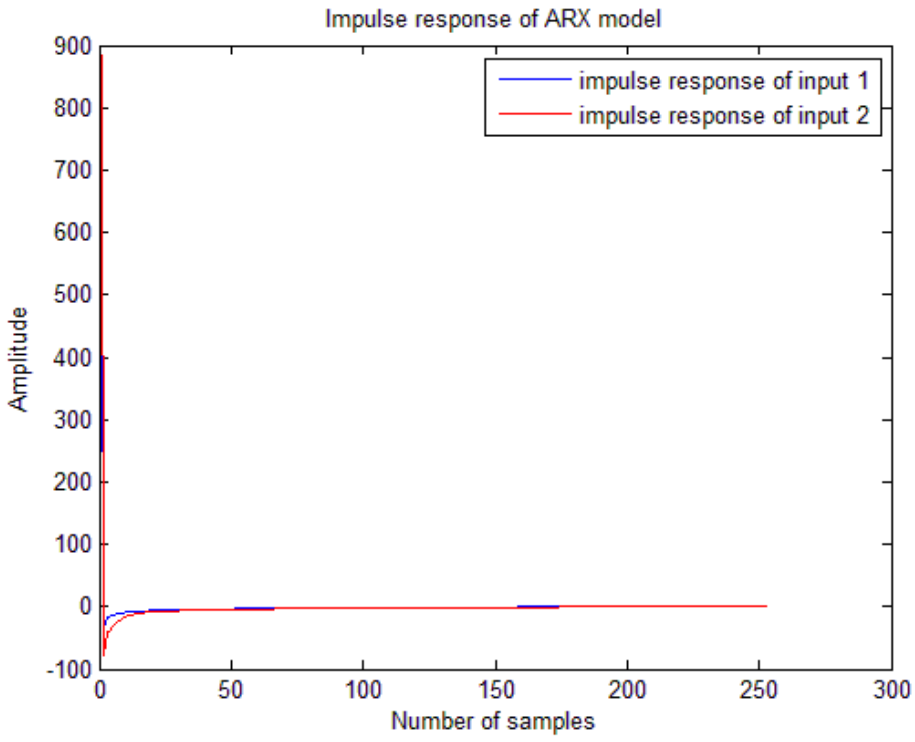

Fig. 60 Impulse response of *Jansen2_S2*, output 2, repetition 5, (jansen_superposition_partII.m).

In Fig. 60 the impulse response of *Jansen2_S2* signal can be observed. As it mentioned above, Jansen's signals were divided into subsystems including both inputs and only one output so in Fig. 60 the impulse responses of one of these subsystems are shown, the subsystem of *Jansen2_S2* signal including both inputs and output 2. Jansen's signals used in the sponge experiments were measured in the loop so every Jansen's signals includes five repetitions and in Fig. 60 the fifth repetition of *Jansen2_S2* is represented.

After a determination of the impulse responses the estimated outputs were obtained according to the definition above, (25).

The last step of this analysis the determination of a correlation coefficients R, (26), between the real measured output and the appropriate estimated output were evaluated in order to confirm the superposition principle and the linear dependence between inputs and outputs.

$$R(i,j) = \frac{C(i,j)}{\sqrt{C(i,i)C(j,j)}} \tag{26}$$

Estimation of correlation coefficients is related to estimation of covariance that is defined for two random variables Y and Z by equation below in Eq. (27).

.

$$cov(Y,Z) = \frac{1}{N-1}\sum_{i=1}^{N}(Y_i - \mu_Y) * (Z_i - \mu_Y) \tag{27}$$

Variable μ_Y is the mean value of Y, μ_Z is the mean value of Z and * denotes the complex conjugate. The covariance matrix C is defined in the way described below, (28), and its values are put into the estimation of correlation coefficients.

$$C = \begin{pmatrix} cov(Y,Y) & cov(Y,Z) \\ cov(Z,Y) & cov(Z,Z) \end{pmatrix} \tag{28}$$

The correlation coefficients assume values in the range from -1 to 1 where the value 0 means no correlation, 1 means direct correlation between two signals and value -1 represents indirect correlation (anticorrelation, the more values in the first group of characters increase, the more values in the second group of character reduce) between two signals.

Based on this fact, the value of the correlation coefficients evaluated between the real output and estimated output can prove the similarity between them. If the value of correlation coefficients is close to 1 the correlation between the real output and the estimated output is significant and it can be said that the superposition principle between real output and both real inputs is relevant and the linear relationship between inputs and output occurs. In that case the sponge phantom could be considered as appropriate to simulate a brain environment and outputs signals from that phantom are a combination of inputs without any significant distortion.

The results of correlation coefficients estimation are introduced below. The first table, Tab. 17, shows the results for *Jansen1_S1* signal. Between real output 1 and estimated output 1 and between real output 2 and estimated output 2 in the first repetition the anticorrelation appeared. It can be caused by measurement error or wrong choice of model describing these subsystems.

In general, a higher values of correlation coefficients for the first real output and estimated first outputs are expected because of the electrode setting S_1. The influence of real inputs to the first real output should be more significant because real output 1 was located closer to inputs than real output 2. In Tab. 17 this conclusion can be observed but some values of the correlation coefficients for the second real output and estimated outputs are low. In the third and the fourth repetitions these values of the correlation coefficients are very low so it can be said that between them no correlation was found.

Tab. 17 Correlation coefficients for *Jansen1_S1* signal.

Jansen1_S1					
	Estimated Outputs, repetition 1	Estimated Outputs, repetition 2	Estimated Outputs, repetition 3	Estimated Outputs, repetition 4	Estimated Outputs, repetition 5
Real Output 1	-0.2581	0.6512	0.6643	0.6324	0.7826
Real Output 2	0.5257	-0.0452	0.3510	0.2888	0.5074

In the rest of Jansen's signals the significant correlation were found (> 0.75) as it can be observed in tables below. In tables Tab. 18 and Tab. 20 the values of the correlation coefficients should be similar because of the electrode setting S_2. In Tab. 18 three exceptions are appeared, the values of correlation coefficients for real output 2 and estimated outputs in the second, third and the fourth repetition. Perhaps a problem with acquired signals during a measurement was appeared because in the previous table, Tab. 17, there are variations from expected values too.

Tab. 18 Correlation coefficients for *Jansen1_S2* signal.

Jansen1_S2					
	Estimated Outputs, repetition 1	Estimated Outputs, repetition 2	Estimated Outputs, repetition 3	Estimated Outputs, repetition 4	Estimated Outputs, repetition 5
Real Output 1	0.9948	0.8858	0.9389	0.9737	0.9837
Real Output 2	0.9783	0.6546	0.7772	0.8964	0.933

The last two tables, Tab. 19 and Tab. 20, show the results which agrees with the theoretical assumptions connected with the electrode settings which are described above.

Tab. 19 Correlation coefficients for *Jansen2_S1* signal.

Jansen2_S1					
	Estimated Outputs, repetition 1	Estimated Outputs, repetition 2	Estimated Outputs, repetition 3	Estimated Outputs, repetition 4	Estimated Outputs, repetition 5
Real Output 1	0.9658	0.9782	0.9719	0.9874	0.961
Real Output 2	0.7469	0.8956	0.7914	0.9595	0.798

Tab. 20 Correlation coefficients for *Jansen2_S2* signal.

Jansen2_S2					
	Estimated Outputs, repetition 1	Estimated Outputs, repetition 2	Estimated Outputs, repetition 3	Estimated Outputs, repetition 4	Estimated Outputs, repetition 5
Real Output 1	0.9963	0.9327	0.9683	0.984	0.9978
Real Output 2	0.9893	0.9413	0.9679	0.9778	0.9907

Significant correlated signals are introduced below in Fig. 61. The amplitude of both signals was normalized.

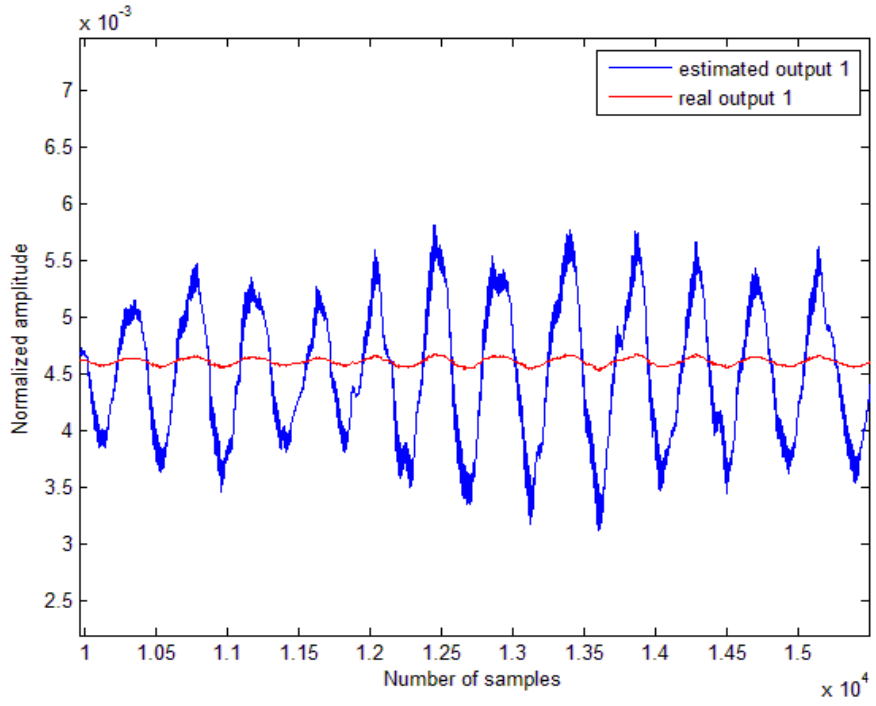

Fig. 61 Significant correlated signals, *Jansen2_S2* signal, output 1, repetition 5, (jansen_superposition_partII.m).

Signals with very low correlation are introduced in Fig. 62. The amplitude of both signals was normalized again.

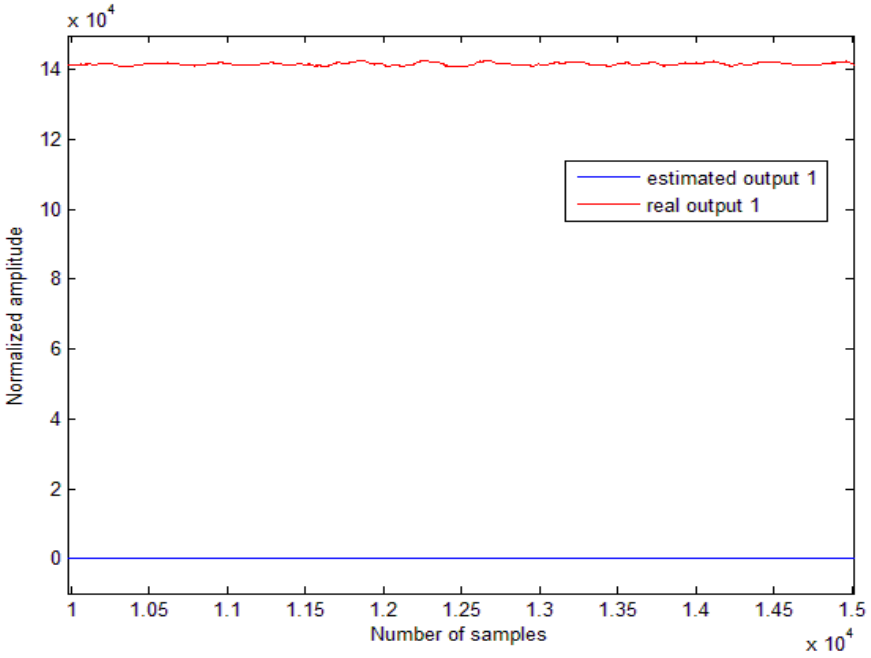

Fig. 62 Not correlated signals, *Jansen1_S1* signal, output 1, repetition 1, (jansen_superposition_partII.m).

11 DISCUSSION

Own programme of Jansen' a single-column model was created in MATLAB in Simulink according to the set of second order differential equations. This programme representing one cortical column generated alpha activity as it was expected. The design of own programme was inspired by mathematical description mentioned in Jansen and Rit study, [16]. The difference between the mathematical description in that study and own programme is that own programme was created in Simulink which is graphically oriented extension of MATLAB. Individual differential equations were represented by mathematical blocks and these blocks were connected into a loop with an external input represented by a white noise ($120 - 320\ Hz$).

Another own programme was an extension of the first one to create Jansen's double-column model. It was inspired by Jansen and Rit study again, [16]. Practical implementation was focused on the interconnection of two cortical columns by the connectivity constants, K_1 and K_2, and the intercolumn delay, a_d. That extension of the first own programme was performed in Simulink again. The result of that extension was a loop where two cortical columns were included and connected by two blocks representing the connectivity constants and the intercolumn delay.

Outputs of that programme were two signals from two cortical columns and their shapes and amplitudes depended on the setting of parameters of the connectivity constants. For the first setting of parameters of the connectivity constants, $K_1 = 7000$ and $K_2 = 10$, two signals both representing alpha activity were received as outputs, for the second setting of parameters of the connectivity constants, $K_1 = 50$ and $K_2 = 500$, two signals representing alpha and beta activity were received as outputs. The intercolumn delay stayed the same in both cases, $a_d \approx 30$.

Spectral analysis was applied to real signals representing alpha and beta activity and to outputs of Jansen's single-column and double-column models. Spectrograms shown some deviations between real signals and simulated signals.

Spectrograms of alpha activity of simulated signals shown the highest intensity in frequency range of $8 - 13\ Hz$. Spectrogram of alpha activity of the real signal shown significant intensity almost till $100\ Hz$. The frequency range of alpha activity was observed but the frequency range of beta activity was observed too. It was caused by an additional noise and bad resolution of the frequency bands.

Spectrograms of beta activity of simulated signals shown the highest activity till $15\,Hz$. So frequency band typical for beta and even for alpha activity was observed. Spectrogram of beta activity of the real signals was very similar like the spectrogram of the alpha activity of the real signal but the intensity of frequencies was lower than in the spectrogram of the alpha activity of the real signal. So in that spectrogram the frequency range typical for alpha and beta activity was present. The high intensity in high frequencies (almost till $100\,Hz$) was caused by the same thing as in previous case, by an additional noise and bad resolution of the frequency bands.

Other models could be used to predict or generate EEG-like signals. They are mentioned in chapter 3 and their brief overview is introduced in [1]. The reason why Jansen's models have been chosen was the mathematical clarity of these models.

In collaboration with the laboratory Gipsa-lab (Grenoble, France), several sponge phantom experiments were performed. These experiments built on previous experiments and the identification of parameters of the measuring system was based on them, [23][24].

Firstly, the sponge experiments included three the simplest signals representing allpass, lowpass and highpass filters. The identification of parameters of these simple systems contained the estimation of the complex gain and the phase, the estimation of the time constant, the estimation of the signal spectrum and the estimation of the transfer function model.

The estimation of the complex gain and the phase was performed by own function created in MATLAB to make a frequency characteristic of measuring signals, [4][28][40]. The estimation of the time constant was performed to find a time delay of the measuring system, [3][18].. The estimation of the signal spectrum included the estimation of the cutting frequency of the measuring signals, [4] [35][36]. The estimation of the transfer function model was performed to express a transfer (transfer function) of measuring systems, [4][35][36].

These estimated parameters were compared to the expected characteristics of ideal allpass, lowpass and highpass filters. The estimated parameters of these systems agreed with the expected ones. It means that the amplitude characteristic of allpass filter was maximal and the phase characteristic was zero line, the amplitude characteristic of lowpass filter was decreasing from the maximum to 0 and the phase characteristic was decreasing from zero value to $\frac{-\pi}{2}$, the amplitude characteristic of highpass filter was increasing from zero value to maximum and the phase characteristic was decreasing from $\frac{\pi}{2}$ to 0.

Secondly, the more complex signals representing highpass filters were included into the sponge experiments. Two types of the electrode setting were used for these experiments, S_1 and S_2, so five signals were used for these experiments in total. The identification of parameters of complex systems was performed in the same way as in previous case and then they were compared to assumptions.

Several deviations between the estimated and the expected parameters were observed. The estimated transfer function models of these systems contained a lowpass components in spite of the fact that these systems were designed to represent highpass filters. The conclusion of this fact was that outputs of these sponge experiments did not describe the ideal highpass filters. The frequency characteristics of these filters indicated the significant similarity with the frequency characteristic of highpass filter. So lowpass components present in the transfer function models were manifestations of nonlinearities that were consequences of using the sponge phantom.

Thirdly, signals representing alpha and beta activity were added to the sponge experiments. The first system contained two signals both representing alpha activity and the second system included two signals representing alpha and beta activity. Two types of the electrode setting were used again so four sponge experiments including five repetitions of Jansen's signals were performed in total.

The analysis was consisted of two main parts, the frequency analysis and the analysis of linear relationship between inputs and outputs. The main tasks of that analysis were to prove that outputs of these systems were similar as inputs, that outputs were the linear combinations of inputs and that the effects of inputs to outputs depended on the distance between inputs and outputs.

The frequency analysis was based on Fourier Transform estimation. Using Fourier Transform the power spectrums of inputs and outputs of these systems were evaluated. Due to the estimation of the power spectrums, it was proved that outputs of these systems were similar as inputs because the highest intensity was observed in the same frequency range.

The analysis of linear relationship between inputs and outputs was based on the assumption of the superposition principle. The impulse responses of both inputs of the measuring systems were found out and according to Eq. (25) both outputs were evaluated. Then evaluated outputs were correlated with real outputs. Based on the correlation coefficients estimation, the degree of similarity between evaluated and real outputs was determined and based on that degree of similarity, the superposition principle between inputs and outputs was confirmed or excluded.

The value of the correlation coefficients in the range of $0.75 - 0.99$ was considered as significant correlation. Values of the correlation coefficients of the first experiment, *Jansen1_S1* signal, were mostly out of that significant range but the rest of these experiments, *Jansen1_S2*, *Jansen2_S1* and *Jansen2_S2* signals, values of the correlation coefficients were in range of $0.75 - 0.99$. Based on that estimations, the superposition principle and then linear relationship was confirmed in these experiments.

Results of analyses of all these experiments suggested that the sponge phantom is appropriate medium to simulate the brain environment including nonlinearities that are present during the real EEG examination.

12 CONCLUSION

Jansen's single-column and Jansen's double-column models were designed in MATLAB, in Simulink. These programmes generated EEG-like signals, alpha and beta activity, according to setting of parameters. Spectrograms were applied to real signals representing alpha and beta activity and to the output signals from own programmes and then these spectrograms were compared.

In the laboratory Gipsa-lab (Grenoble, France), several experiments with the sponge phantom were performed. Firstly, experiments with the simplest signals representing allpass, lowpass and highpass filters were performed and the identification of parameters of these systems was done. Results of that identification were compared to assumptions.

Secondly, more complex signals were added to the sponge experiments. These complex systems represented highpass filters and the identification of parameters of these systems was done in the same way as the identification of parameters of the simplest systems.

Thirdly, signals from Jansen's models were included into the sponge experiments. Two types of analysis were applied to outputs of these experiments. The first one was frequency analysis including the estimation of the power spectrums. This type of analysis was useful to show that the high power was observed in the same frequency range in inputs and in outputs of these measuring systems. It was important to confirm the similarity between inputs and outputs of the measuring systems. The second type was analysis of linear relationship between inputs and outputs of the measuring experiments. This type of analysis was based on the confirmation of the superposition principle. Based on the correlation coefficients estimation between real output of the measuring system and the estimated output of the measuring system linear relationship was confirmed.

Results of all performed sponge experiments suggested that the sponge phantom is appropriate conductive medium to simulate the brain environment.

LITERATURE

[1] SHAYEGH, Farzaneh, Rassoul Amir FATTAHI, Saeid SADRI a Karim ANSARI-ASL. A brief survey of computational models of normal and epileptic EEG signals: a guideline to model-based seizure prediction. *A brief survey of computational models of normal and epileptic EEG signals: a guideline to model-based seizure prediction*. 2011, (Journal of Medical Signals & Sensors, 1)

[2] A Difference Amplifier. In: *A Difference Amplifier* [online]. 2015 [cit. 2015-01-04]. Dostupné z: http://www.play-hookey.com/analog/feedback_circuits/difference_amplifier.html

[3] HISCOCKS, Peter D. A Laplace Transform cookbook. *A Laplace Transform cookbook* [online]. 2008 [cit. 2015-07-26]. Dostupné z: http://www.syscompdesign.com/assets/Images/AppNotes/laplace-cookbook.pdf

[4] ANDERSSON, Lennart, JÖNSSON Ulf, JOHANSSON Karl Henrik a BENGTSSON Johan. *A manual for system identification* [online]. [cit. 2015-07-26].

[5] OLIVIER, David a Karl J. FRISTON. A neural mass model for MEG/EEG: coupling and neuronal dynamics. *A neural mass model for MEG/EEG: coupling and neuronal dynamics*. 2003, (NeuroImage, 20).

[6] LILEY, David T.J., Peter J. CADUSCH a Mathew P. DAFILIS. A spatially continuous mean field theory of electrocortical activity. *A spatially continuous mean field theory of electrocortical activity* [online]. 2002, (Comput. Neural Syst. 13) [cit. 2015-07-27]. Dostupné z: http://opax.swin.edu.au/~dliley/papers/NE2103.pdf

[7] Action potential. In: *Action potential* [online]. [cit. 2015-01-04]. Dostupné z:http://www.zerobio.com/central/actionpotential.htm

[8] *Analýza EEG signálu* [online]. Praha, 2010 [cit. 2015-01-04]. Dostupné z:http://cyber.felk.cvut.cz/research/theses/papers/92.pdf. Diplomová práce. ČVUT, Fakulta elektrotechnická.

[9] GRIMBERT, Francois a Olivier FAUGERAS. Bifurcation analysis of Jansen's neural mass model. *Bifurcation analysis of Jansen's neural mass model* [online]. 2005 [cit. 2015-01-04]. Dostupné z: ftp://ftp-sop.inria.fr/odyssee/Publications/2006/grimbert-faugeras:06.pdf

[10] Brain and electroencephalogramme (EEG). In: *Brain and electroencephalogramme (EEG)* [online]. 2009 [cit. 2015-01-04]. Dostupné z: http://www.elin.ttu.ee/mesel/Study/Courses/Biomedel/Content/BioElect/BESignal/EEG.htm

[11] EEG. In: *EEG* [online]. 2004 [cit. 2015-01-04]. Dostupné z:http://ftplf2.agarek.com/fyzio/prvak/biofyzika/semin/helcas_eeg.php

[12] EEG activity before and during process meditation alpha band (7-12 cycles). In: *EEG activity before and during process meditation alpha band (7-12 cycles)* [online]. [cit. 2015-01-04]. Dostupné z:http://thulea.org/pages/avallach/av117.html

[13] EEG-Holter. *EEG-Holter* [online]. 2013 [cit. 2015-01-04]. Dostupné z: http://sourceforge.net/projects/eegholter/

[14] NUNEZ, Paul L. a Ramesh SRINIVASAN. *Electric fields of the brain: The neurophysics of EEG*. New York, USA: OUP USA, 2006. ISBN 978-0-19-505038-7.

[15] Elektroencefalografie. *Elektroencefalografie* [online]. [cit. 2015-01-04]. Dostupné z:http://www.wikiskripta.eu/index.php/Elektroencefalografie

[16] JANSEN, Ben H. a Vincent G. RIT. Electroencephalogram and visual evoked potential generation in a mathematical model of coupled cortical columns. *Electroencephalogram and visual evoked potential generation in a mathematical model of coupled cortical columns*. 1995, (Biol. Cybern., 73).

[17] Electroencephalography. In: *Wikipedia: the free encyclopedia* [online]. San Francisco (CA): Wikimedia Foundation, 2001-2015 [cit. 2015-01-04]. Dostupné z: http://en.wikipedia.org/wiki/Electroencephalography

[18] *Electronics tutorial: Passive low pass filter* [online]. 2015 [cit. 2015-07-26]. Dostupné z: http://www.electronics-tutorials.ws/filter/filter_2.html

[19] Elektrofyziologie. In: *Elektrofyziologie* [online]. [cit. 2015-01-04]. Dostupné z:http://fbmi.cvut.cz/files/nodes/657/public/Elektrofyziologie.pdf

[20] Elektronika 3. *Elektronika 3* [online]. [cit. 2015-07-26]. Dostupné z: http://www.isibrno.cz/~joe/elektronika/elektronika_3.pdf

[21] *Evaluating goodness of fit* [online]. 2015 [cit. 2015-07-27]. Dostupné z: http://www.mathworks.com/help/curvefit/evaluating-goodness-of-fit.html

[22] Holter EEG with ECG medical device. In: *Holter EEG with ECG medical device* [online]. [cit. 2015-01-04]. Dostupné z:http://www.alibaba.com/showroom/ecg-holter.html

[23] SOTELO, David. *Identification of the parameters of an electroencephalographic recording system: Part I - Modeling of the propagation of the electrical activity in a random medium*. Grenoble, France, 2014. Master thesis. Université Joseph Fourier, Laboratory Gipsa-lab, Département Automatique.

[24] SOTELO, Carlos. *Identification of the parameters of an electroencephalographic recording system: Part II - Modeling and simulation of the electrical activity of a neural network*. Grenoble, France, 2014. Master thesis. Université Joseph Fourier, Laboratory Gipsa-Lab, Département Automatique.

[25] Introduction to the Analysis of Brain Waves. In: *Introduction to the Analysis of Brain Waves* [online]. 2012 [cit. 2015-01-04]. Dostupné z: http://matlabsproj.blogspot.cz/2012/06/introduction-to-analysis-of-brain-waves.html

[26] THOMPSON, Marc T. *Intuitive analog circuit design: A problem-solving approach using design case studies, Livre 3 Electronics & Electrical*. Elsevier Newnes, 2006. ISBN 0750677864.

[27] LEAP for the Assessment and Correction of Specific Learning Difficulties. In: *LEAP for the Assessment and Correction of Specific Learning Difficulties* [online]. [cit. 2015-01-04]. Dostupné z: http://www.positivehealth.com/article/kinesiology/leap-for-the-assessment-and-correction-of-specific-learning-difficulties

[28] SCHOUKENS, Johan, Rik PINTELON a Yves ROLAIN. *Mastering System Identification in 100 Excercises*. John Wiley & Sons, Inc., 2012. ISBN 9780470936986.

[29] Neocortex stellate cell. In: *Neocortex stellate cell* [online]. [cit. 2015-01-04]. Dostupné z:http://neurolex.org/wiki/Category:Neocortex_stellate_cell

[30] Neurons, nerve tissues, the nervous system. In: *Neurons, nerve tissues, the nervous system* [online]. [cit. 2015-01-04]. Dostupné z: http://biomedicalengineering.yolasite.com/neurons.php

[31] Normal EEG Brain Waves. In: *Normal EEG Brain Waves* [online]. [cit. 2015-01-04]. Dostupné z:http://besttoddlertoys.eu/tag/normal-eeg-brain-waves

[32] Obecná neurofyziologie. In: *Obecná neurofyziologie* [online]. [cit. 2015-01-04]. Dostupné z: http://www.profmartinik.cz/wp-content/soubory/obecna-neurofyziologie.pdf

[33] Ocular Movement and Cardiac Rhythm Control using EEG Techniques. In: *Ocular Movement and Cardiac Rhythm Control using EEG Techniques* [online]. 2013 [cit. 2015-01-04]. Dostupné z: http://www.intechopen.com/books/medical-imaging-in-clinical-practice/ocular-movement-and-cardiac-rhythm-control-using-eeg-techniques

[34] *PhysioNet: EEG motor movement/imagery dataset* [online]. 2000 [cit. 2015-07-26]. Dostupné z: http://www.physionet.org/pn4/eegmmidb/

[35] BIBBY, John a TOUTENBERG. *Prediction and improved estimation in linear models*. John Wiley & Sons Ltd, 1978. ISBN 978-0471016564.

[36] Selecting a model structure in the system identification process. In: *Selecting a model structure in the system identification process* [online]. 2010 [cit. 2015-07-26]. Dostupné z: http://www.ni.com/white-paper/4028/en/

[37] LJUNG, Lennart. *System Identification toolbox: For use with MATLAB* [online]. [cit. 2015-07-27]. Dostupné z: http://serdis.dis.ulpgc.es/~ii-its/MatDocen/laboratorio/manuales/IDENT.PDF

[38] The effects of cryopreservation on the cat, Part 3. In: *The effects of cryopreservation on the cat, Part 3* [online]. [cit. 2015-01-04]. Dostupné z:http://chronopause.com/chronopause.com/index.php/2012/02/21/the-effects-of-cryopreservation-on-the-cat-part-3/index.html

[39] The Thalamus and Cerebral Cortex (Integrative Systems) Part 1. In: *The Thalamus and Cerebral Cortex (Integrative Systems) Part 1* [online]. [cit. 2015-01-04]. Dostupné z: http://what-when-how.com/neuroscience/the-thalamus-and-cerebral-cortex-integrative-systems-part-1/

[40] CHAVEZ, M., M. BESSERVE, C. ADAM a J. MARTINERIE. Towards a proper estimation of phase synchronization from time series. *Towards a proper estimation of phase synchronization from time series*. 2005, (Journal of Neuroscience Methods, 154).

[41] LA ROSA, A. Transfer function, Laplace transform, Low pass filter. In: *Transfer function, Laplace transform, Low pass filter*[online]. [cit. 2015-07-26]. Dostupné z: http://www.pdx.edu/nanogroup/sites/www.pdx.edu.nanogroup/files/NOTES_Transfer%20function%20Laplace%20Transormation%20Active%20filter_0.pdf

[42] What is qEEG / Brain Mapping?. In: *What is qEEG / Brain Mapping?* [online]. [cit. 2015-01-04]. Dostupné z:http://qeegsupport.com/what-is-qeeg-or-brain-mapping/

[43] *Zpracování elektroencefalografických signálů* [online]. Brno, 2011 [cit. 2015-01-04]. Dostupné z:http://www.vutbr.cz/www_base/zav_prace_soubor_verejne.php?file_id=37132. Diplomová práce. VUT, Fakulta elektrotechniky a komunikačních technologií.

[44] *Zpracování signálů EEG ve frekvenční oblasti* [online]. Brno, 2014 [cit. 2015-01-04]. Dostupné z: https://www.vutbr.cz/www_base/zav_prace_soubor_verejne.php?file_id=86564. Bakalářská práce. VUT, Fakulta elektrotechniky a komunikačních technologií.

13 APENDIX

Results of the estimation of the time constants of *C1_S1_ch0, C1_S1_ch1, C1_S2_ch0, C1_S2_ch1* and *C1_bip* signals are introduced in figures below, from Fig. 63 to Fig. 72.

Next, results of the estimation of the signal spectrum of *C1_S1_ch0, C1_S1_ch1, C1_S2_ch0, C1_S2_ch1* and *C1_bip* signals performed in *Ident* toolbox are represented, from Fig. 73 to Fig. 77.

In tables below, from Tab. 21 to Tab. 24, results of MSE and FIT estimation of *C1_S1_ch0, C1_S1_ch1, C1_S2_ch0* and *C1_bip* signals are shown. Based on these results the structure of ARX models using for the estimation of the transfer function models has been chosen.

Illustration of *Ident* toolbox interface is shown in the last figure. This toolbox has been used for the estimation of the transfer function models of all signals represented in that work.

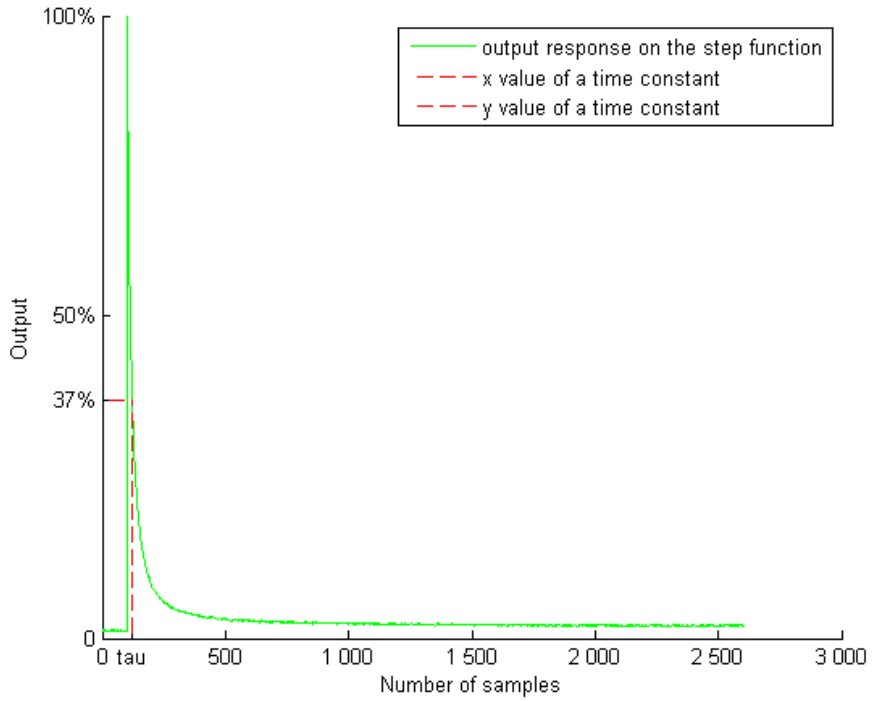

Fig. 63 The step response of *C1_S1_ch0* signal, output 1, (step_response.m).

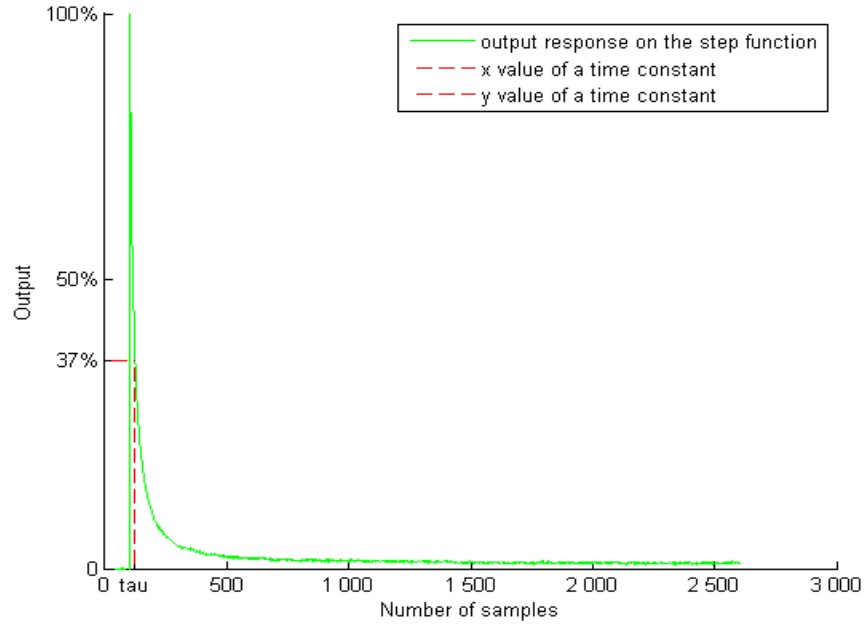

Fig. 64 The step response of *C1_S1_ch0* signal, output 2, (step_response.m).

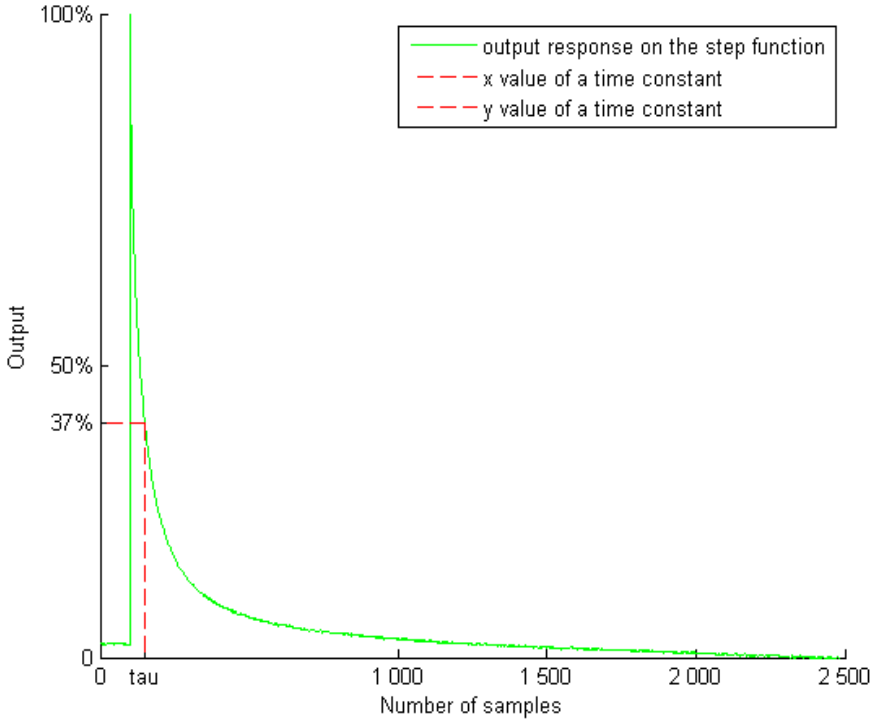

Fig. 65 The step response of *C1_S1_ch1* signal, output 1, (step_response.m).

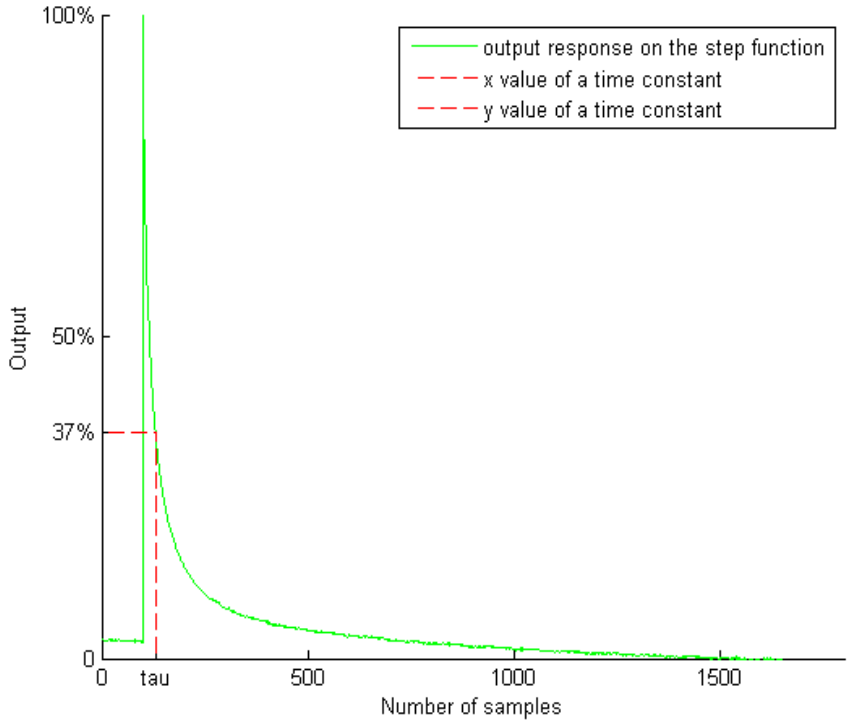

Fig. 66 The step response of *C1_S1_ch1* signal, output 2, (step_response.m).

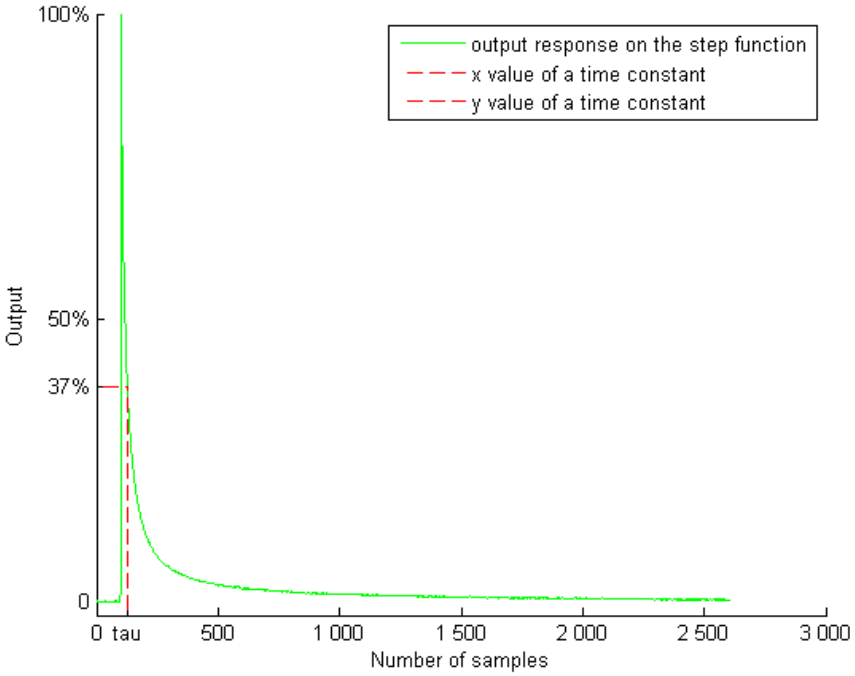

Fig. 67 The step response of *C1_S2_ch0* signal, output 1, (step_response.m).

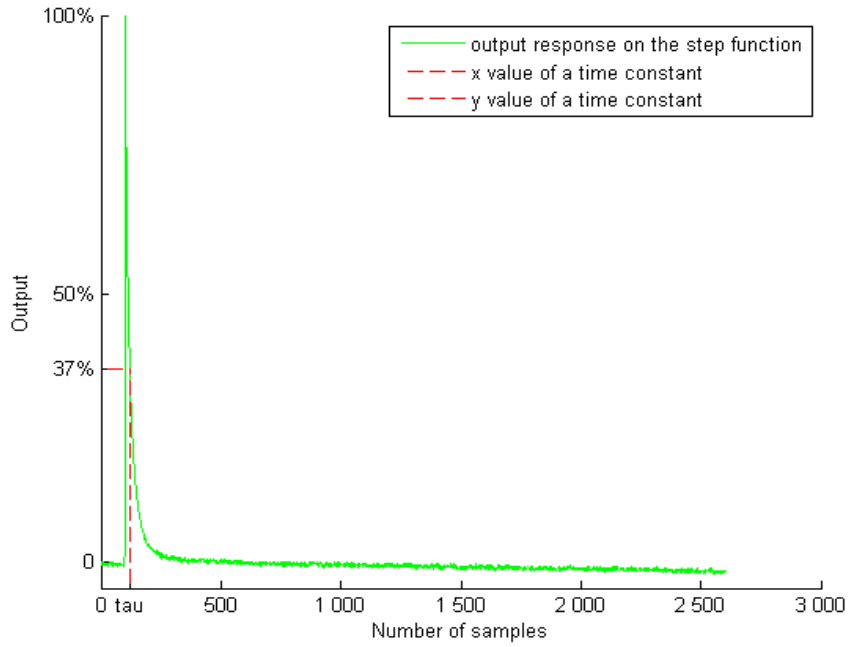

Fig. 68 The step response of *C1_S2_ch0* signal, output 2, (step_response.m).

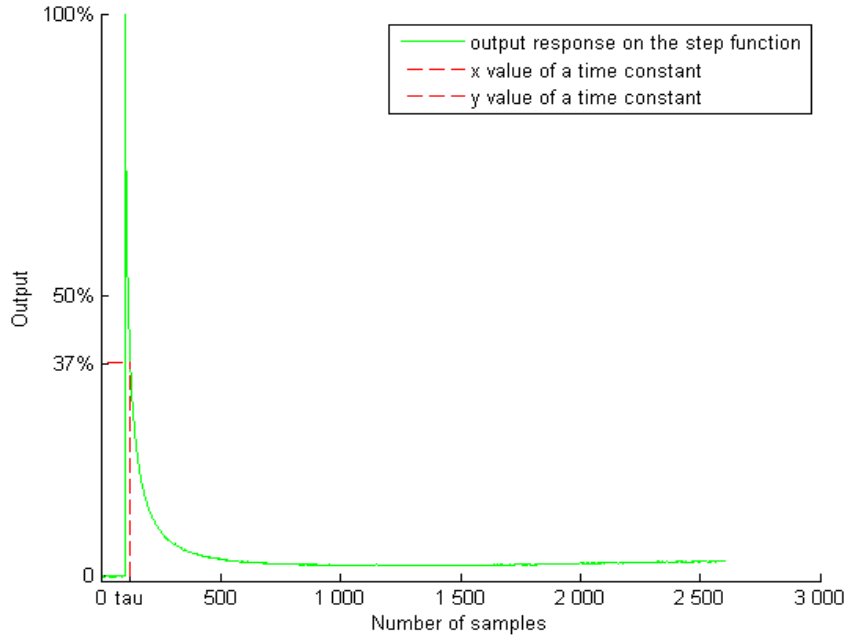

Fig. 69 The step response of *C1_S2_ch1* signal, output 2, (step_response.m).

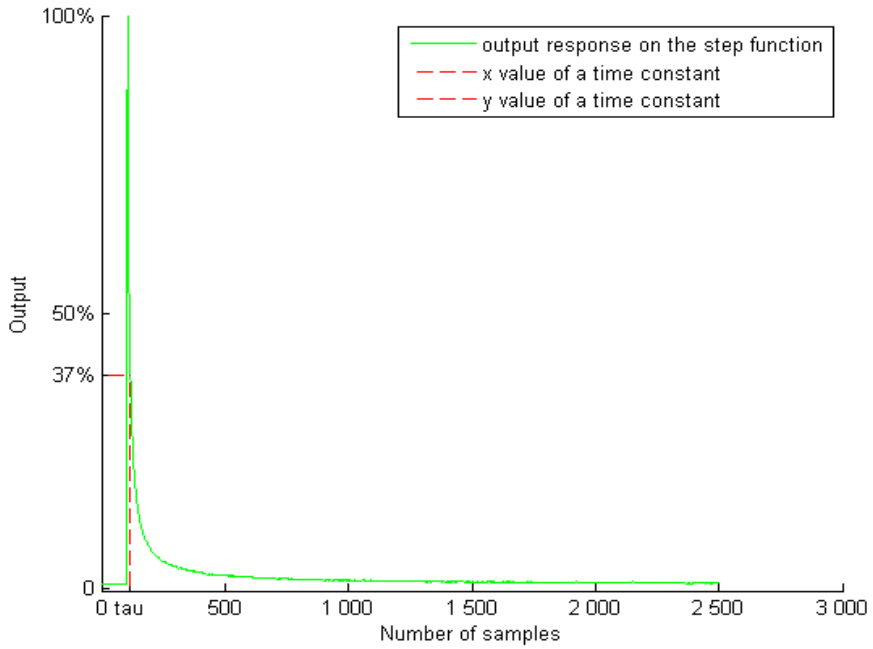

Fig. 70 The step response of *C1_bip* signal, output 1, (step_response.m).

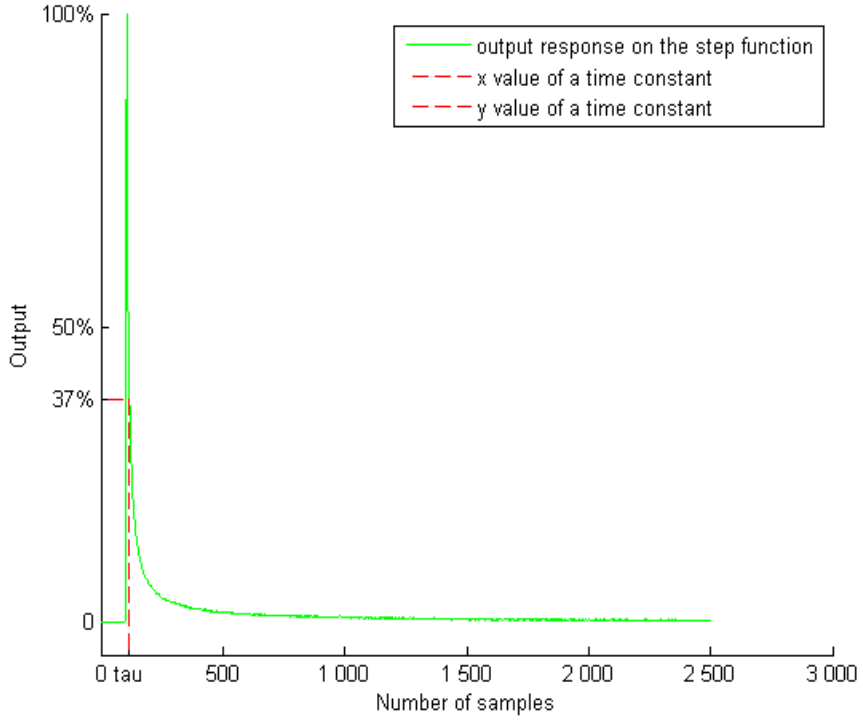

Fig. 71 The step response of *C1_bip* signal, output 2, (step_response.m).

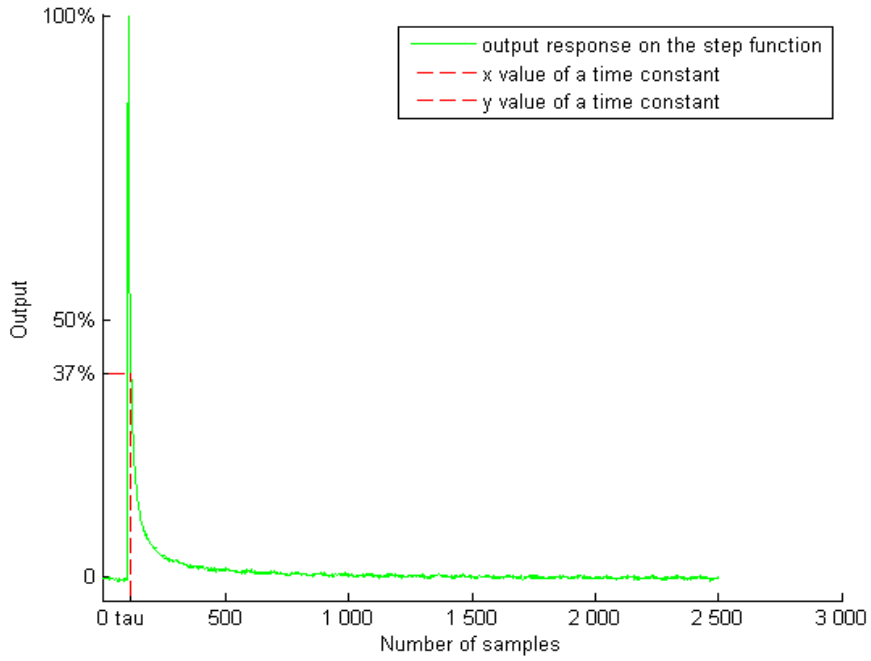

Fig. 72 The step response of *C1_bip* signal, output 3, (step_response.m).

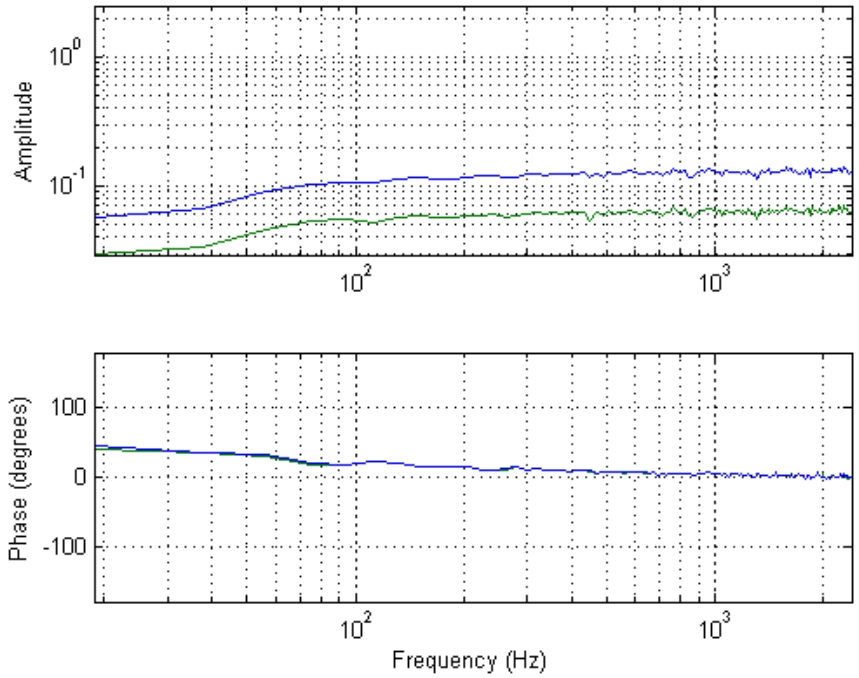

Fig. 73 The spectrum of *C1_S1_ch0* signal, (S1_ch0_out1.sid, S1_ch0_out2.sid).

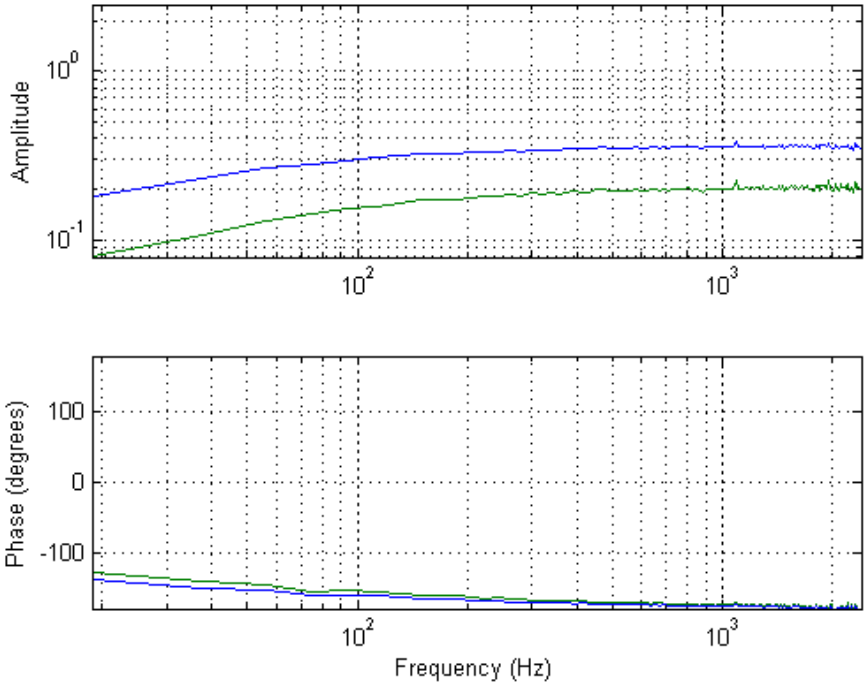

Fig. 74 The spectrum of *C1_S1_ch1* signal, (S1_ch1_out1.sid, S1_ch1_out2.sid).

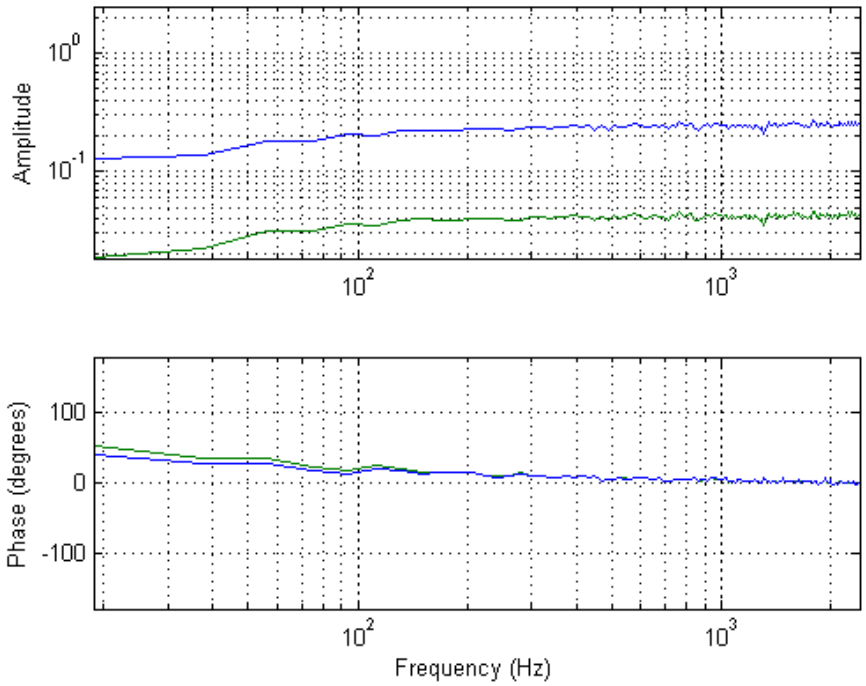

Fig. 75 The spectrum of *C1_S2_ch0* signal, (S2_ch0_out1.sid, S2_ch0_out2.sid).

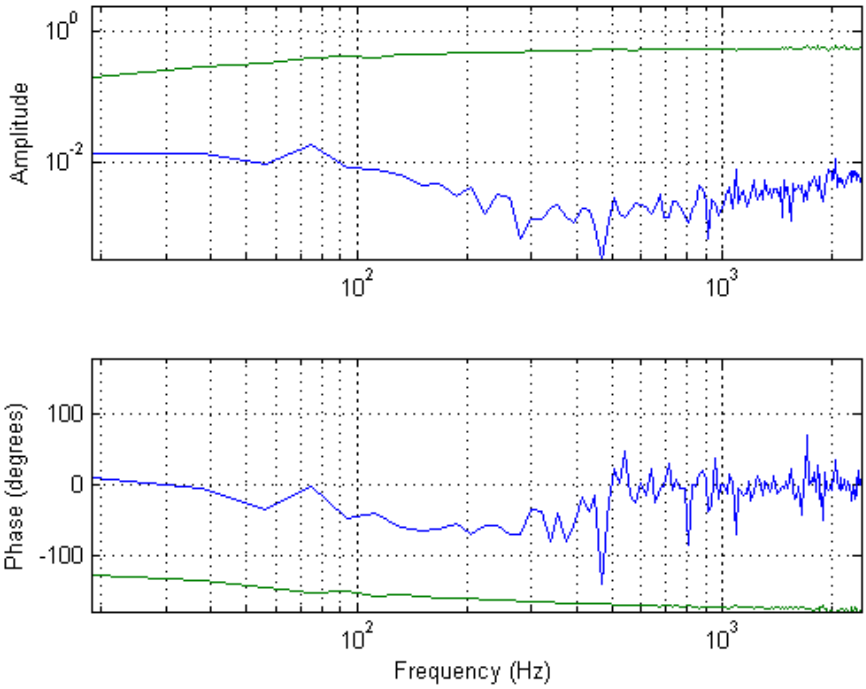

Fig. 76 The spectrum of *C1_S2_ch1* signal, ((S1_ch1_out1.sid, S1_ch1_out2.sid).)

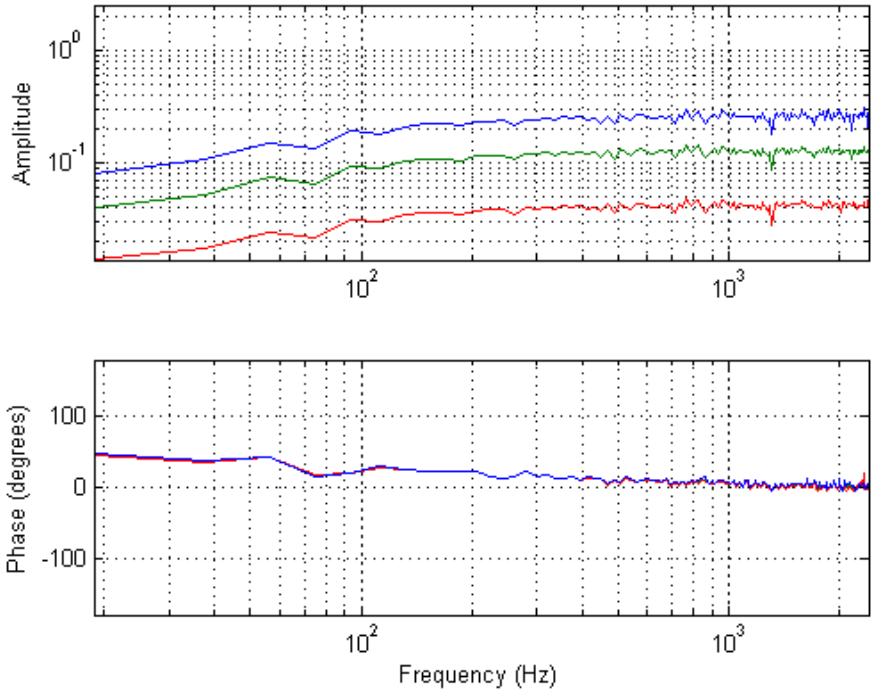

Fig. 77 The spectrum of *C1_bip* signal, (bip_out1.sid, bip_out2.sid, bip_out3.sid)

Tab. 21 Comparison of MSE and FIT values of *C1_S1_ch0* signal.

	(n_a, n_b)	MSE	FIT [%]
Output 1	**(1, 1)**	4 510 000	64.96
	(2, 1)	35 774 000	1.4
	(3, 1)	46 277 000	-12.15
	(4, 1)	37 872 000	-1.45
	(5, 1)	37 538 000	-1
Output 2	**(1, 1)**	2 640 800	49.65
	(2, 1)	8 961 900	7.26
	(3, 1)	27 704 000	-63.05
	(4, 1)	9 144 400	6.32
	(5, 1)	1 289 400 000	-1 010

Tab. 22 Comparison of MSE and FIT values of *C1_S1_ch1* signal.

	(n_a, n_b)	MSE	FIT [%]
Output 1	**(1, 1)**	1 861 000	73.12
	(2, 1)	25 518 000	0.49
	(3, 1)	25 837 000	-0.13
	(4, 1)	26 722 000	-1.83
	(5, 1)	25 761 000	0.01
Output 2	**(1, 1)**	1 550 000	56.59
	(2, 1)	8 036 500	1.33
	(3, 1)	9 516 000	-7.36
	(4, 1)	8 193 800	0.37
	(5, 1)	9 512 300	-7.34

Tab. 23 Comparison of MSE and FIT values of *C1_S2_ch0* signal.

	(n_a, n_b)	MSE	FIT [%]
Output 1	**(1, 1)**	4 334 200	81.76
	(2, 1)	4 362 000 000	-478.44
	(3, 1)	127 910 000	0.94
	(4, 1)	5 158 100 000	-529.01
	(5, 1)	131 300 000	-0.36
Output 2	**(1, 1)**	2 031 100	31.53
	(2, 1)	3 878 400	5.39
	(3, 1)	28 014 000	-154.25
	(4, 1)	3 989 800	4.05
	(5, 1)	3 856 500	5.66

Tab. 24 Comparison of MSE and FIT values of *C1_bip* signal.

	(n_a, n_b)	MSE	FIT [%]
Output 1	**(1, 1)**	5 265 600	74.82
	(2, 1)	1 465 800 000	-320
	(3, 1)	83 558 000	-0.3
	(4, 1)	84 276 000	-0.73
	(5, 1)	83 029 000	0.02
Output 2	**(1, 1)**	1 925 900	68.9
	(2, 1)	19 523 000	0.99
	(3, 1)	20 237 000	-0.8
	(4, 1)	20 354 000	-1.1
	(5, 1)	19 977 000	-0.16
Output 3	**(1, 1)**	1 387 200	23
	(2, 1)	2 230 800	2.4
	(3, 1)	3 673 500	-25.2
	(4, 1)	29 93 100	-13.02
	(5, 1)	2 456 000	-2.38

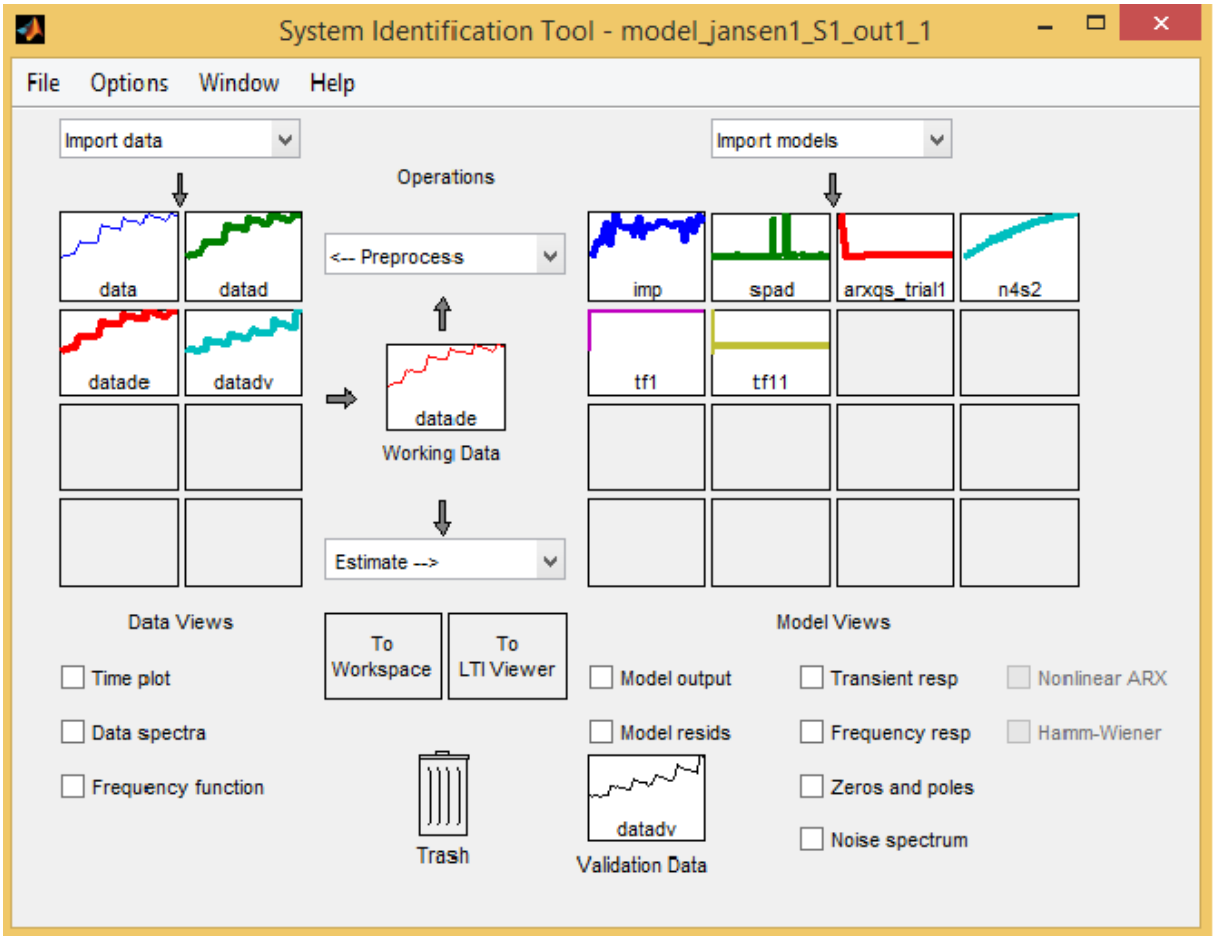

Fig. 78 Illustration of *Ident* toolbox interface.